EXPERIMENTAL AND NUMERICAL STUDY OF SPRING-IN ANGLE IN CORNER SHAPED COMPOSITE PARTS

A THESIS SUBMITTED TO
THE GRADUATE SCHOOL OF NATURAL AND APPLIED SCIENCES
OF
MIDDLE EAST TECHNICAL UNIVERSITY

BY
KEREM FURKAN ÇİÇEK

IN PARTIAL FULLFILLMENT OF THE REQUIREMENTS
FOR
THE DEGREE OF MASTER OF SCIENCE
IN
MECHANICAL ENGINEERING

SEPTEMBER 2014

Approval of the thesis:

EXPERIMENTAL AND NUMERICAL STUDY
OF
SPRING-IN ANGLE IN CORNER SHAPED COMPOSITE PARTS

submitted by **KEREM FURKAN ÇİÇEK** in partial fulfillment of the requirements for the degree of **Master of Science in Mechanical Engineering Department, Middle East Technical University** by,

Prof. Dr. Canan Özgen _____
Dean, Graduate School of **Natural and Applied Sciences**

Prof. Dr. Süha Oral _____
Head of Department, **Mechanical Engineering**

Assist. Prof. Dr. Merve Erdal _____
Supervisor, **Mechanical Engineering Dept., METU**

Prof. Dr. Altan Kayran _____
Co-Supervisor, **Aerospace Engineering Dept., METU**

Examining Committee Members:

Prof. Dr. Haluk Darendeliler _____
Mechanical Engineering Dept., METU

Assist. Prof. Dr. Merve Erdal _____
Mechanical Engineering Dept., METU

Prof. Dr. Altan Kayran _____
Aerospace Engineering Dept., METU

Prof. Dr. Levend Parnas _____
Mechanical Engineering Dept., METU

Prof. Dr. Serkan Dağ _____
Mechanical Engineering Dept., METU

Date: 02/09/2014

I hereby declare that all information in this document has been obtained and presented in accordance with academic rules and ethical conduct. I also declare that, as required by these rules and conduct, I have fully cited and referenced all material and results that are not original to this work.

Name, Last name : Kerem Furkan ÇİÇEK

Signature :

ABSTRACT

EXPERIMENTAL AND NUMERICAL STUDY OF SPRING-IN ANGLE IN CORNER SHAPED COMPOSITE PARTS

Çiçek, Kerem Furkan

M. S., Department of Mechanical Engineering

Supervisor: Assist. Prof. Dr. Merve Erdal

Co-supervisor: Prof. Dr. Altan Kayran

September 2014, 110 Pages

In this study, spring-in problem encountered in corner shaped composite parts which are made of Hexcel's AS4/8552 unidirectional (UD) prepregs is investigated. For that purpose, a simple two dimensional (2-D) geometrical model available in the literature is implemented and spring-in is calculated according to this model. Then using autoclave process, U-shaped composite parts are manufactured and spring-in measurements are performed on these parts. Finally, a three dimensional (3-D) numerical model in ABAQUS is constructed by taking tool-part interaction, cure shrinkage and state transformations of resin into account and spring-in simulation is performed. Spring angle of 0.92° found by numerical analysis model is found to be in good agreement with the spring angle of 0.85° found by experimental method. Consequently, an efficient 3-D ABAQUS model is developed for spring-in analysis of corner shaped composite parts.

Keywords: Spring-in, Composites, Autoclave Manufacturing Process, ABAQUS.

ÖZ

KÖŞELİ GEOMETRİYE SAHİP KOMPOZİT PARÇALARDA OLUŞAN GERİ YAYLANMANIN DENEYSEL VE NÜMERİK OLARAK İNCELENMESİ

Çiçek, Kerem Furkan
Yüksek Lisans, Makina Mühendisliği Bölümü,
Tez Yöneticisi: Yard. Doç. Dr. Merve Erdal
Ortak Tez Yöneticisi: Prof. Dr. Altan Kayran

Eylül 2014, 110 Sayfa

Bu çalışmada, köşeli geometriye sahip ve Hexcel'in AS4/8552 UD prepreglerinden üretilen kompozit parçalarda karşılaşılan geri yaylanma problemi araştırılmıştır. Bu amaçla, literatürede bulunan iki boyutlu (2-B) basit bir geometrik model oluşturmuş ve bu modele göre geri yaylanma hesabı yapılmıştır. Daha sonra otoklav işlemi ile U şekline sahip parçalar üretilmiş ve bu parçalar üzerinde geri yaylanma ölçümleri yapılmıştır. Son olarak, ABAQUS içerisinde kalıp-parça etkileşimini, kürlenme büzülmesini ve reçinenin hal değişimlerini hesaba katan üç boyutlu (3-B) bir model oluşturulmuş ve geri yaylanma simülasyonları gerçekleştirilmiştir. Nümerik analiz modeli ile bulunan 0.92°'lik geri yaylanma açısının deneysel yöntem ile bulunmuş olan 0.85°'lik geri yaylanma açısına oldukça yakın olduğu görülmüştür. Sonuç olarak, köşeli geometriye sahip kompozit parçaların geri yaylanma analizini gerçekleştirebilmek için 3-B etkili bir ABAQUS modeli geliştirilmiştir.

Anahtar Kelimeler: Geri yaylanma, Kompozitler, Otoklav Üretim İşlemi, ABAQUS

To my fiancée and my family,

ACKNOWLEDGEMENTS

I gratefully acknowledge the support and guidance of my thesis advisors Assist. Prof. Dr. Merve Erdal and Prof. Dr. Altan Kayran. With their thoughtful encouragement and discreet supervision, I was able to finish my thesis.

I would like to express my sincere gratitude to my supervisors Tahir Fidan and Suphi Yılmaz, at ASELSAN Inc. for their support and patience throughout my thesis studies.

I am also grateful to İhsan Otabatmaz from EPSİLON Composite for his contributions on the experiments I conducted during my thesis. My thanks also go out to my colleague, Oğuz Doğan, who helped me during ABAQUS modeling.

I extend my sincere thanks to my parents Sevda and Atalay Çiçek for their encouragement and support in every moment of my life.

Finally, my deepest thanks go to my fiancée, Merve Soyarslan, for her love and never-ending support.

TABLE OF CONTENTS

LIST OF TABLES

LIST OF FIGURES

NOMENCLATURE

C_{ij}	Stiffness matrix of ply *i,j* planes, *i,j=1,2,3 or x,y,z*
$\overline{C}_{ij}^{l}$	Stiffness matrix of laminate on *i,j* planes, *i,j= x,y,z*
C_p	Specific heat capacity of ply
E_i	Young's moduli of ply on *i* planes, *i=11,22,33*
G_i	Shear moduli of ply on *i* planes, *i=12,13,23*
K_i	Summation of thermal loads belonging to each ply, *i=x,y,z,xy*
k_{cij}	Thermal conductivity of ply on *ij* planes, *ij=11,22,33*
S_{ij}	Compliance matrix of ply *i,j* planes, *i,j=1,2,3 or x,y,z*
$\bar{S}_{ij}$	Compliance matrix of laminate on *i,j* planes, *i,j= x,y,z*
T_g	Glass transition temperature
T_{ij}	Transformation matrix
α	Degree of cure
α_θ	Effective CTE of laminate in in-plane tangential direction
α_r	Effective CTE of laminate in through the thickness direction
α_i	CTEs of ply on *i* planes, *i=11,22,33*
α_i^l	Effective CTEs of laminate, *i=x,y,z*
ε_i	Strains of ply on *i* planes, *i=1,2,3,23,13,12 or x,y,z,yz,xz,xy*
ε_i^l	Strains of laminate on *i* planes, *i=x,y,z,yz,xz,xy*
ε_i^{cure}	Cure shrinkage of ply on *i* planes, *i=11,22,33*
$\Delta\theta_L$	Spring-in angle of corner section
ΔT	Temperature difference between cure temperature and room temperature
θ	Enclosed angle of corner section
ϑ_{ij}	Poisson's ratios of ply on *i* planes, *i=12,13,23*
σ_i	Stresses of ply on *i* planes, *i=1,2,3,23,13,12 or x,y,z,yz,xz,xy*
σ_i^l	Stresses of laminate on *i* planes, *i= x,y,z,yz,xz,xy*
ϕ_θ	Cure shrinkage strain of laminate in in-plain tangential direction
ϕ_r	Cure shrinkage strain of lamiante in through thickness direction

LIST OF ABBREVIATIONS

CAD	Computer Aided Design
CLT	Classical Lamination Theory
CMC	Ceramic Matrix Composite
CNC	Computer Numerical Control
CTE	Coefficient of Thermal Expansion
FEA	Finite Element Analysis
FEM	Finite Element Method
FRPC	Fiber-reinforced Plastic Composite
MMC	Metal Matrix Composite
PMC	Polymer Matrix Composite
RTM	Resin Transfer Molding
UD	Unidirectional
USDFLD	User Defined Field
3-D	Three dimensional
2-D	Two dimensional

CHAPTER 1

INTRODUCTION

1.1 COMPOSITE MATERIALS

A composite material, or sometimes called as a composite, is a combination of at least two materials which have different physical and chemical properties. The concept of composite is first encountered in the nature although today, composite materials are commonly considered as engineered materials. For example, natural wood is a composite material. It consists of cellulose fibers embedded in polysaccharide lignin. Here, cellulose fibers are responsible from providing good strength and stiffness properties while the polysaccharide lignin as the resin matrix ensures the integrity of the wood [1].

Composite materials with their changeable mechanical properties allow designers to overcome difficult engineering problems by making tougher and lighter designs possible. Moreover, manufacturing complex shaped parts with the use of composites is easier than with the use of conventional materials such as metals. The composite materials have many other advantageous properties which are good dimensional stability, corrosion resistance, slowness of damage propagation, good fatigue strength, and aging resistance [2]. Therefore, the use of composite materials takes place in various industries such as automotive industry, building and civil engineering industry, aeronautics, space, armaments, shipbuilding, electricity and electronics, sports and leisure industries, and many other industries like packaging, art, and decoration [3].

Modern composite materials can be classified in four categories based on their matrices: polymer matrix composite (PMC), metal matrix composite (MMC), ceramic matrix composite (CMC), and carbon matrix composite. Much lower manufacturing temperatures are required for PMC when compared to MMC and

CMC. Also, there has been an increasing demand over the last 30 years in the usage of PMC, particularly for fiber-reinforced plastic composites (FRPC) [4]. PMC contains thermoset or thermoplastic resins which are reinforced with glass, carbon, aramid, or boron fibers. MMC includes metals or alloys reinforced with boron, carbon, or ceramic fibers. CMC, on the other hand, is composed of ceramic matrix and ceramic fibers. Carbon matrix composites employ graphite yarn or fabric in carbon or graphite matrix [9].

In this study, the focus will be on PMC which has two different types in terms of its polymer matrices such as thermoset composites and thermoplastic composites. As will be explained in the following chapters, these composites are reinforced with fiber structures and manufactured by different processes.

1.1.1 Thermoset Composites

A set of manufacturing methods are available for thermoset composites such as hand lay-up, liquid composite moulding (e.g. resin transfer molding or RTM process), and autoclave-forming [5].

Thermoset resins become hardened (solid-like) material when they are cured by applying heat for a specific time interval. However, when a thermoset resin is heated or cured, the process is irreversible which means the resin can not be remolded after the initial heat-forming or curing process. Heating a thermoset resin forms three-dimensional (3-D) network structure between the molecules of resin as chemical reactions (chemical crosslinking or sometimes called as polymerization reactions) take place during curing process. Therefore, once cured, thermoset resins still sustain their strength and shape at high temperatures and they will not become liquid when they are reheated. But above a certain temperature, a dramatic fall in the mechanical properties of thermoset resin is observed. This temperature is called as glass transition temperature (T_g). T_g differs for each thermoset resin depending upon the specific cure-cycle parameters such as time, temperature, and pressure [4].

As the thermoset resins can stay in liquid state at low temperatures before the cure process, embedding continuous fiber reinforcements into the resin matrix can be performed relatively easily. For that reason, thermoset composites are widely available with continuous fiber reinforcements. Epoxy, vinyl ester, furan, cyanate ester, bismaleimide, phenolic resin, and unsaturated polyester can be given as examples to the thermoset resins that are used in the fiber reinforced composites [4].

1.1.2 Thermoplastic Composites

Thermoplastic composites can be processed by different manufacturing methods. For instance, autoclave-forming, diaphragm forming, and compression-forming are the most commonly used methods [5].

Thermoplastic resins, on the other hand, become softened when they are heated and become hardened or solidified when they are cooled down. It is possible to heat up and cool down a thermoplastic resin system as many times as needed without causing a chemical change in the resin's molecular structure. This means the manufacturing process of thermoplastic resin composites is reversible [6, 22].

PET, polyproplyene, polycarbonate, PBT, vinyl, polyethylene, PVC, PEI, and nylon can be given as examples to commonly used thermoplastic resins. Thermoplastic composites with short-chopped fiber reinforcements have been widely employed in thermoplastic composite industry and this type of thermoplastic composites generally contains glass or carbon fiber as the reinforcement. However, for the last decade, it has been possible to see long fiber thermoplastic composite applications in composite industries, especially in automotive industry. These materials have advantages in terms of material properties and manufacturing processes such as adjustable and reproducible fiber length distribution, single heat history, high productivity, and short cycle times [7, 8].

1.1.3 Fiber Reinforcements

In FRPC, fibers can be in different structural forms such as small particles, whiskers (discontinuous fibers) or continuous fibers (filaments). Glass, carbon, and aramid are the most commonly used fiber types in engineering composites and there are some other types of fibers available like boron and ceramic [9]. Fiber arrangement in a laminate can be two dimensional (2-D) or three dimensional (3-D). For the 2-D fiber arrangement, there is no fiber aligned in through thickness direction (Figure 1). However, this leads to poor mechanical properties in terms of stiffness and strength in this direction. As the through-thickness direction of the laminate is dominated with resin which has weaker mechanical properties when compared to the in-plane fiber dominated properties [10]. (Figure 2)

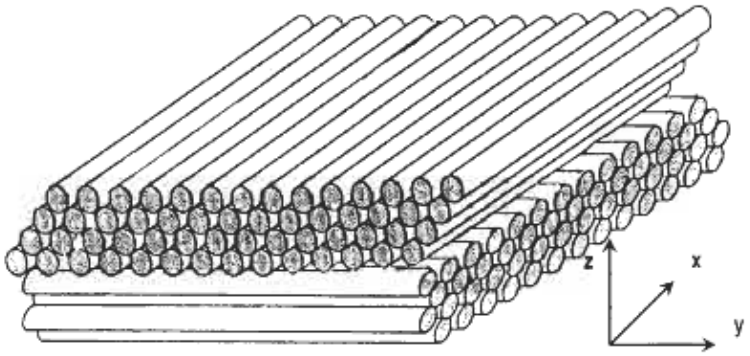

Figure 1: Schematic of 2-D fiber arrangement [10]

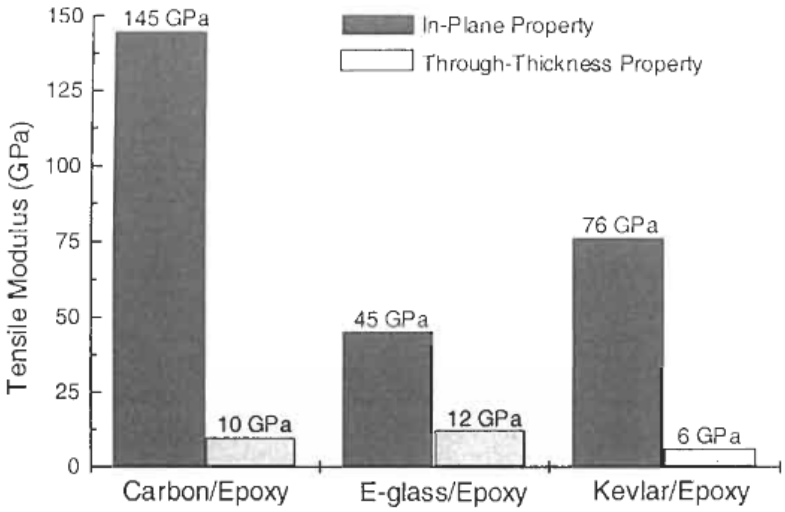

Figure 2: Comparison of in-plane and through thickness tensile modulus of some engineering composites having 2-D fiber arrangement [10]

Unidirectional (UD) composites, for instance, have continuous 2-D fiber arrangement in which all fibers are parallel to each other. (Figure 3) There are other types of continuous 2-D fiber composites such as crossply or woven fabric reinforced composites in which the fibers are oriented at right angles to each other [9]. (Figure 4)

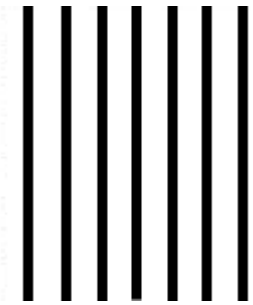

Figure 3: UD continuous 2-D fiber arrangement

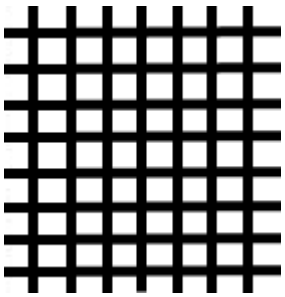

Figure 4: Crossply or woven fabric 2-D fiber arrangement in a composite

3-D fiber arrangement, on the other hand, establishes stiffer and stronger mechanical properties in the through-thickness direction of composite laminate. Since the late-1960s, a processing technique called as braiding has been used to manufacture 3-D fiber structures. 3-D braided fiber structures are utilized in space applications and rocket propulsion, transportation industry, and medical sector as plate, stiffened panels, beams and spars, shell or skin structures, and medical devices [11]. An example to the multi-axis 3-D braided para-aramid preform is shown in Figure 5. Para-aramid is a fiber type with high elastic modulus developed in 1960s by DuPont and Nobel.

Figure 5: 3-D braided para-aramid perform [11]

1.1.4 Manufacturing Processes

In manufacturing, continuous-fiber composites are laminated such that individual layers, plies, or laminae are oriented in desired directions to provide necessary strength properties. This structure is called as laminate in which different lay-up configurations can be performed [12]. (Figure 6, Figure 7) For instance, a symmetric and balanced laminate has a symmetric stacking sequence with respect to its midplane and any ply or lamina in the laminate with orientation angle θ on one side is accompanied by the same ply or lamina with the orientation angle of –θ on the other side of the midplane (symmetry line) as shown in Figure 7 [13].

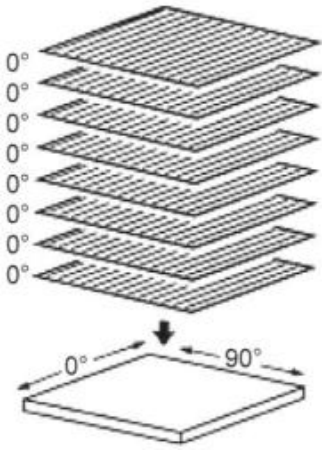

Figure 6: Unidirectional lay-up configuration [12]

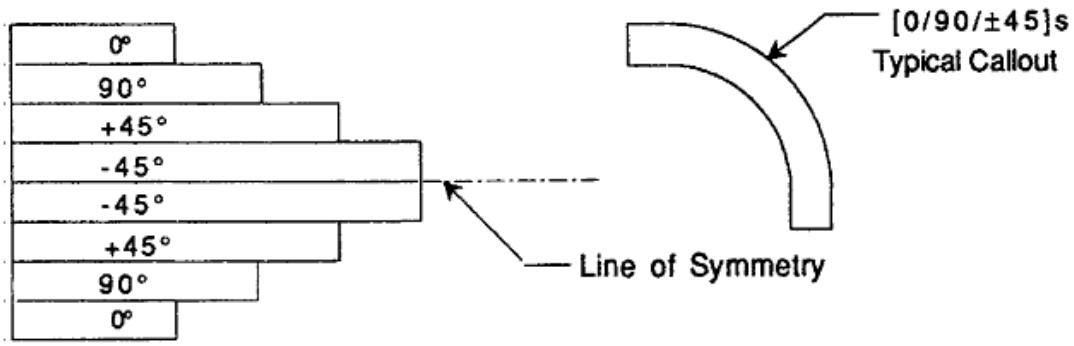

Figure 7: Symmetric and balanced lay-up configuration [14]

In composite industry, various types of manufacturing processes are available and the application of each process depends on different parameters such as the cost, design criteria, required quality and quantity. Some of the significant manufacturing processes for thermoset and thermoplastic composites are going to be explained in the following paragraphs.

In hand lay-up or wet lay-up process, dry reinforcement, mostly woven fabric or mat material, is laid up on the mold manually. During hand lay-up process, low viscosity resin is employed to impregnate each ply. (Figure 8) This method is practicable when the required quantities are small [12].

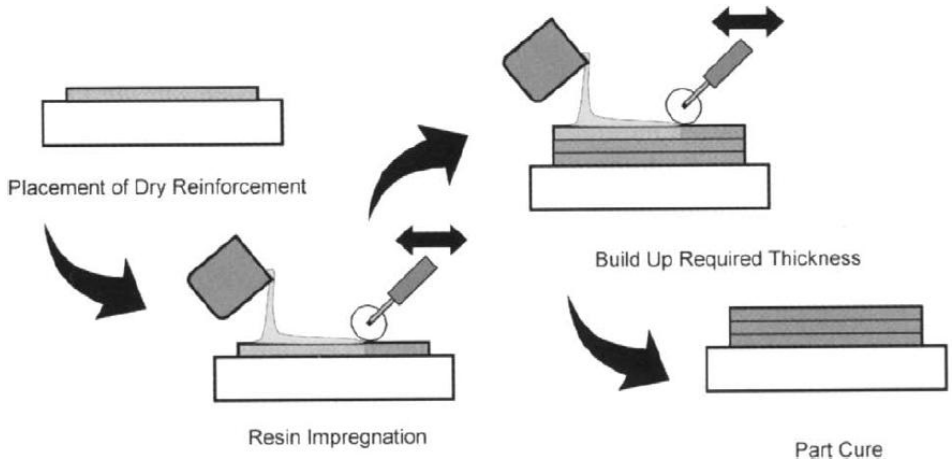

Figure 8: Hand lay-up process [12]

In resin transfer molding (RTM) process, which is one of the liquid forming processes for thermoset composites, a dry perform or lay-up is placed in a metal two-part mold and the mold is clamped. Then, pressurized low viscosity resin is infused inside the mold using the inlet gates. (Figure 9) In order to facilitate the escape of air trapped inside the mold, sometimes vacuum is applied at specific air vents. Very tight tolerances are achievable via this method since this is a matched-die process. Moreover, the mold can accommodate internal heaters to accelerate the curing process if needed [12, 15].

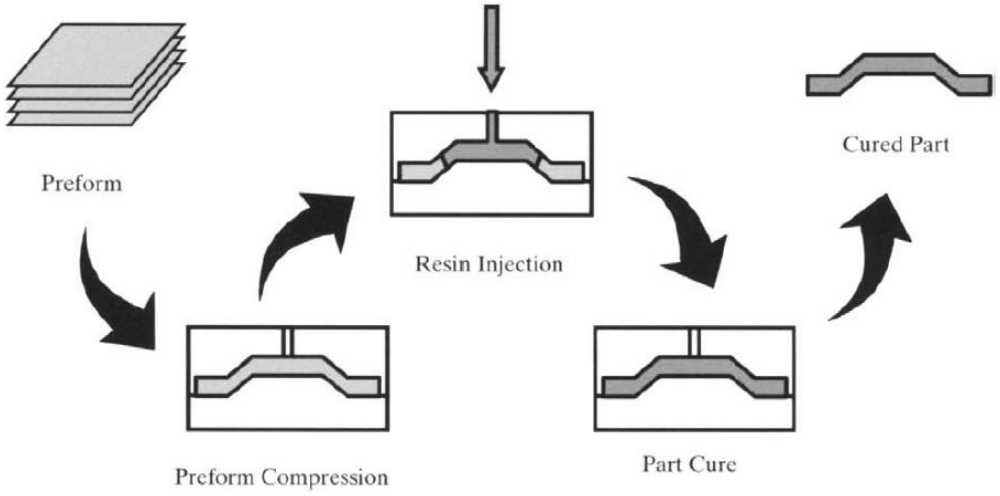

Figure 9: RTM process [12]

Autoclave forming process, which is another important manufacturing process for composites, is generally preferred in aerospace industry. High quality composite parts can be manufactured with this method. However, the process requires significant amount of time. Main steps of autoclave forming process can be stated as preparation of prepregs, tool preparation, laying up prepregs on the tool to make the part, curing of the part, removal of the part from the tool, inspection, and finishing steps [16]. (Figure 10)

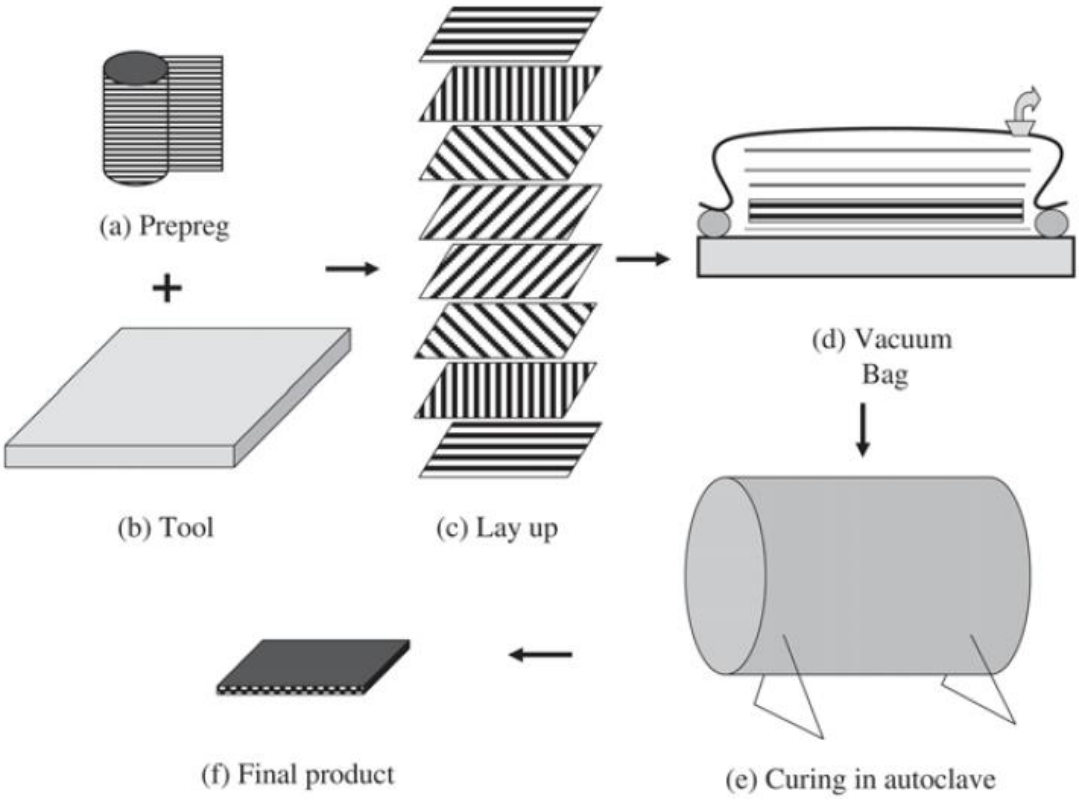

Figure 10: Autoclave forming process [16]

The prepreg is a combination of matrix and fiber reinforcement which is readily available to be used in autoclave forming process. The schematic view of a UD prepreg is shown in Figure 11. In a prepreg, fibers are pre-impregnated with resin, and the resin is partially cured to so that the prepreg is still formable. To prevent further curing and hardening, the prepreg is stored in a refrigerator at 0 ºF [17, 22].

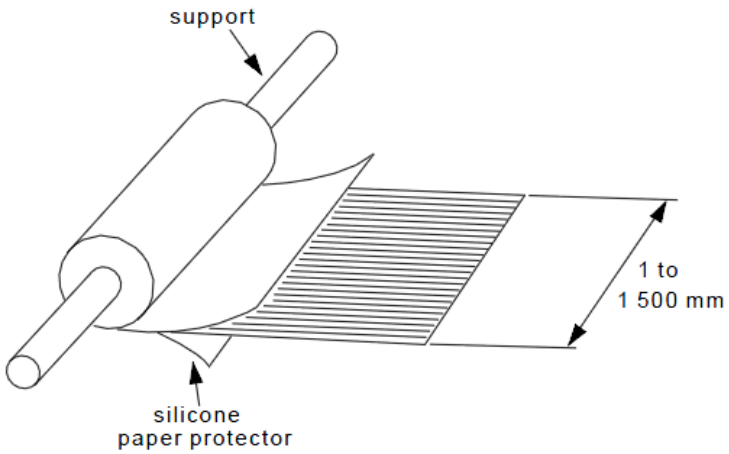

Figure 11: Schematic view of a UD prepreg [17]

As seen in Figure 10, prepregs are cut in suitable size and desired orientations for each layer. They are placed on the tool according to the lay-up configuration. Then prepreg lay-up is vacuum bagged with the tool for consolidation of the composite. Finally, the vacuum bagged manufacturing assembly is put inside the autoclave where heat and pressure applied and cured with respect to a specific cure cycle.

Diaphragm forming is a thermoforming process which is implemented to manufacture thermoplastic composites. In the course of this process, a flat laminate prepreg preform is positioned between two diaphragms (or foils) and these foils are clamped to a mold. The manufacturing assembly including laminate, foils, and mold are then placed in an autoclave machine. Necessary process temperature and pressure are applied inside the autoclave chamber. Due to the usage of autoclave, this process gives high quality products [19].

1.2 MANUFACTURING INDUCED SHAPE DISTORTION PROBLEMS IN THERMOSET COMPOSITES VIA AUTOCLAVE FORMING PROCESS

1.2.1 Vacuum Bagging and Cure Cycle

In autoclave forming process, as mentioned earlier, first prepreg layers are prepared to be draped on mold surface. After draping process is finished, vacuum bagging process takes place. A vacuum bag covers prepreg layup, mold, and other auxiliary equipment as illustrated in Figure 12.

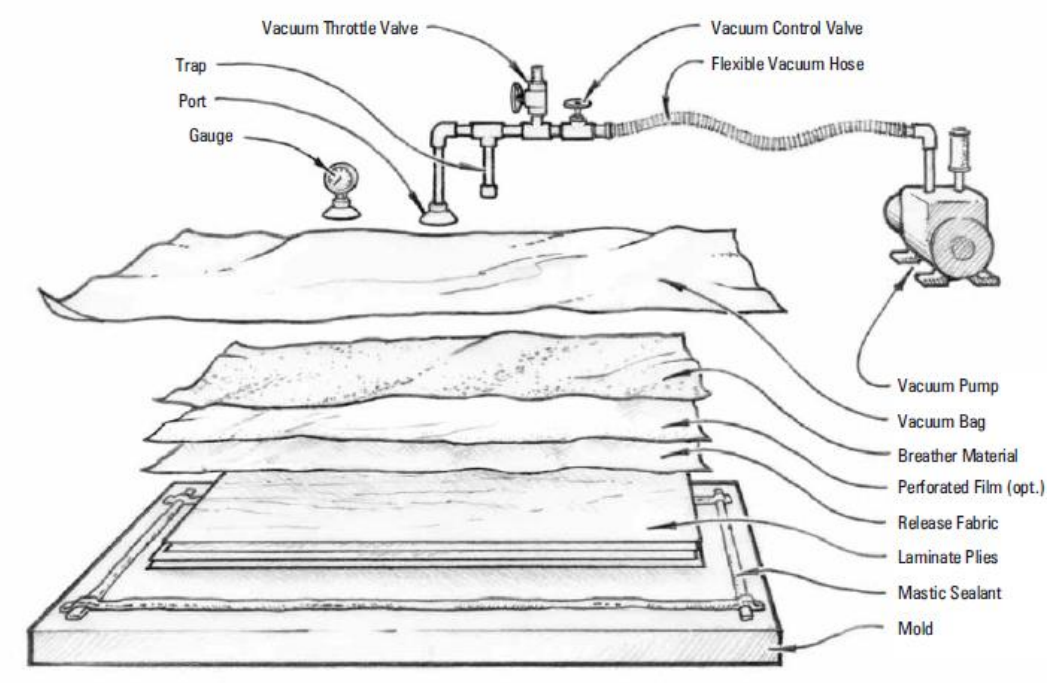

Figure 12: A typical vacuum bagging process [18]

Vacuum bagging is a clamping process which employs atmospheric pressure to consolidate prepreg layers until the curing process inside the autoclave machine ends. When the bag is sealed to the mold, a vacuum pump starts to work and it evacuates the air inside the bag such that air pressure inside the bag is reduced.

Then atmospheric pressure puts equal force on everywhere of the vacuum bag surface. The pressure gradient between inside and outside of the vacuum bag drives the amount of clamping force [18].

Breather material shown in Figure 12 is a perforated film which endures high temperatures in autoclave chamber. It allows the escape of vapor of gases formed during curing process. Release fabric, on the other hand, is a smooth fabric which does not stick to the laminate. It provides a good surface quality for the laminate. Sometimes, release agents are applied on the mold surface to prevent laminates from bonding to the mold surface [16, 18].

Mastic sealant or sealant tape is used during vacuum bagging process for sealing the interface between mold and bagging film. The sealant should adhere to mold surface properly in order to provide an airtight seal [20].

After vacuum bagging process is completed, manufacturing assembly is placed in to autoclave chamber. Inside the autoclave, in order to accomplish curing process, the manufacturing assembly is subjected to temperature and pressure cycles with respect to a time cycle. The combination of these cycles is called as cure cycle and as an example, cure cycle for a specific prepreg is shown in Figure 13 [16].

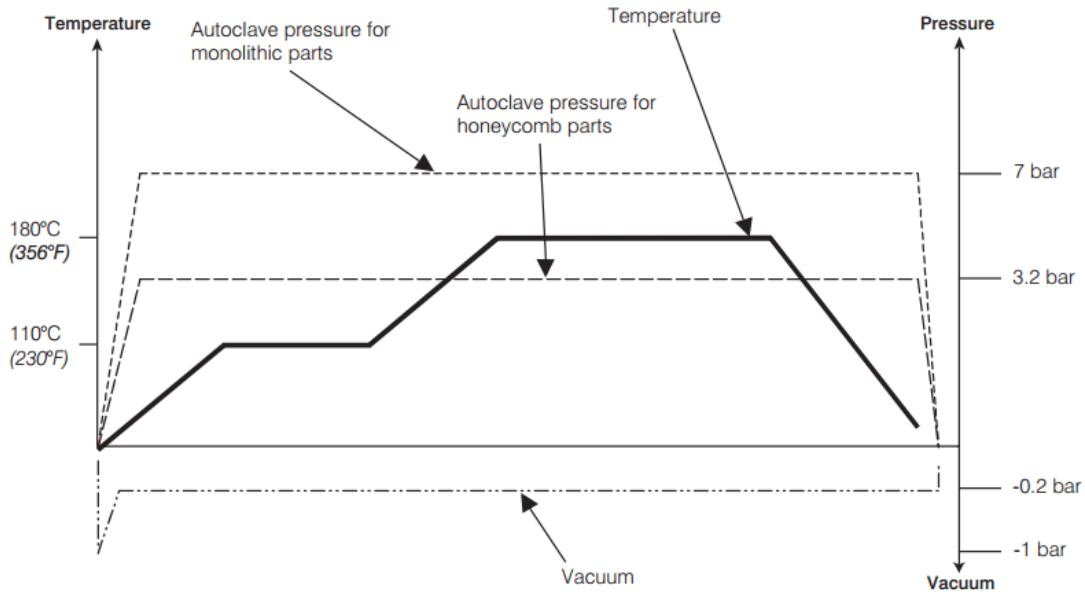

Figure 13: Cure cycle for Hexcel's AS4/8552 UD prepregs [21]

During cure cycle of thermoset composites, exothermic polymerization reactions take place and phase changes occur in the polymeric resin. Thermoset resins are usually in viscous state at room temperature and degree of cure is zero initially. However, when curing process starts, crosslinking reactions occur between polymer molecules and then a network structure develops in the resin [4].

A viscous resin reaches gelation with enough number of crosslinks such that it transforms from a viscous state to a rubbery state. Hereafter, consolidation of polymeric resin accelerates. Crosslinking or polymerization reactions continue intensively until a point that glass transition temperature (T_g) reaches cure temperature and polymer transforms into a glassy state as reported in [24]. After vitrification or full cure as shown in Figure 14, denser and insoluble solid-like composite is obtained, and the degree of cure reaches to one (100% cure). The degree of cure (α) is determined by taking the fraction of heat generated up to a specific point during cure to the total heat generation in one cycle [23].

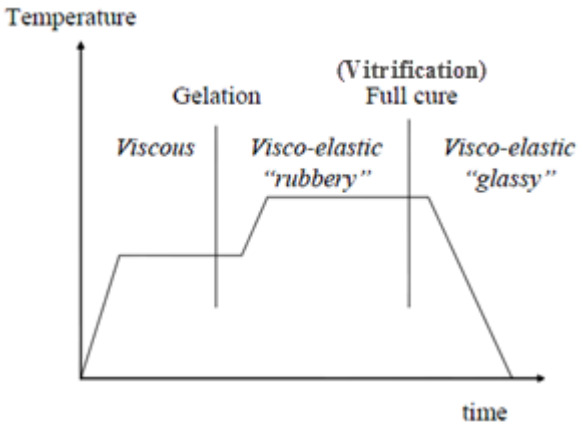

Figure 14: Material behavior of a thermosetting composite during a typical cure cycle [23]

1.2.2 Shape Distortion Problems in Autoclave Forming Process

In general, some problems reducing the quality of final product might be encountered during manufacturing of composites. These problems can be insufficient curing of resin, voids or air bubbles in the resin, wrinkles around the corner of a part, overlapping of fibers during draping, delaminated regions, resin cracks in transverse directions, and shape distortions in the geometry of the part [1].

As mentioned earlier, prepregs are used during autoclave forming process of a composite part. Products containing prepreg lay-ups decrease some of the manufacturing problems such as insufficient curing and voids in the resin because fiber to resin ratio is controlled in prepregs. This provides uniformity and repeatability in manufactured composite parts. However, in typical hand lay-ups, obtaining less than 50% resin is almost impracticable and problems such as resin rich areas, dry spots, and voids (air bubbles) can be seen at many locations in finished parts [25].

It should also be noted that voids and foreign particles trapped between layers later cause delamination in the composite part. Therefore, clean rooms are employed

during draping of prepreg layers in order to prevent foreign particles from sticking to layer surfaces and vacuum bag is utilized in autoclave forming process to decrease the amount of voids present in the resin. It is particularly important to apply vacuum bagging to reduce voids since interlaminar shear strength reduces by 7% for each 1% void present in the resin [28].

Resin cracks are considered to initiate from manufacturing defects such as resin voids, densely grouped fiber arrangement, and fiber-resin de-bonding. These cracks can grow within planes normal to the ply mid-plane and finally result in failure [29].

Some computer programs perform draping simulations for each prepreg layer on mold surface so that overlapping of fibers or wrinkling of a prepreg fabric can be observed and solved before actually draping them [26]. For instance, software called PAM-QUIKFORM provides a CATIA integrated solution for composite design and manufacturing. It calculates the drapability of a ply beforehand and shows critical regions such as the red regions in Figure 15.

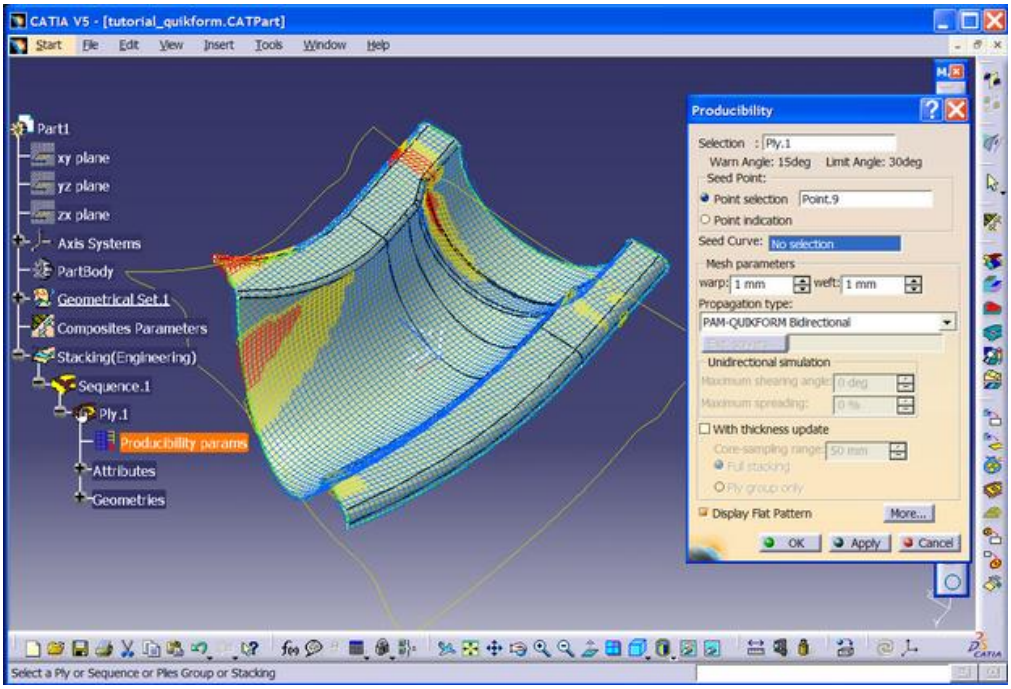

Figure 15: Drapability Simulation in PAM-QUIK FORM [27]

Manufacturing problems mentioned up to this point can be controlled and eliminated in the course of an autoclave forming process. However, shape distortions which occur due to unavoidable residual stress formations during cure are not easy to overcome [23]. Because of shape distortions, assembling of composite parts becomes difficult and this leads to an increase in manufacturing costs. In the following sections, shape distortion types and mechanisms causing residual stresses and shape distortions are going to be explained in detail.

1.2.2.1. Shape Distortion Types

Shape distortions can be classified in two major groups as warpage and spring-in. As shown in Figure 16, warpage is described as the distortion of geometry for a manufactured part which is initially thin and flat [23, 30, 32].

Figure 16: Warpage on an initially flat part [30]

On the other hand, spring-in, which is the main focus of the thesis, can be defined as the decrease of the enclosed angle in a corner shaped composite part. It is also called as spring-forward and the spring-in mechanism is displayed in Figure 17. For a thermoset composite part, change in the enclosed angle of a perpendicular corner is in the order of 1˚to 3˚[33].

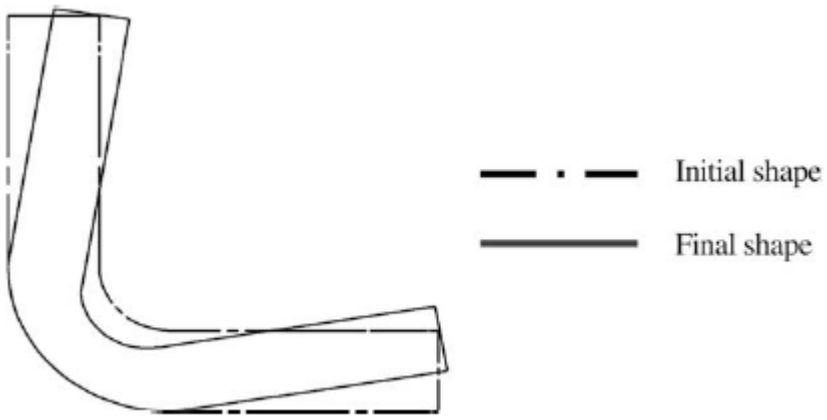

Figure 17: Spring-in on a corner section [34]

1.2.2.2. Effective Mechanisms Causing Residual Stresses and Shape Distortions

In the course of curing process, residual stresses build-up in the resin. During the first stages of curing process, thermoset resin in its viscous state cannot retain appreciable stresses. When the resin transforms to rubbery state, it has significant amount of bulk modulus such that hydrostatic stresses might arise in three-dimensionally constrained areas due to tooling. This can create cracks on thick composites in the early stages of curing process [30, 37]. After vitrification, the Young's modulus and shear modulus of a resin in glassy state are about hundred times the modulus values of the same resin in the rubbery state [36]. Therefore, a vitrified resin behaves like an elastic solid and thermal strains are much more dominant in this state than chemical strains (cure shrinkage strains) due to crosslinking reactions.

There are different mechanisms such as anisotropy in coefficient of thermal expansion (CTE) properties, cure shrinkage of resin, and tool-part interaction that induce residual stresses and cause shape distortions on composite parts [30, 33, 35, 36].

Anisotropy in CTEs

There are three mechanisms causing residual stresses because of anisotropic CTE properties. These mechanisms are due to fiber and matrix level (micromechanical level), ply-level, and laminate-level differential thermal expansion properties respectively [30].

In the first mechanism, it is stated that CTE of polymer-matrix is generally higher than the CTE of fiber. In addition to this, fibers generally have orthotropic thermal expansion coefficients. This means CTE's of a fiber are unique and independent in three mutually perpendicular directions. These factors result in residual stresses at the micromechanical level as the part is cooled-down from the cure temperature to the room temperature. The residual stresses developed at this level do not contribute much to the shape distortions, however; they might cause the progress of matrix cracking and have a negative effect on the mechanical properties of the composites [30, 37].

Unidirectional plies have much larger CTE in the transverse directions than in the fiber direction because the fiber direction is dominated by fibers whereas the transverse directions are dominated by resin. Furthermore, the mechanical stiffness properties of unidirectional composites are much weaker in transverse direction when compared to the fiber direction [36]. Therefore, in the second mechanism, when the temperature of a ply is increased, transverse expansion is more than expansion observed in the fiber direction and as a result warpage in the initially flat ply is encountered [30].

The third mechanism is similar to the second mechanism but this time it is in the laminate-level. Laminates, having higher transverse CTE's compared to fiber dominated longitudinal CTE, tend to distort with the application of temperature gradient [30]. However, transverse expansion of a laminate is greatly dependent up on the lay-up configuration. If an initially flat laminate is symmetric and balanced, then all stretch-bending couplings are eliminated such that transverse expansions of

plies cancel each other independent of the stacking sequence and warpage due to anisotropy in CTEs is not observed. [33] This is similar to the situation that when a tensile force is applied to a balanced laminate having *(+θ/-θ)* sequence, tension-shear coupling effect are neutralized as shown in Figure 18 [1].

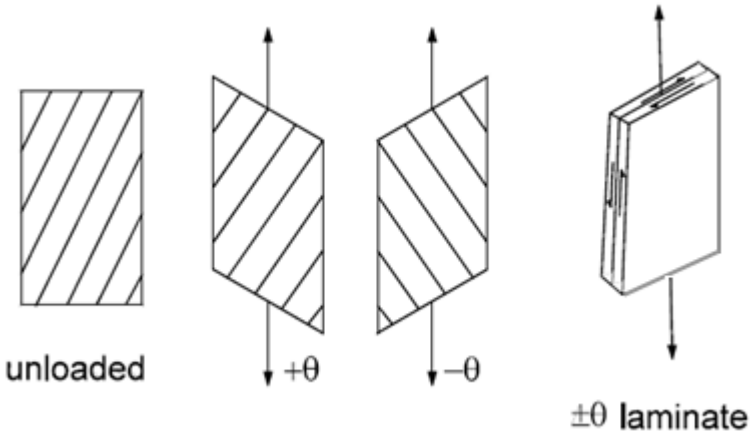

Figure 18: Elimination of tension-shear coupling when a tensile force applied on balanced laminate [1]

However, for a corner shaped laminate, having symmetric and balanced lay-up configuration would not prevent spring-in shape distortion due to anisotropy in CTEs since the neutral axis of the laminate is shifted from the mid-plane due to the corner curvature [32].

Cure Shrinkage of Resin

Due to chemical reactions between resin molecules during the cure process, resins shrink in volume. Volumetric shrinkage for a typical epoxy resin is around 6-7% when fully cured [39]. Moreover, thermal gradients and chemical conversion gradients are observed in the resin during cure because of strong linkage between reaction kinetics and heat transfers, and also low thermal diffusivity of resin. In

thick laminates, thermal gradients through thickness direction have significant effect on curing process and they can change the cure shrinkage trend [40]. The difference in degree of cure between the surface and core of a neat resin reaches to 15% of the total degree of cure [39]. This causes residual stresses and cure gradients in the resin and leads to variation in mechanical properties. In addition to this, chemical shrinkage causes shape distortions in curved or cylindrical laminates due to the different chemical shrinkage buildup between in-plane and transverse directions [41].

Cure shrinkage can be minimized through the use of different cure cycles. For that purpose, time and temperature parameters of cure cycle are modified [42]. However, modifying cure cycle parameters to reduce residual stresses is not always feasible since there might be an increase in the time of curing process or undesired mechanical properties can be obtained at the end.

Tool-part Interaction

Regardless of the lay-up configuration, laminates manufactured on flat tooling displays a concave down warpage [30, 31]. Tools generally have higher CTE properties when compared to composites. Under these conditions, both tool and composite part are subjected to temperature changes inside the autoclave chamber and layers close to the tool are stretched more than the plies far away from the tool. This non-uniform strain distribution cause residual stresses in the composite part since the viscosity and the mechanical properties of the composite change during the curing process and any shape change is cured-in. After the demolding process, composite part is warped according to the mechanism shown in Figure 19. Depending on the frictional forces at the tool-part interface, there is a relative slip between tool and part which also result in shape distortion [31, 43].

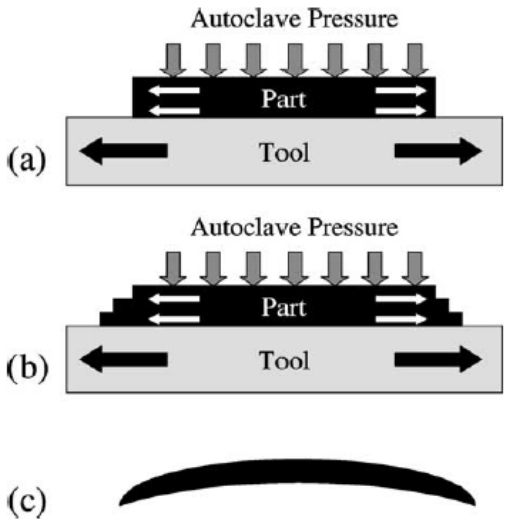

Figure 19: Warpage Mechanism: a) Tool expansion due to heating of tool up to cure temperature b) Inter-ply slippage due to stress gradients in the through thickness direction c) Initially flat part is curved after demolding [31]

1.3 OBJECTIVE OF THE THESIS

The objective of this thesis is to develop a 3-D numerical analysis model that predicts the spring-in problem in corner shaped composite parts manufactured via autoclave forming process. It is considered that with such a predictive analysis method, tool geometry can be modified beforehand such that the cured part comes out of the mold without any appreciable shape distortion. For this purpose, an efficient and reliable numerical analysis model which considers anisotropic material behavior, cure shrinkage of resin, and tool-part interaction is developed.

1.4 THESIS OUTLINE

This thesis consists of five main chapters. In the first three chapters, spring-in problem on corner shaped composite parts which are made of AS4/8552 composite system is investigated by different methods. AS4/8552 is a UD prepreg which

consists of carbon fibers and epoxy resin. Then, in the last two chapters, results are presented and discussed, and conclusions are made respectively.

2-D analytical solution for spring-in problem available in the literature is presented in Chapter 2. The analytical solution finds and uses 3-D effective CTEs of a symmetric and balanced laminate. Furthermore, the effect of cure shrinkage is also taken into account here and for that purpose; effective cure shrinkage strains of a symmetric and balanced laminate are also found. Then strains due to anisotropy in CTEs and cure shrinkage are utilized in a simple geometric formula to find spring-in angle of a corner shaped composite part.

In Chapter 3, spring-in behavior of U-shaped composite parts is examined by manufacturing composite specimens using autoclave forming process. For that purpose, details of spring-in angle measurement using an optical scanning device are described. Also, in this chapter it is explained how the surface temperature field of a specific manufacturing assembly inside the autoclave chamber is monitored during the curing process.

A 3-D ABAQUS model simulating the spring-in of U-shaped composite parts is developed in Chapter 4. The numerical model considers changing rubbery and glassy state composite properties and takes spring-in mechanisms such as anisotropy in material properties, cure shrinkage of resin and tool-part interaction into account. In addition to these, the effects of cure shrinkage and tool-part interaction mechanisms on spring-in problem are separately identified numerically.

Results of analytical, experimental and numerical spring-in values are given and discussed in Chapter 5. Comments are made on the effects of cure shrinkage and tool-part interaction mechanisms on spring-in problem. In addition to these, the effect of coefficient of friction between tool and part is discussed.

In Chapter 6, conclusions are made and recommendations for further research are provided.

CHAPTER 2

ANALYTICAL DETERMINATION OF SPRING-IN

In this chapter, a 2-D theoretical computation method available in the literature for spring-in on corner sections is explained and a solution is obtained with this method. The method includes both the anisotropy in CTE and the cure shrinkage effects, but excludes tool-part interaction. The aim is to compare the results obtained using the analytical method with experimental measurements and the FEM solution.

2.1 GEOMETRIC DEFINITION OF SPRING-IN

Spring-in is already discussed in Chapter 1 and it can be defined as the decrease in the enclosed angle of a corner section which has anisotropic material properties. There have been many studies conducted to determine spring-in angle theoretically over the past years. [33, 34, 41, 44, 45, 46] In this chapter, a theoretical model solving the spring-in angle of a corner section on a laminate is introduced. Theoretical model utilizes 2-D Radford model [46] to take both cure shrinkage and anisotropy of CTE into account during cooling down from cure temperature to room temperature with the help of studies available in the literature [33, 44].

Corner section of a U-shaped or L-shaped composite part in cured and uncured states is displayed in Figure 20 where θ, l_o, l_i, and t represent the enclosed angle, outer length, inner length and thickness of the corner section in uncured state, respectively.

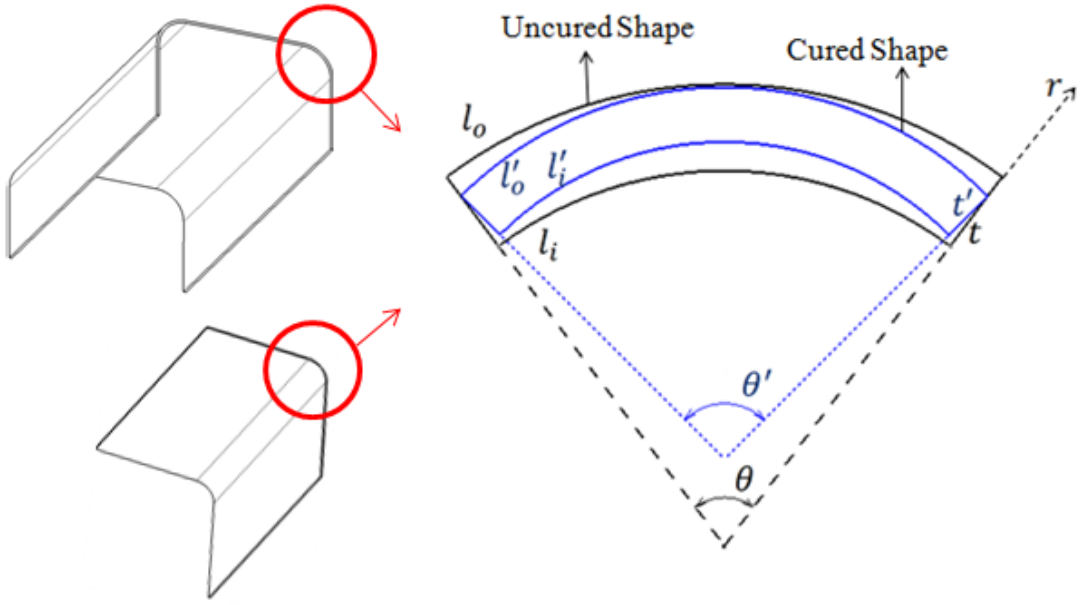

Figure 20: Change in the enclosed angle *(θ)* of corner section after curing process

The change in the enclosed angle can be written in the following form:

$$\Delta\theta=\theta'-\theta=\frac{l'_o-l'_i}{t'}-\frac{l_o-l_i}{t} \qquad (1)$$

Knowing that $l'_o=(1+\varepsilon_\theta)l_o$, $l'_i=(1+\varepsilon_\theta)l_i$, and $t'=(1+\varepsilon_r)t$, Equation (1) can be rearranged as shown in Equation (2):

$$\Delta\theta=\theta\left(\frac{\varepsilon_\theta-\varepsilon_r}{1+\varepsilon_r}\right) \qquad (2)$$

where ε_θ is the strain of laminate in the in-plane tangential direction and ε_r is the strain of the laminate in the through thickness direction, as shown in Figure 20.

Using Equation (2), the sources of in-plane and through thickness strains such as anisotropy in CTE ($\Delta\theta_{CTE}$) and cure shrinkage ($\Delta\theta_{CS}$) are included and expanded in Equation (3).

$$\Delta\theta=\Delta\theta_{CTE}+\Delta\theta_{CS}=\theta\left(\frac{(\alpha_\theta-\alpha_r)\Delta T}{1+\alpha_r\Delta T}\right)+\theta\left(\frac{\phi_\theta-\phi_r}{1+\phi_r}\right) \quad (3)$$

where, α_θ, α_r, ϕ_θ, ϕ_r, and ΔT denote CTE in in-plane tangential direction, CTE in through the thickness direction, cure shrinkage strain in in-plane tangential direction, cure shrinkage strain in through the thickness direction, and temperature difference between the cure temperature and the room temperature, respectively.

Although, the formula given in Equation (3) models a 2-D spring-in problem, the need for calculating effective CTEs (α_r and α_θ) of the laminate in through the thickness and in-plane directions requires a 3-D approach. Therefore, later in this chapter, derivation of effective CTEs is explained. The represented model considers only symmetric and balanced laminates which has quasi-isotropic lay-up configuration. A quasi-isotropic laminate exhibits isotropic material behavior in in-plane directions but for the out of plane direction or through thickness direction, this isotropic material behavior does not hold. It should also be noted that Equation (3) uses constant CTE values while taking the cooling down process into account.

The cure shrinkage strains of the laminate seen in the second term of Equation (3) are calculated using experimental data for one ply. The method for obtaining cure shrinkage strains of a symmetric and balanced laminate is also presented in this chapter.

For the cross-section of an L-shaped part shown in Figure 21, the angle between two legs can be denoted as θ_L. An increase in the enclosed angle *(θ)* causes an equal amount of decrease in the angle of θ_L. Therefore, using the relationship between θ

and θ_L, Equation (3) can be reorganized to account for the angle θ_L as demonstrated in Equation (4).

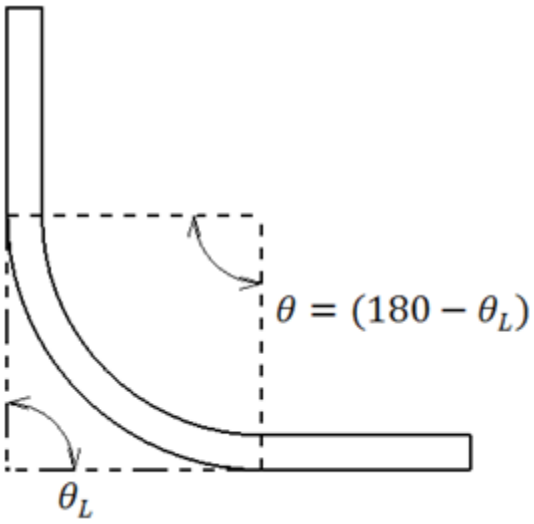

Figure 21: Cross-section of an L shaped part

$$\Delta\theta_L=(180-\theta_L)\left[\left(\frac{(\alpha_r-\alpha_\theta)\Delta T}{1+\alpha_r\Delta T}\right)+\left(\frac{\phi_r-\phi_\theta}{1+\phi_r}\right)\right] \quad (4)$$

Determining mechanical and thermal properties of a laminate experimentally is not always feasible since the parameters related to each manufacturing process such as time, applied temperature and pressure or manufacturing method might differ considerably. Thus, models have been generated to estimate some mechanical and thermal properties of composites in different levels such as from micromechanical level like the fiber-matrix interphase to macromechanical level like laminates. In the remaining parts of this chapter, a model which predicts three dimensional stiffness matrix for a symmetric laminate made of UD plies is introduced first [47]. This is followed by obtaining three dimensional effective CTE values of a symmetric and balanced laminate by using the method proposed by Dong [44]. Then, a cure shrinkage model is generated to predict laminate's shrinkage strain by using

experimental data. The results are then implemented in Equation (4) to have a quick estimation of spring-in angle for a symmetric and balanced laminate.

2.2 3-D EFFECTIVE THERMOMECHANICAL PROPERTIES OF A SYMMETRIC AND BALANCED LAMINATE

Classical lamination theory (CLT) assumes plane stress solution and ignores through thickness stresses. It is limited for the analysis of thin plates [33]. Therefore, CLT becomes useless for the cases such as spring-in of corner shaped geometries where through the thickness effects are important. For that reason, to predict 3-D effective mechanical properties, averaging methods are used in studies [47, 48, 49]. In this section, the method represented by Chen and Tsai [47] is explained in detail and employed for the solution.

2.2.1 Effective Stiffness Matrix

Figure 22 presents a small portion of an L-shaped laminate made of differently oriented UD plies. There are two different coordinate systems: a local 123-coordinate system defined on each ply and a global xyz-coordinate system. In each ply, the 1-axis coincides with the fiber direction and the 2-axis, which is the other in-plane axis, is perpendicular to the fiber direction. The 3-axis, on the other hand, is in the through-thickness direction and coincides with global z-axis. For each ply, fiber reinforcements (or local 1-axis) are oriented at an angle of θ with the global x-axis.

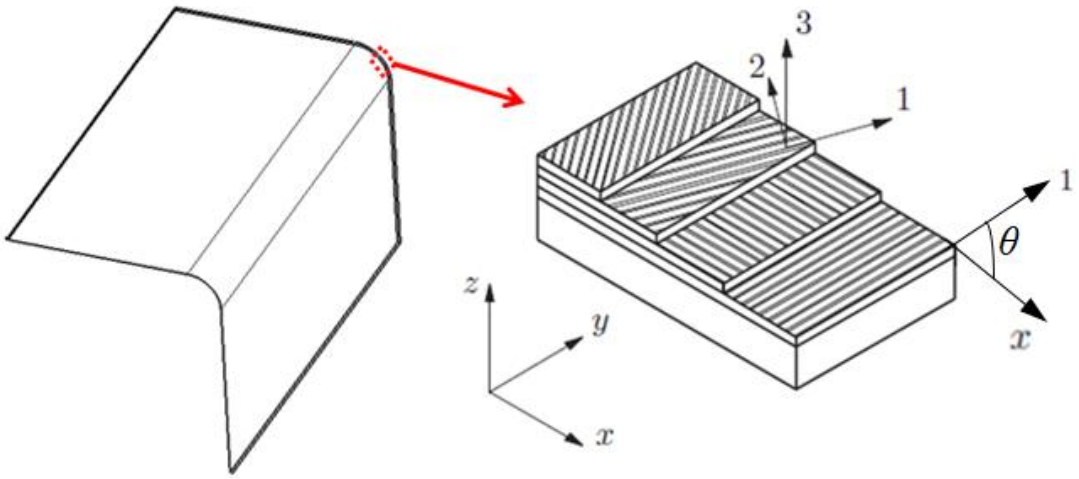

Figure 22: L shaped laminate made of differently oriented UD prepregs [33]

The linear-elastic tensorial constitutive equation defining stress-strain relationship can be written with respect to the local coordinate system as shown in Equation (5).

$$\{\sigma\}=[C]\{\varepsilon\} \tag{5}$$

where $[C]$ is the stiffness matrix of an orthotropic (or transversely isotropic) ply and it is the inverse of the compliance matrix $[S]$:

$$[C]=[S]^{-1} \tag{6}$$

If the fiber arrangement is assumed to be the identical in directions of local *2*- and *3*-axes, then the material properties may also be assumed to be same in these directions. These composite materials, such as the ones composed of perfectly aligned UD, plies are called as transversely isotropic. By using the compliance matrix $[S]$, strain can be related to stress:

$$\{\varepsilon\}=[S]\{\sigma\} \tag{7}$$

Equation (7) can be written explicitly as below:

$$\begin{Bmatrix}\varepsilon_1\\ \varepsilon_2\\ \varepsilon_3\\ \gamma_{23}\\ \gamma_{13}\\ \gamma_{12}\end{Bmatrix}=\begin{bmatrix}\frac{1}{E_1} & \frac{-\nu_{12}}{E_1} & \frac{-\nu_{13}}{E_1} & 0 & 0 & 0\\ \frac{-\nu_{12}}{E_1} & \frac{1}{E_2} & \frac{-\nu_{23}}{E_2} & 0 & 0 & 0\\ \frac{-\nu_{13}}{E_1} & \frac{-\nu_{23}}{E_2} & \frac{1}{E_3} & 0 & 0 & 0\\ 0 & 0 & 0 & \frac{1}{G_{23}} & 0 & 0\\ 0 & 0 & 0 & 0 & \frac{1}{G_{13}} & 0\\ 0 & 0 & 0 & 0 & 0 & \frac{1}{G_{12}}\end{bmatrix}\begin{Bmatrix}\sigma_1\\ \sigma_2\\ \sigma_3\\ \sigma_{23}\\ \sigma_{13}\\ \sigma_{12}\end{Bmatrix} \tag{8}$$

where γ_{ij} is the engineering shear strain which is equal to two times the tensorial shear strain, as shown by Equation (9):

$$\gamma_{ij}=2\varepsilon_{ij,}\quad i,j=1,2,3,\quad i\neq j \tag{9}$$

It should be noted that in Equation (8) Glassy state mechanical properties are used.. It is now time to define each ply's constitutive equation in global *xyz*-coordinate system. Both the stresses and strains should be transformed from the local *123*-coordinate system to global *xyz*-coordinate system:

$$\{\sigma\}_{xyz}=[T]^{T}\{\sigma\}_{123},\quad \{\varepsilon\}_{xyz}=[T]^{-T}\{\varepsilon\}_{123} \tag{10}$$

where the transformation matrix [*T*] converts the local *1*- and *2*-axes into global *x*- and *y*-axes about the global *z*-axis or local *3*-axis which are same as can be seen from Figure 3. [*T*] is expressed as:

$$[T]=\begin{bmatrix} \cos^2(\theta) & \sin^2(\theta) & 0 & 0 & 0 & -2\sin(\theta)\cos(\theta) \\ \sin^2(\theta) & \cos^2(\theta) & 0 & 0 & 0 & 2\sin(\theta)\cos(\theta) \\ 0 & 0 & 1 & 0 & 0 & 0 \\ 0 & 0 & 0 & \cos(\theta) & \sin(\theta) & 0 \\ 0 & 0 & 0 & -\sin(\theta) & \cos(\theta) & 0 \\ \sin(\theta)\cos(\theta) & -\sin(\theta)\cos(\theta) & 0 & 0 & 0 & \cos^2(\theta)-\sin^2(\theta) \end{bmatrix} \tag{11}$$

where, as mentioned earlier, θ is the angle between local *1*- and global *x*-axes shown in Figure 22. The transformation matrix [*T*] is not required to be reduced by defining a Reuter's matrix for which a detailed explanation is given in [50] since it already considers engineering strain γ_{ij} *(i,j=1,2,3, i≠j)* being twice the tensorial shear strain ε_{ij} *(i,j=1,2,3, i≠j)*. Therefore, the transformed constitutive equation can be written as shown in Equation (12):

$$\{\sigma\}_{xyz}=[T][C][T]^T\{\varepsilon\}_{xyz}=[\bar{C}]\{\varepsilon\}_{xyz} \tag{12}$$

In Equation (12), $[\bar{C}]$ denotes the transformed stiffness matrix of a ply. The equation (12) for each transformed orthotropic ply is stated in the explicit form as:

$$\begin{Bmatrix} \sigma_x \\ \sigma_y \\ \sigma_z \\ \sigma_{yz} \\ \sigma_{xz} \\ \sigma_{xy} \end{Bmatrix}^{(k)} = \begin{bmatrix} \overline{C}_{11} & \overline{C}_{12} & \overline{C}_{13} & 0 & 0 & \overline{C}_{16} \\ \overline{C}_{12} & \overline{C}_{22} & \overline{C}_{23} & 0 & 0 & \overline{C}_{26} \\ \overline{C}_{13} & \overline{C}_{23} & \overline{C}_{33} & 0 & 0 & \overline{C}_{36} \\ 0 & 0 & 0 & \overline{C}_{44} & \overline{C}_{45} & 0 \\ 0 & 0 & 0 & \overline{C}_{45} & \overline{C}_{55} & 0 \\ \overline{C}_{16} & \overline{C}_{26} & \overline{C}_{36} & 0 & 0 & \overline{C}_{66} \end{bmatrix}^{(k)} \begin{Bmatrix} \varepsilon_x \\ \varepsilon_y \\ \varepsilon_z \\ \gamma_{yz} \\ \gamma_{xz} \\ \gamma_{xy} \end{Bmatrix}^{(k)} \tag{13}$$

where superscript *k* denotes the label of a ply in the laminate which is composed of *n* plies.

Up to this point, the transformed stress-strain relationship of a ply including the stiffness matrix is obtained as in Equation (13). The next step is to find the three dimensional (3-D) effective laminate stiffness matrix ($[\overline{C}^{l}]$) using transformed stiffness matrix ($[\overline{C}]$) of each ply (or lamina). For that purpose, a method proposed by Chen and Tsai [47] is implemented to find the 3-D effective stiffness matrix of a symmetric laminate. In this method, a symmetric inhomogeneous laminate having variable material properties at each ply is considered to be a homogeneous and anisotropic material with three dimensional effective moduli.

The effective constitutive equation of a symmetric and balanced laminate is given as:

$$\begin{Bmatrix} \sigma_x^l \\ \sigma_y^l \\ \sigma_z^l \\ \sigma_{yz}^l \\ \sigma_{xz}^l \\ \sigma_{xy}^l \end{Bmatrix} = \begin{bmatrix} \overline{C}_{11}^l & \overline{C}_{12}^l & \overline{C}_{13}^l & 0 & 0 & 0 \\ \overline{C}_{12}^l & \overline{C}_{22}^l & \overline{C}_{23}^l & 0 & 0 & 0 \\ \overline{C}_{13}^l & \overline{C}_{23}^l & \overline{C}_{33}^l & 0 & 0 & 0 \\ 0 & 0 & 0 & \overline{C}_{44}^l & 0 & 0 \\ 0 & 0 & 0 & 0 & \overline{C}_{55}^l & 0 \\ 0 & 0 & 0 & 0 & 0 & \overline{C}_{66}^l \end{bmatrix} \begin{Bmatrix} \varepsilon_x^l \\ \varepsilon_y^l \\ \varepsilon_z^l \\ \gamma_{yz}^l \\ \gamma_{xz}^l \\ \gamma_{xy}^l \end{Bmatrix} \tag{14}$$

Chen and Tsai [47] define the effective stresses and strains of a laminate in terms of stresses and strains belonging to each lamina:

$$\sigma_i^l = \frac{1}{h}\int_h \sigma_i^k dz \qquad i=x,y,z,yz,xz,xy \quad k=1,\ldots,n \tag{15}$$

$$\varepsilon_i^l = \frac{1}{h}\int_h \varepsilon_i^k dz \qquad i=x,y,z,yz,xz,xy \quad k=1,\ldots,n \tag{16}$$

where h is the total thickness of the laminate and, as described before, superscript k refers to the k^{th} lamina. It is also assumed that the distribution of in-plane strains and interlaminar normal stresses are constant through the thickness of the laminate:

$$\varepsilon_i^l = \varepsilon_i^k \qquad i=x,y,xy \quad k=1,\ldots,n \tag{17}$$

$$\sigma_z^l = \sigma_z^k \qquad k=1,\ldots,n \tag{18}$$

In the study of Chen and Tsai [47], the 3-D effective elastic coefficients represented in Equation (14) are obtained by applying appropriate deformation modes and employing assumptions indicated in Equations (17) and (18) along with the stress-strain relationship given in Equation (13) for each lamina. For the derivation of 3-D effective stiffness properties of a symmetric laminate using each ply's stiffness matrix elements, one is referred to the study of Chen and Tsai [47]. In Equations (19), (20), (21), and (22) some of the 3-D stiffness matrix elements of a symmetric and balanced laminate as $\overline{C}_{11}^l$, $\overline{C}_{22}^l$, $\overline{C}_{12}^l$, $\overline{C}_{13}^l$, $\overline{C}_{23}^l$, $\overline{C}_{33}^l$, $\overline{C}_{66}^l$ are given:

$$\overline{C}_{33}^{l}=\left(\sum_{k=1}^{n}\frac{t^{k}}{C_{33}^{k}}\right)^{-1} \tag{19}$$

$$\overline{C}_{i3}^{l}=\overline{C}_{33}^{l}\sum_{k=1}^{n}t^{k}\frac{C_{i3}^{k}}{C_{33}^{k}} \qquad i=1,2 \tag{20}$$

$$\overline{C}_{ij}^{l}=\sum_{k=1}^{n}t^{k}C_{ij}^{k}+\frac{\overline{C}_{i3}^{l}\overline{C}_{j3}^{l}}{\overline{C}_{33}^{l}}-\sum_{k=1}^{n}t^{k}\frac{C_{i3}^{k}C_{j3}^{k}}{C_{33}^{k}} \qquad i=1,2 \tag{21}$$

$$\overline{C}_{66}^{l}=\sum_{k=1}^{n}t^{k}C_{66}^{k}-\sum_{k=1}^{n}t^{k}\frac{\left(C_{63}^{k}\right)^{2}}{C_{33}^{k}} \qquad i=1,2 \tag{22}$$

where t^k is the volume fraction of the k^{th} lamina in the whole laminate. Moreover, Chen and Tsai [47] showed that the through-thickness shear compliance coefficients of a symmetric and balanced laminate ($\overline{S}_{44}^{l}$, $\overline{S}_{55}^{l}$, $\overline{S}_{45}^{l}$) is obtained as follows:

$$\overline{S}_{ij}^{l}=\sum_{k=1}^{n}t^{k}S_{ij}^{k} \quad i,j=4,5 \tag{23}$$

Interlaminar shear stiffness coefficients $\overline{C}_{44}^{l}$, $\overline{C}_{55}^{l}$, $\overline{C}_{45}^{l}$ can be expressed as:

$$\begin{bmatrix}\overline{C}_{44}^{l} & \overline{C}_{45}^{l}\\ \overline{C}_{45}^{l} & \overline{C}_{55}^{l}\end{bmatrix}=\begin{bmatrix}\overline{S}_{44}^{l} & \overline{S}_{45}^{l}\\ \overline{S}_{45}^{l} & \overline{S}_{55}^{l}\end{bmatrix}^{-1} \tag{24}$$

However, in a symmetric and balanced laminate, the individual plies occur in $\pm\theta$ pairs. Due to this reason, by combining Equations (8), (11), (13), (23), it can be concluded that $\bar{S}_{45}^{l}$ becomes zero for a symmetric and balanced laminate. This means that:

$$\begin{bmatrix} \bar{C}_{44}^{l} & 0 \\ 0 & \bar{C}_{55}^{l} \end{bmatrix} = \begin{bmatrix} \bar{S}_{44}^{l} & 0 \\ 0 & \bar{S}_{55}^{l} \end{bmatrix}^{-1} \tag{25}$$

where $\bar{S}_{44}^{l}$, $\bar{S}_{55}^{l}$ can be calculated using Equation (23).

2.2.2 Effective Coefficient of Thermal Expansions (CTEs)

The strains in a ply include thermal and mechanical components as shown in Equation (26):

$$\{\varepsilon\}_{xyz}^{(k)} = \{\varepsilon^{M}\}_{xyz}^{(k)} + \{\alpha\}_{xyz}^{(k)} \Delta T \tag{26}$$

where $\{\varepsilon^{M}\}$ stands for the mechanical component of the strain, $\{\alpha\}$ consists of the CTEs in vectorial form, ΔT denotes the difference between the cure temperature and room temperature. For an orthotropic ply (or lamina), the CTEs in local *123*-coordinate system can be transferred to the global *xyz*-coordinate system with the help of transformation matrix *[T]* which is represented in Equation (11):

$$\begin{Bmatrix} \alpha_x \\ \alpha_y \\ \alpha_z \\ 0 \\ 0 \\ \alpha_{xy} \end{Bmatrix} = [T]^{-T} \begin{Bmatrix} \alpha_1 \\ \alpha_2 \\ \alpha_3 \\ 0 \\ 0 \\ 0 \end{Bmatrix} \tag{27}$$

When there is no mechanical load applied and only thermal stresses are considered, the constitutive relationship for a ply oriented at an angle of θ given in Equation (13) becomes:

$$\begin{bmatrix} \overline{C}_{11} & \overline{C}_{12} & \overline{C}_{13} & 0 & 0 & \overline{C}_{16} \\ \overline{Q}_{12} & \overline{Q}_{22} & \overline{Q}_{23} & 0 & 0 & \overline{C}_{26} \\ \overline{C}_{13} & \overline{C}_{23} & \overline{C}_{33} & 0 & 0 & \overline{C}_{36} \\ 0 & 0 & 0 & \overline{C}_{44} & \overline{C}_{45} & 0 \\ 0 & 0 & 0 & \overline{C}_{45} & \overline{C}_{55} & 0 \\ \overline{C}_{16} & \overline{C}_{26} & \overline{C}_{36} & 0 & 0 & \overline{C}_{66} \end{bmatrix}^{(k)} \begin{Bmatrix} \varepsilon_x - \alpha_x \Delta T \\ \varepsilon_y - \alpha_y \Delta T \\ \varepsilon_z - \alpha_z \Delta T \\ \gamma_{yz} \\ \gamma_{xz} \\ \gamma_{xy} - 2\alpha_{xy} \Delta T \end{Bmatrix}^{(k)} = \begin{Bmatrix} 0 \\ 0 \\ 0 \\ 0 \\ 0 \\ 0 \end{Bmatrix}^{(k)} \tag{28}$$

Equation (28) can be rearranged as:

$$\begin{bmatrix} \overline{C}_{11} & \overline{C}_{12} & \overline{C}_{13} & 0 & 0 & \overline{C}_{16} \\ \overline{C}_{12} & \overline{C}_{22} & \overline{C}_{23} & 0 & 0 & \overline{C}_{26} \\ \overline{C}_{13} & \overline{C}_{23} & \overline{C}_{33} & 0 & 0 & \overline{C}_{36} \\ 0 & 0 & 0 & \overline{C}_{44} & \overline{C}_{45} & 0 \\ 0 & 0 & 0 & \overline{C}_{45} & \overline{C}_{55} & 0 \\ \overline{C}_{16} & \overline{C}_{26} & \overline{C}_{36} & 0 & 0 & \overline{C}_{66} \end{bmatrix}^{(k)} \begin{Bmatrix} \varepsilon_x \\ \varepsilon_y \\ \varepsilon_z \\ \gamma_{yz} \\ \gamma_{xz} \\ \gamma_{xy} \end{Bmatrix}^{(k)} = \begin{bmatrix} \overline{C}_{11}\alpha_x + \overline{C}_{12}\alpha_y + \overline{C}_{13}\alpha_z + 2\overline{C}_{16}\alpha_{xy} \\ \overline{C}_{12}\alpha_x + \overline{C}_{22}\alpha_y + \overline{C}_{23}\alpha_z + 2\overline{C}_{26}\alpha_{xy} \\ \overline{C}_{13}\alpha_x + \overline{C}_{23}\alpha_y + \overline{C}_{33}\alpha_z + 2\overline{C}_{36}\alpha_{xy} \\ 0 \\ 0 \\ \overline{C}_{16}\alpha_x + \overline{C}_{26}\alpha_y + \overline{C}_{36}\alpha_z + 2\overline{C}_{66}\alpha_{xy} \end{bmatrix} \Delta T \tag{29}$$

As given in Equation (17), Dong [44] assumes that all plies are bonded strictly to each other and they have the same strains. This means that strains of a laminated

composite part are equal to the strains of each lamina. Hence, when the thermal loads of each ply shown in Equation (29) are summed up, the stress-strain relationship of a symmetric and balanced laminate given in Equation (14) can be rewritten as:

$$\begin{bmatrix} \overline{C}_{11}^{l} & \overline{C}_{12}^{l} & \overline{C}_{13}^{l} & 0 & 0 & 0 \\ \overline{C}_{12}^{l} & \overline{C}_{22}^{l} & \overline{C}_{23}^{l} & 0 & 0 & 0 \\ \overline{C}_{13}^{l} & \overline{C}_{23}^{l} & \overline{C}_{33}^{l} & 0 & 0 & 0 \\ 0 & 0 & 0 & \overline{C}_{44}^{l} & 0 & 0 \\ 0 & 0 & 0 & 0 & \overline{C}_{55}^{l} & 0 \\ 0 & 0 & 0 & 0 & 0 & \overline{C}_{66}^{l} \end{bmatrix} \begin{Bmatrix} \varepsilon_x \\ \varepsilon_y \\ \varepsilon_z \\ \gamma_{yz} \\ \gamma_{xz} \\ \gamma_{xy} \end{Bmatrix} = \begin{Bmatrix} K_x \\ K_y \\ K_z \\ 0 \\ 0 \\ K_{xy} \end{Bmatrix} \tag{30}$$

where K_x, K_y, K_z, and K_{xy} are the summation of thermal loads belonging to each ply:

$$\begin{aligned} K_x &= \sum_{k=1}^{n} (\overline{C}_{11})_k (\alpha_x)_k + (\overline{C}_{12})_k (\alpha_y)_k + (\overline{C}_{13})_k (\alpha_z)_k + 2(\overline{C}_{16})_k (\alpha_{xy})_k \\ K_y &= \sum_{k=1}^{n} (\overline{C}_{12})_k (\alpha_x)_k + (\overline{C}_{22})_k (\alpha_y)_k + (\overline{C}_{23})_k (\alpha_z)_k + 2(\overline{C}_{26})_k (\alpha_{xy})_k \\ K_z &= \sum_{k=1}^{n} (\overline{C}_{13})_k (\alpha_x)_k + (\overline{C}_{23})_k (\alpha_y)_k + (\overline{C}_{33})_k (\alpha_z)_k + 2(\overline{C}_{36})_k (\alpha_{xy})_k \\ K_{xy} &= \sum_{k=1}^{n} (\overline{C}_{16})_k (\alpha_x)_k + (\overline{C}_{26})_k (\alpha_y)_k + (\overline{C}_{36})_k (\alpha_z)_k + 2(\overline{C}_{66})_k (\alpha_{xy})_k \end{aligned} \tag{31}$$

Due to the symmetric and balanced nature of the laminate, K_{xy} given in Equation (31) becomes zero. (For the derivation please refer to study of Dong [44]. Therefore, Equation (30) can be simplified as:

$$\begin{bmatrix} \overline{C}_{11}^{l} & \overline{C}_{12}^{l} & \overline{C}_{13}^{l} \\ \overline{C}_{12}^{l} & \overline{C}_{22}^{l} & \overline{C}_{23}^{l} \\ \overline{C}_{13}^{l} & \overline{C}_{23}^{l} & \overline{C}_{33}^{l} \end{bmatrix} \begin{Bmatrix} \varepsilon_x \\ \varepsilon_y \\ \varepsilon_z \end{Bmatrix} = \begin{Bmatrix} K_x \\ K_y \\ K_z \end{Bmatrix} \Delta T \tag{32}$$

By applying Cramer's rule to equation (32), the 3-D effective CTEs of symmetric and balanced laminate such as α_x^l, α_y^l, α_z^l are obtained as follows:

$$\alpha_x^l = \frac{\varepsilon_x}{\Delta T} = \frac{\begin{vmatrix} K_x & K_y & K_z \\ \overline{C}_{12}^{l} & \overline{C}_{22}^{l} & \overline{C}_{23}^{l} \\ \overline{C}_{13}^{l} & \overline{C}_{23}^{l} & \overline{C}_{33}^{l} \end{vmatrix}}{\begin{vmatrix} \overline{C}_{11}^{l} & \overline{C}_{12}^{l} & \overline{C}_{13}^{l} \\ \overline{C}_{12}^{l} & \overline{C}_{22}^{l} & \overline{C}_{23}^{l} \\ \overline{C}_{13}^{l} & \overline{C}_{23}^{l} & \overline{C}_{33}^{l} \end{vmatrix}}$$

$$\alpha_y^l = \frac{\varepsilon_y}{\Delta T} = \frac{\begin{vmatrix} \overline{C}_{11}^{l} & \overline{C}_{12}^{l} & \overline{C}_{13}^{l} \\ K_x & K_y & K_z \\ \overline{C}_{13}^{l} & \overline{C}_{23}^{l} & \overline{C}_{33}^{l} \end{vmatrix}}{\begin{vmatrix} \overline{C}_{11}^{l} & \overline{C}_{12}^{l} & \overline{C}_{13}^{l} \\ \overline{C}_{12}^{l} & \overline{C}_{22}^{l} & \overline{C}_{23}^{l} \\ \overline{C}_{13}^{l} & \overline{C}_{23}^{l} & \overline{C}_{33}^{l} \end{vmatrix}} \tag{33}$$

$$\alpha_z^l = \frac{\varepsilon_z}{\Delta T} = \frac{\begin{vmatrix} \overline{C}_{11}^{l} & \overline{C}_{12}^{l} & \overline{C}_{13}^{l} \\ \overline{C}_{12}^{l} & \overline{C}_{22}^{l} & \overline{C}_{23}^{l} \\ K_x & K_y & K_z \end{vmatrix}}{\begin{vmatrix} \overline{C}_{11}^{l} & \overline{C}_{12}^{l} & \overline{C}_{13}^{l} \\ \overline{C}_{12}^{l} & \overline{C}_{22}^{l} & \overline{C}_{23}^{l} \\ \overline{C}_{13}^{l} & \overline{C}_{23}^{l} & \overline{C}_{33}^{l} \end{vmatrix}}$$

For a symmetric and balanced laminate, α_x^l and α_y^l are expected to be the same. While calculating the spring-in angle due to anisotropy in CTEs, α^θ and α^r shown in

the first term of Equation (4) are replaced by α_x^l and α_z^l, respectively, in accordance with the compatibility of the coordinate system shown in Figure 23.

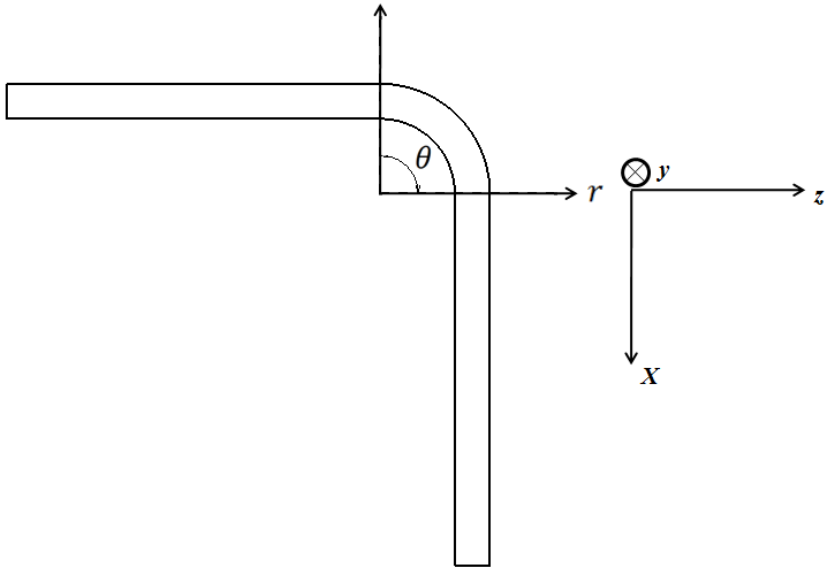

Figure 23: r-θ and x-y-z coordinate systems displayed on the cross section of an L-shaped part

Therefore, according to coordinate systems defined in Figure 23, the first term of equation (4) becomes:

$$\Delta\theta_L=(180-\theta_L)\left[\left(\frac{(\alpha_z^l-\alpha_x^l)\Delta T}{1+\alpha_z\Delta T}\right)\right] \tag{34}$$

2.3 EFFECTIVE CURE SHRINKAGE OF A SYMMETRIC AND BALANCED LAMINATE

For a UD ply, it is assumed that fiber reinforcement is uniformly distributed in the resin matrix. Therefore, experimentally determined cure shrinkage strains through

the resin dominant transverse directions, namely *2*- and *3*-directions in the local coordinate system shown in Figure 22, can be treated as the same. (i.e. $\varepsilon_{22}^{cure}=\varepsilon_{33}^{cure}$) However, in the longitudinal direction or in the local *1*-direction, due to fiber reinforcement, lamina is subjected to very little cure shrinkage which can be regarded as zero, (i.e., $\varepsilon_{11}^{cure}=0$) [51].

It can be considered that each ply in a laminate is subjected to the same amount of cure shrinkage in through the thickness direction, therefore; they contract equally in this direction. Consequently, effective through-thickness cure shrinkage strain ($\emptyset_r$) of a laminate can be written as:

$$\emptyset_r=\sum_{k=1}^{n} t^k(\varepsilon_{33}^{cure})^k \tag{35}$$

where t^k is the volume fraction of the k^{th} ply (or lamina). On the other hand, the in–plane cure shrinkage strain of a laminate ($\emptyset_\theta$) due to transverse cure shrinkage strains (ε_{33}^{cure}) of each lamina can be written as follows:

$$\emptyset_\theta=\sum_{k=1}^{n} t^k(\varepsilon_{33}^{cure}\cos\theta)^k \tag{36}$$

where θ is the orientation angle of each ply as mentioned earlier. Cure shrinkage strains, ($\emptyset_r$) and ($\emptyset_\theta$) are shown on an L-shaped composite laminate in Figure 24.

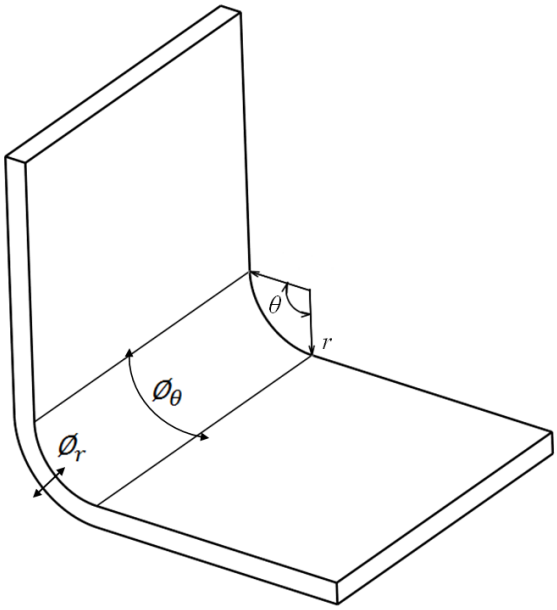

Figure 24: Cure shrinkage strains ($\emptyset_r$) and ($\emptyset_\theta$) with the corresponding r-θ coordinate system displayed on an L-shaped part

2.4 MATERIAL PROPERTIES NEEDED FOR THE CALCULATION OF SPRING-IN ANGLE

During this thesis, U-shaped composite laminate which is made of made of AS4/8552 composite system with a lay-up configuration of $[45°/-45°/90°/0°]_s$ is studied to determine spring-in angle. (Figure 25)

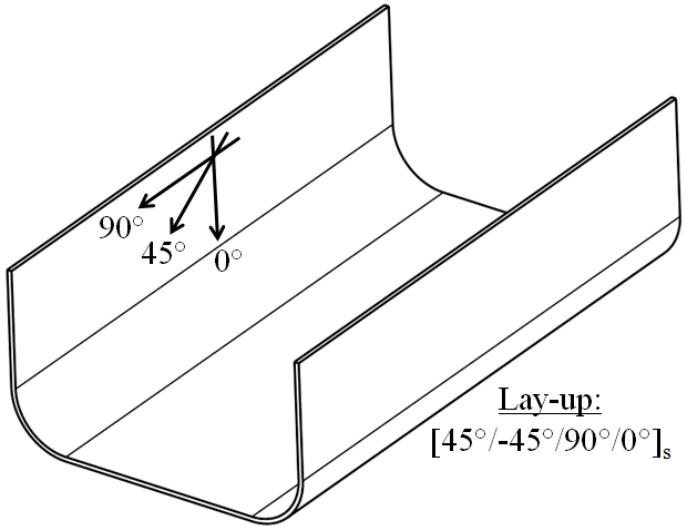

Figure 25: U-shaped composite laminate studied in the thesis

In order to calculate the spring-in angle of these composite parts, Young's moduli (E_{11}, E_{22}, E_{33}), shear moduli (G_{12}, G_{13}, G_{23}), Poisson's ratios (ϑ_{12}, ϑ_{13}, ϑ_{23}), CTEs (α_{11},α_{22},α_{33}) and cure shrinkage strain in transverse direction (ε_{33}^{cure}) shown in Table 1 are used in the analytical solution. For Hexcel's AS4/8552 composite system, HexTow®AS4 represents the type of carbon fiber used in the prepreg. AS4 carbon fiber is a continuous, high strength, high strain, polyacrylonitrile based fiber, and it is surface treated to be able to meet improved interlaminar shear properties, handling characteristics, and structural properties according to the product data [52]. On the other hand, Hexply® 8552 epoxy matrix is an amine cured, toughened epoxy resin system, and it is confirmed for structural applications which call for high strength, stiffness, and damage tolerance. When fully cured, it can be used for temperatures up to 121℃ [53].

Table 1 – Some of the Necessary Material Properties of Hexcel's AS4/8552 Composite System for Analytical Spring-in Calculation [51]

Property	**Unit**	**Value**
E_{11}	MPa	135000
$E_{22}=E_{33}$	MPa	9500
$G_{12}=G_{13}$	MPa	4900
G_{23}	MPa	4900
$\vartheta_{12}=\vartheta_{13}$	-	0.3
ϑ_{23}	-	0.45
α_{11}	με/°C	0[a]
$\alpha_{22}=\alpha_{33}$	με/°C	32.6
$\varepsilon_{22}^{cure}=\varepsilon_{33}^{cure}$	%	0.48

CHAPTER 3

EXPERIMENTAL INVESTIGATION OF SPRING-IN

A number of U-shaped composite laminates consisting of UD plies has been manufactured via autoclave forming process in order to investigate the spring-in problem experimentally. Surface temperature of the tool-part assembly has been monitored during the complete cure cycle by using thermocouples and the spring-in measurement for the manufactured parts has been conducted using an optical scanning device after completion of the manufacturing process. The details related to autoclave forming process including the cure cycle, thermocouple installations for temperature measurements and the spring-in measurement are presented in this chapter.

3.1. LAY-UP CONFIGURATION, MATERIAL TYPE AND DIMENSIONS

Designing a laminate with symmetric and balanced configuration prevents warpage formation by cancelling out the bending effects of thermal and cure strains. On the other hand, for laminates having corner shaped geometries such as U-shaped composite parts manufactured within the scope of this thesis, spring-in problem will still be present even though the laminates have symmetric and balanced lay-up configuration mainly because of anisotropy in CTEs and other factors like tool-part interaction and cure shrinkage. Therefore, to minimize warpage problem and not to have "warpage and spring-in" couplings in the manufactured composite parts, a symmetric and balanced lay-up configuration is considered. Quasi-isotropic laminate configuration that is studied in the thesis is taken as $[45°/-45°/90°/0°]_s$.

Hexcel's UD carbon-epoxy prepreg (AS4/8552) is used to manufacture U-shaped composite parts with autoclave manufacturing technique. Details related to AS4/8552 composite system have already been explained in the previous chapter.

Aluminum 6061 series with T6 heat treatment is used as the tool material. Aluminum is not recommended as a tool material when shape distortion is an important issue because the CTE of aluminum is generally too high when compared to composite part's CTE. However, in the experiment, to see the shape distortion problem clearly, aluminum alloy is chosen for tooling.

Dimensions of composite parts and tools are shown in Figure 26 and Figure 27, respectively. Each ply has a thickness of 0.13mm when fully cured [53].

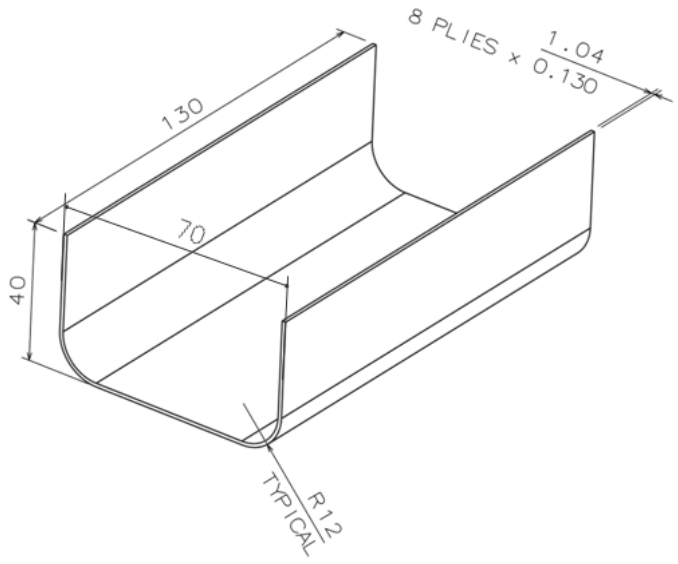

Figure 26: Dimensions of Composite Parts (in mm)

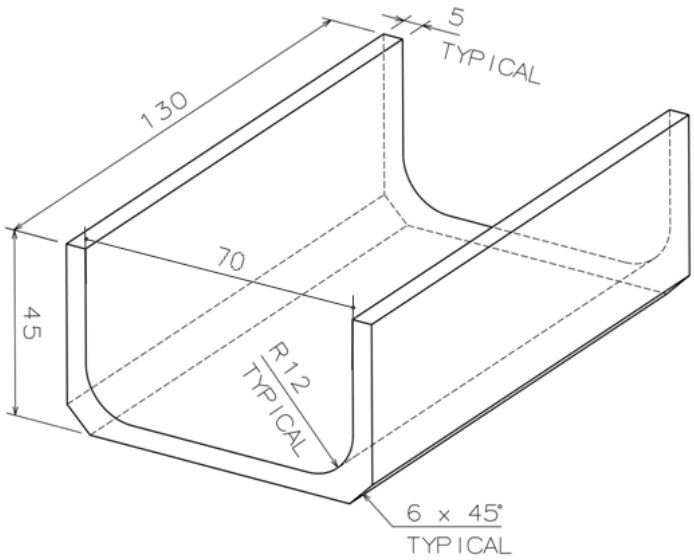

Figure 27: Dimensions of Tools (in mm)

3.2. AUTOCLAVE FORMING PROCESS

Four identical composite parts in terms of material type, lay-up configuration, geometry, tooling, and curing process are manufactured in a single autoclave cycle. Temperatures of one of the specific composite parts and its tool are monitored by using thermocouples during the cure cycle. However, attaching thermocouple might affect spring-in behavior of that composite part. Therefore, for spring-in of the composite part with thermocouples installed is not measured.

3.2.1. Preparing the Tool Surface and Prepregs

A mold release agent called Frekote 700-NC is applied on clean and dry mold (or tool) surfaces. Epoxies, polyester resins, thermoplastics, rubber compounds, and other molded polymers can be released by using this agent [54]. Then for each composite part, 8 layers of prepregs are tailored in suitable sizes for the lay-up

configuration $[45°/-45°/90°/0°]_s$. The nesting process is performed manually due to the noncomplex geometries of composite parts.

3.2.2. Intermediate Vacuum Bagging Process

Each ply or layer is draped on tool surfaces in accordance with the lay-up configuration and intermediate vaccum bagging is applied after draping two plies. In total, three intermediate vacuum bagging processes have taken place. The purpose of having intermediate vacuum processing is to apply compaction on draped plies so that plies can firmly take the shape of the mold, and any possible delamination may be prevented. AIRTECH KM1300 vacuum bag, AIRTECH AIRWEAVE N4 breather material, AIRTECH A4000R release fabric, and Aerovac LTS90B sealant tape are used for intermediate vacuum bagging process and all manufacturing assemblies are vacuumed in a single bag as shown in Figure 28. One intermediate vacuum bagging process takes approximately 10 minutes and a vacuum pressure of 0.75 bar is applied.

Figure 28: Intermediate vacuum bagging process

3.2.3. Final Vacuum Bagging Process

When draping of the last ply group is completed for each manufacturing assembly, final vacuum bagging process is carried out to be able to start curing via autoclave forming process. However, this time, separate vacuum bags are applied to each manufacturing assembly and vacuum bag sealants are carefully inspected to prevent any possible leakage before placing them in the autoclave chamber. Special care is taken while using mastic sealant for vacuum bagging manufacturing assembly with thermocouples since it is most likely expected to have leakage problem due to thermocouple cables coming out of the sealed vacuum bag. AIRTECH WL5200 release film, AIRTECH N10 breather, AIRTECH KM1300 vacuum bag, and AIRTECH GS 213 mastic sealant are used for the final vacuum process, as shown in Figure 29. Approximately, 0.8 bar is applied as the vacuum pressure.

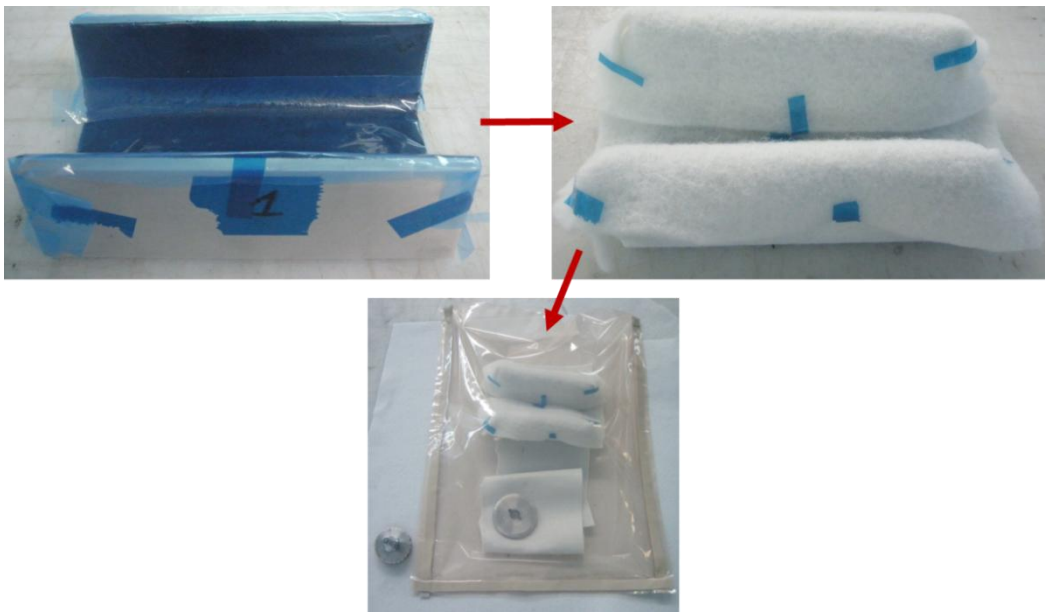

Figure 29: Final Vacuum Bagging Process

In order to provide well air circulation during curing process, vacuum bagged manufacturing assemblies are placed on a grilled plate instead of mono block plate, as shown in Figure 30. Sometimes due to high temperatures reached during the cure cycle, vacuum bag might stick to the autoclave plate. To prevent this problem, a thin breather film which can also be seen in Figure 30 is placed beneath the vacuum bagged manufacturing assemblies.

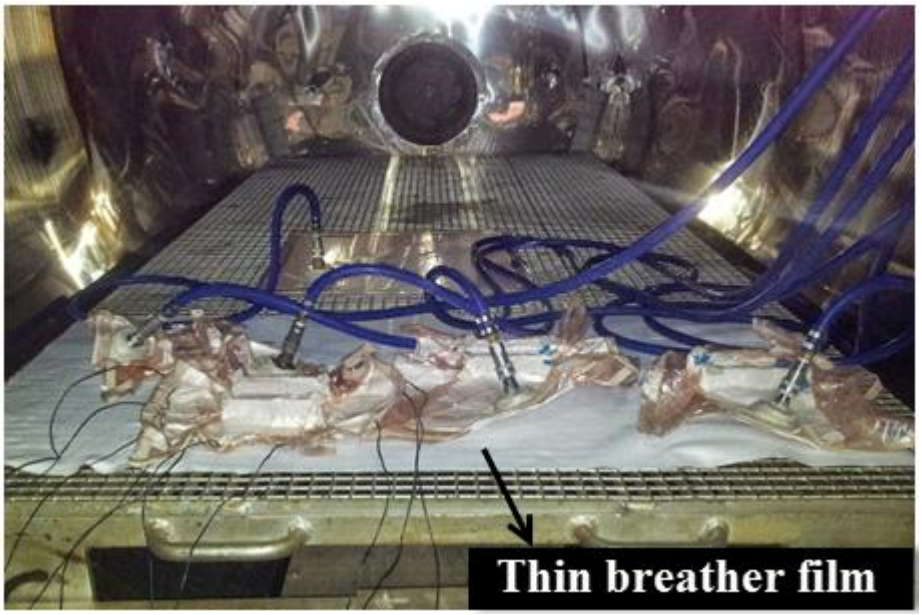

Figure 30: Vacuum bagged manufacturing assemblies inside the autoclave chamber

3.2.4. Thermocouple Installation to a Specific Manufacturing Assembly

Four composite parts are manufactured in the experiment as described before and three of them are used for spring-in angle measurements. The temperature change of one manufacturing assembly is monitored during the cure cycle and for temperature measurement purpose, 10 thermocouples are placed on that manufacturing assembly. The schematic view of thermocouple installation can be seen in Figure 31.

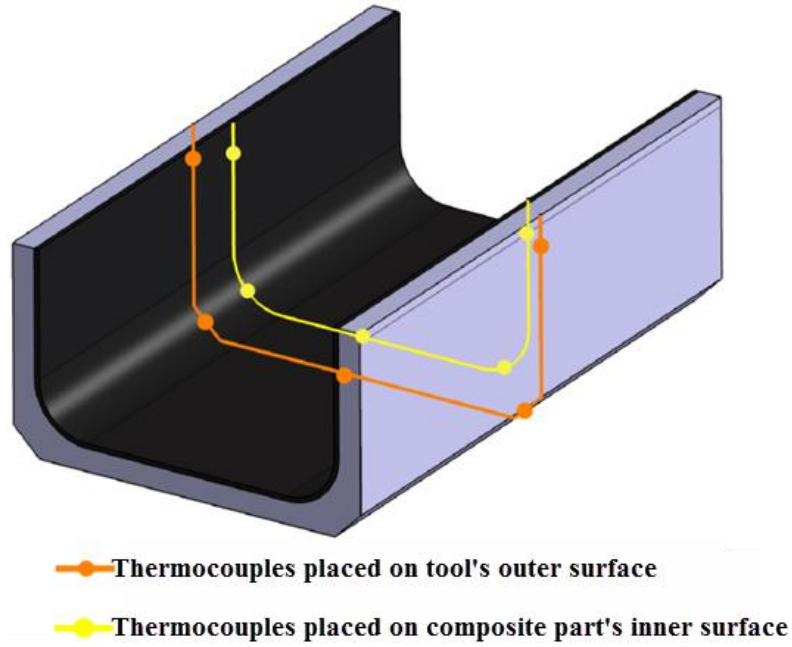

Figure 31: Schematic View of Thermocouple Installation

The objective of using thermocouples is to observe temperature fields of composite part's inner surface and tool's outer surface in the course of the curing process. In other words, the uniformity of temperature distribution on the surfaces of manufacturing assembly in the autoclave chamber is examined by gathering temperature data. If any major temperature gradient is observed on aforementioned surfaces, it is decided that the temperature field data of surfaces obtained from thermocouples has to be given as input to the ABAQUS finite element analysis model to obtain a more realistic analysis model. During the experiment temperature gradient through the thickness of the manufacturing assembly is not monitored because of the low thickness of the laminate. It should be noted that in the study of Çinar et al. [55], temperature through the thickness of the AS4/8552-Al manufacturing assembly is measured at 8 stations in a 16 ply laminate which is thicker than the composite parts manufactured in the current experiments. Moreover, tool dimensions used by Çinar et al. [55] are also larger than the dimensions of the tools used in the current experimental campaign. It is also noted

that the maximum temperature variation through the thickness was found to be within 3℃ throughout the cure cycle by Çinar et al. [55]. Based on the results obtained by Çinar et al. [55] with regard to the temperature distribution through the thickness, in the current study, uniform temperature is assumed through the thickness of the laminate.

Each thermocouple has a different code and each of them is connected to different measurement ports in thee autoclave oven. Thermocouple data is then processed in the central processing unit of the autoclave. The thermocouple codes and their locations on the manufacturing assembly are given in Figure 32. The autoclave oven used in this experiment can gather data from 10 thermocouples at maximum since it has 10 measurement ports.

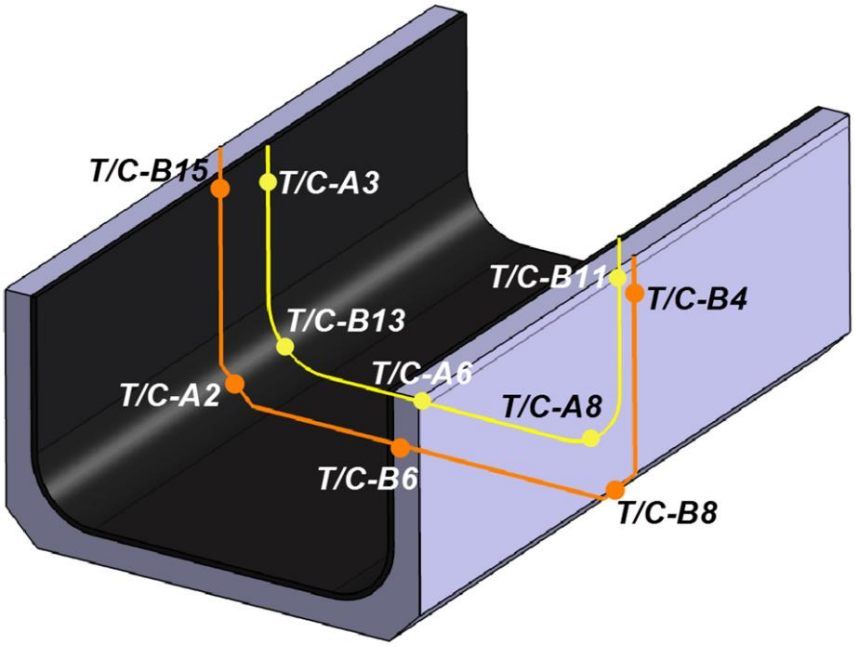

Figure 32: Thermocouple codes and their locations

3.2.5. Cure Cycle

Cure cycle graph for Hexcel's AS4/8552 UD prepreg was already shown in Figure 13 and Hexcel [53] describes manufacturer's recommended cure cycle (MRCC) steps as follows:

a) Apply full vacuum (1 bar),
b) Apply 7 bar gauge autoclave pressure,
c) Reduce the vacuum to a safety value of 0.2 bar when the autoclave pressure reaches approximately 1 bar gauge,
d) Heat at 1- 3°C/min (2-8°F/min) to 110°C ± 5°C (230°F ± 9°F),
e) Hold at 110°C ± 5°C (230°F ± 9°F) for 60 minutes ± 5 minutes,
f) Heat at 1-3°C/min (2-8°F/min) to 180°C ± 5°C (356°F ± 9°F),
g) Hold at 180°C ± 5°C (356°F ± 9°F) for 120 minutes ± 5 minutes,
h) Cool at 2 - 5°C (4-9°F) per minute,
i) Vent autoclave pressure when the component reaches 60°C (140°F) or below.

3.2.6. Temperature Field Data Obtained From Thermocoupled Manufacturing Assembly

Temperature data is collected from the thermocoupled manufacturing assembly until the end of manufacturing process every 2 minutes for a total duration of 360 minutes. Temperature vs. time graph along with the thermocouple codes, as shown in Figure 32, is generated using MS Excel and MATLAB® together. Figure 33 gives the temperature vs. time graph generated for each thermocoupleç

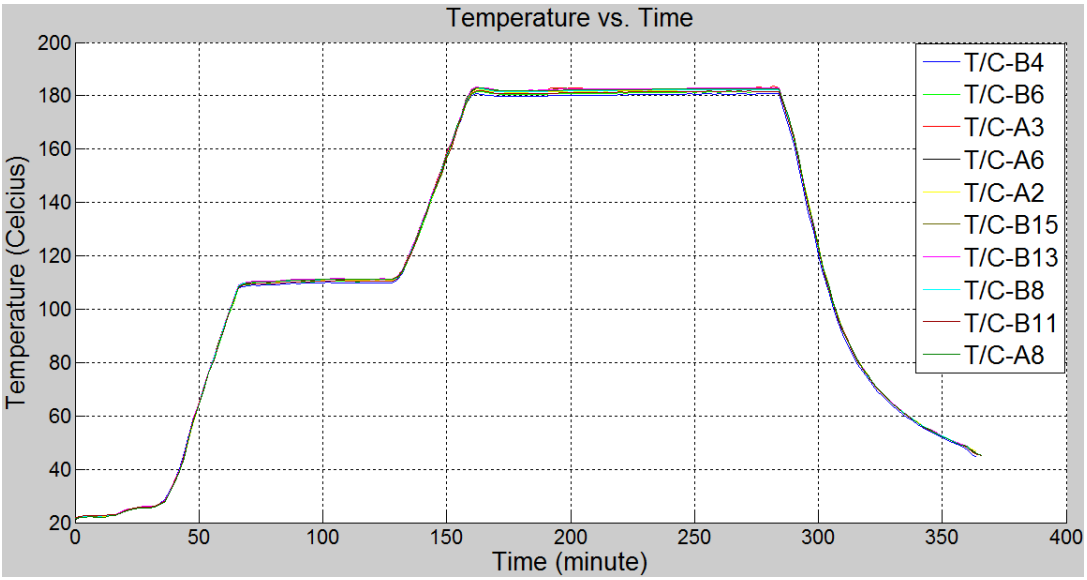

Figure 33: Temperature vs. Time Graph Showing Each Thermocouple Data

By looking at Figure 33 and the original cure cycle shown in Figure 13, it can be deduced that temperature is uniformly distributed on the surfaces of manufacturing assembly since maximum temperature deviation between thermocouple readings at a specific time is about 2°C. Therefore, variation of the temperature with the position on the part's surface and in the thickness direction can be neglected and while performing the FEM analysis, homogeneous temperature fields can be assigned to the simulation models.

3.3. MEASURING THE SPRING-IN ANGLE

3.3.1. Scanning Mating Surfaces of the Composite and the Tool via Optical Measuring Device

After the autoclave forming process is completed, as shown in Figure 34, a set square is used to observe spring-in angle of composite parts by eye inspection. However, in order to obtain more reliable measurements, mating (contacting)

surfaces of the composite parts and aluminum tools are scanned by using GOM Atos 3-D optical measuring device. This device is used for inspection of industrial components with a working volume of 350 x 280 x 280 mm.

Figure 34: Spring-in of a composite part by eye inspection

Although aluminum tools are machined in CNC with tight tolerances, there is always manufacturing induced errors in the tools, and these errors in turn affect the spring-in behavior of composite parts. Therefore, in the present study surfaces of the tool are also scanned.

The optical measuring device is calibrated first, and then reference markers are stuck on all parts' and tools' desired surfaces. Reference markers help the optical measuring device to recognize the surface in spatial coordinates. Zaimovic and Lemes [56], stated that black colored surfaces give the poorest scanning results and gray color is the most appropriate surface color for 3-D optical scanning. As the color of composite parts is black, gray spray is applied on the scanning surfaces of composite parts. The same procedure is implemented for aluminum tools having shiny surfaces. It is pointed out by Zaimovic and Lemes [56] that shiny surfaces of

aluminum tools are difficult to scan as shiny surfaces reflections. Sprayed surfaces of the composite part and the aluminum tool are displayed in Figure 35.

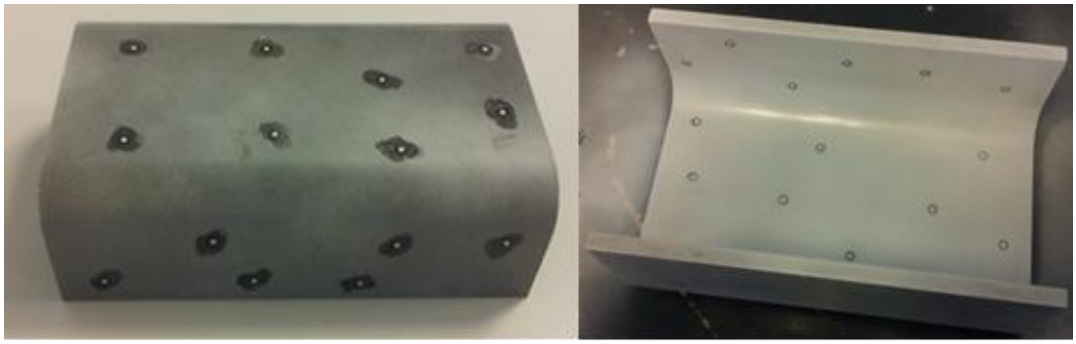

Figure 35: Reference markers and the application of gray spray on: a) Composite Part Surface b) Tool Surface

As an example, scanning process of the aluminum tool is shown in Figure 36. When the scanning process is completed for all contacting surfaces, point cloud data of surfaces is obtained and meshed by using the computer program ATOS Professional, andsurface geometries in .stl format, which can be edited, are generated.

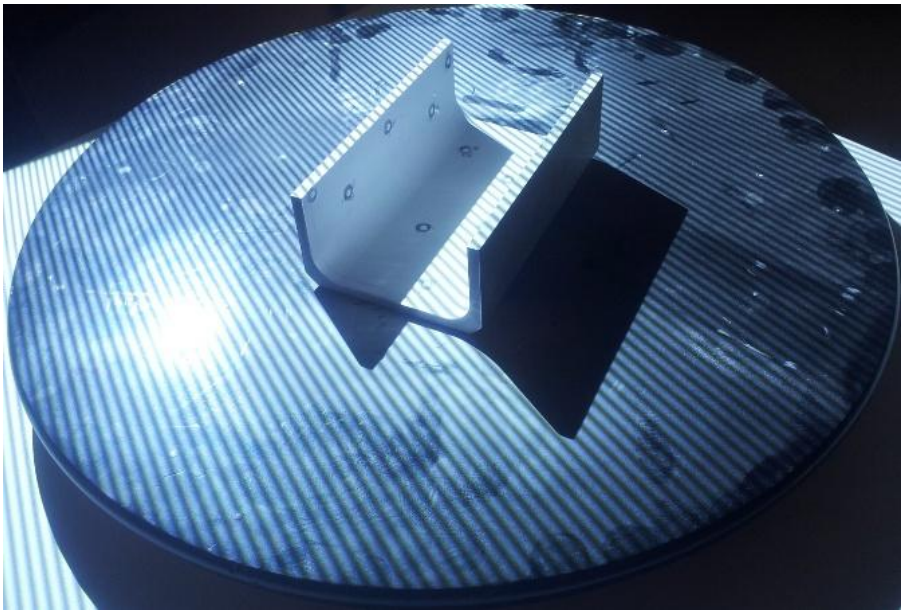

Figure 36: Scanning Process of the Tool

3.3.2. Processing Scanned Surfaces in CATIA Environment

CATIA's Reverse Engineering module is used to obtain CAD surfaces from point cloud data in .stl format and CATIA's Generative Shape Design module is employed to construct the necessary measurement geometries on these surfaces for the determination of the spring-in.

In the following, the procedure carried out in CATIA is explained with an example. Scanned surface of the composite part in .stl format is imported into CATIA's Reverse Engineering module. Automatic CAD surface is created using this .stl data as shown in Figure 37.

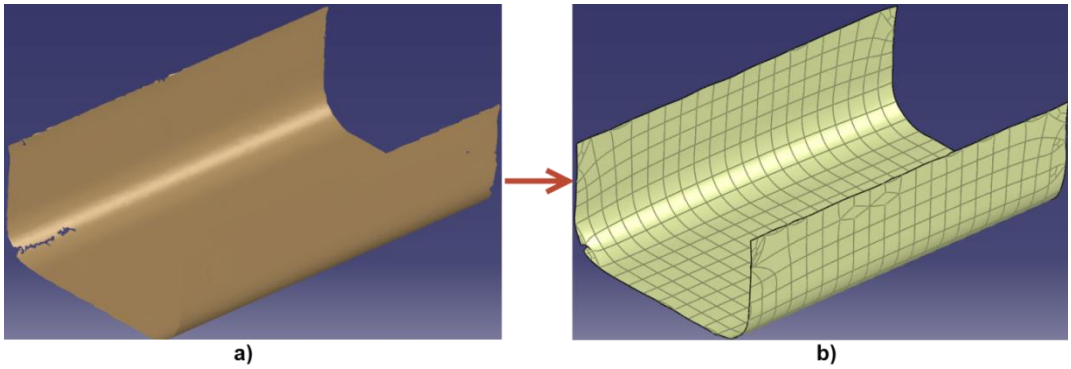

Figure 37: a) Importing the scanned surface of the composite part in .stl format b) Creating automatic surface from the .stl data

The viability of the generated surface is checked by running a deviation analysis in which scanned data is taken as reference. Figure 38 shows the deviation analysis which shows how much the newly created surface deviates from the scanned data.

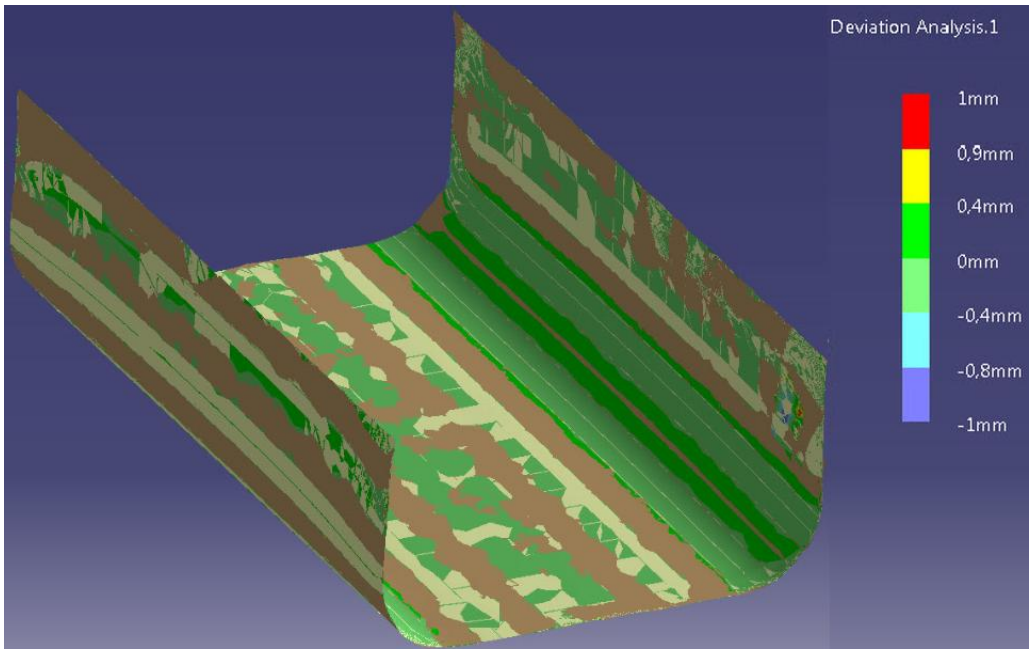

Figure 38: Deviation analysis performed on newly generated surface with respect to the scanned data

The generated CAD surface shown in Figure 38 is found to be satisfactory as the deviation does not exceed ±0.4mm. All other contacting surfaces of composite parts and tools are generated in CATIA using the same procedure.

It is only possible to measure angle between planar geometries, therefore; CAD surfaces need to be processed further in the CATIA environment to be able to obtain spring-in angle measurements. Necessary geometric elements are constructed on the generated surfaces using Generative Shape Design module in CATIA. For that purpose, geometric elements on two sides and three sections of the U shaped parts are generated along the length of contacting surfaces such that angles α_{ij} *(i=A,B and j=1,2,3)* and β_{ij} *(i=A,B and j=1,2,3)* on composite parts and tools, are measured in CATIA, respectively. Figure 39 and Figure 40 show the angles measured on the composite part and tool part, respectively.

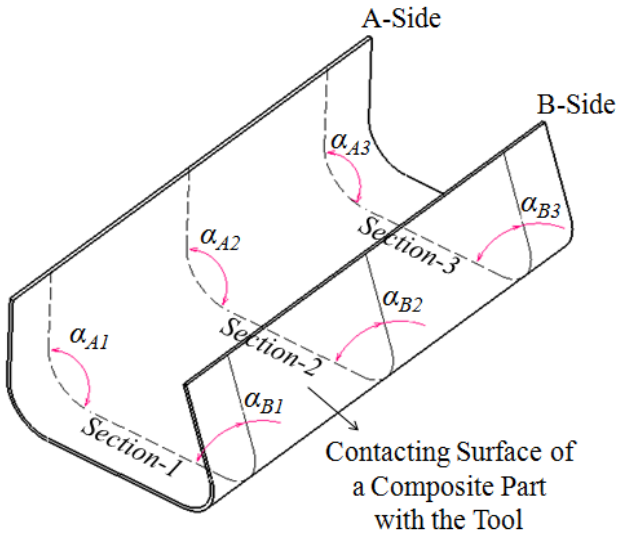

Figure 39: Angles α_{ij} *(i=A,B and j=1,2,3)* measured in CATIA for composite parts

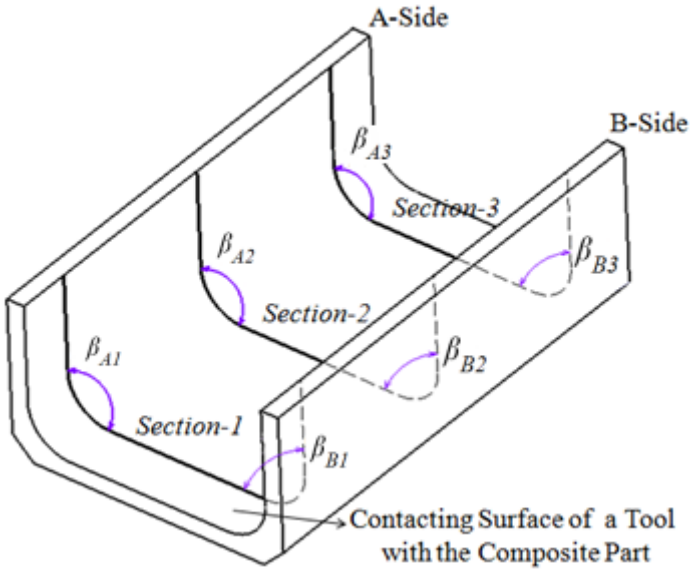

Figure 40: Angles β_{ij} *(i=A,B and j=1,2,3)* measured in CATIA for tools

In Figure 39 and Figure 40, Section-2 is located at the mid span of the U shaped part and Section-1 and Section-3 are located 50mm away from Section-2. Angles α_{ij} and β_{ij} are measured in CATIA and spring-in angles $\Delta\theta_{ij}$ *(i=A,B and j=1,2,3)* are calculated at each measuring point shown in Figure 39 and Figure 40 after extracting α_{ij} for the composite part and β_{ij} for the toolwhich are conjugate to each other. Equation (37) gives the calculation of the spring-in angle at each section.

$$\Delta\theta_{ij}=\beta_{ij}-\alpha_{ij} \tag{37}$$

The results are provided in the "Results and Discussions" Chapter.

CHAPTER 4

NUMERICAL ANALYSIS MODEL FOR SPRING-IN SIMULATION

For numerical analysis of spring-in, the material properties of the composite are needed. For material characterization of thermoset composite, cure kinetics models which predict the trend of cure and state transformations of resin such as gelation and vitrification are generated. Via these models, material properties such as glass transition temperature, modulus development during curing process, and CTEs can be found. The cure shrinkage can be monitored in the course of curing process [37, 40, 51, 57].

For cure kinetics modeling of a thermoset composite, data is obtained via experiments using differential scanning calorimeter (DSC), dynamic mechanical analyzer (DMA) and/or thermal mechanical analyzer (TMA) are conducted. DSC is used to obtain heat flow measurements of a specimen as a function of temperature, and these measurements determine the amount of heat needed to raise a specimen's temperature to a certain degree. Therefore, the degree of cure (α) in one cycle can be found by using DSC. DMA, on the other hand, is used to understand the viscoelastic behavior of polymers in terms of temperature, time, frequency, stress, atmosphere or a combination of these parameters. Material properties of the composite system such as glass transition temperature (T_g), CTEs, and cure shrinkage along the thickness direction can be found by using DMA. Thermal mechanical analyzer (TMA) which measures the deformation of a specimen under non-oscillating stress conditions with respect to time and temperature can be used for determining glass transition temperature (T_g) and CTEs of the composite material [37, 67].

After performing material characterization, effective mechanisms causing the spring-in problem should be implemented in the numerical analysis model properly. Ersoy et al. [58] stated that in any numerical analysis model, effective mechanisms

such as tool-part interaction, thermal expansion and contraction, cure shrinkage, and modulus development should be included to predict the manufacturing distortion accurately.

4.1. MATERIAL PROPERTIES OF AS4/8552 COMPOSITE SYSTEM AND ALUMINUM TOOL

The most involved material properties related to the spring-in and the residual stress modeling are the degree of cure, glass transition temperature, cure shrinkage strains, thermal expansion coefficients, elastic properties, and the gel point which instantaneously change during the curing process [51]. However, when a thermal analysis is preferred, in addition to the aforementioned material properties, thermal conductivity and specific heat capacity are also needed. As will be explained in detail, a fully coupled thermal-stress analysis model called as "coupled temperature-displacement" is generated in ABAQUS since this kind of an analysis is preferred when mechanical and thermal solutions have strong influences on each other [59]. Obviously, in the course of the curing process, residual stress development is strongly dependent on temperature changes. In this type of analysis, if needed, heat transfer such as conduction between composite part and tool, and convection between manufacturing assembly and autoclave environment can also be considered and implemented.

Ersoy et al. [51] constructed a cure kinetics model for the AS4/8552 composite system. Using this cure kinetics model, some of the necessary material properties for spring-in modeling are determined as constant and average values for both rubbery and glassy states. The total through the thickness cure shrinkage strain (ε_{33}^{cure}), Young's moduli (E_{11}, E_{22}, E_{33}), shear moduli (G_{12}, G_{13}, G_{23}), Poisson's ratios ($\vartheta_{12}, \vartheta_{13}, \vartheta_{23}$), and CTEs ($\alpha_{11},\alpha_{22},\alpha_{33}$) are obtained in this study. Table 2 summarizes the material properties of Hexcel AS4/8552 composite system required

for spring-in modeling. For the details of cure kinetics modeling, one should refer to the study of Ersoy et al. [51].

Table 2 – Some of the Necessary Material Properties of Hexcel's AS4/8552 Composite System for Spring-in Modeling [51]

Property	Unit	Rubbery	Glassy
E_{11}	MPa	132200	135000
$E_{22}=E_{33}$	MPa	165	9500
$G_{12}=G_{13}$	MPa	44.3	4900
G_{23}	MPa	41.6	4900
$\vartheta_{12}=\vartheta_{13}$	-	0.346	0.3
ϑ_{23}	-	0.982	0.45
α_{11}	με/°C	0[b]	0[b]
$\alpha_{22}=\alpha_{33}$	με/°C	-31.7	32.6
ε_{11}^{cure}	%	0[b]	0[b]
$\varepsilon_{22}^{cure}=\varepsilon_{33}^{cure}$	%	0.48	0[b]
ρ^{a}	g/cm^3	1.58	1.58

[a] Density (ρ) is taken from Hexcel Product Data [53]

[b] Assumed to be zero

Johnston [60], determined the thermal conductivity and specific heat properties of AS4/8552 composite system. Orthotropic thermal conductivity properties such that k_{c11}, k_{c22}, and k_{c33} are found by Johnston [60] who conducted thermal conductivity tests according to ASTM E 1225 standard. Here, transverse thermal conductivity properties (k_{c33} and k_{c22}) are taken equal to each other since both directions are dominated by resin matrix and their conductivities can be treated as the same. Moreover, thermal conductivity tests for k_{c33} are carried out when the resin is at cured and uncured states, as shown in Figure 41.

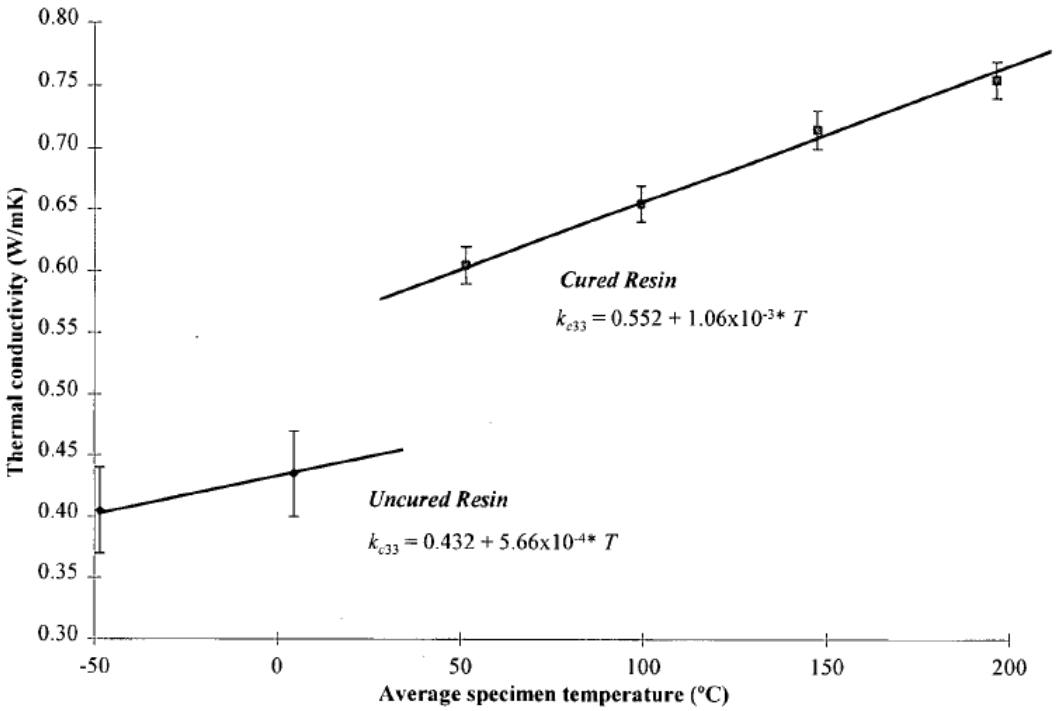

Figure 41: Transverse thermal conductivity (k_{c33}) obtained for AS4/8552 in cured and uncured states [60]

For longitudinal thermal conductivity (k_{c11}) tests, only fully cured samples are tested by Johnston [60], because the fiber dominant longitudinal thermal conductivity does not change too much from rubbery to glassy states. Results of the longitudinal conductivity tests are shown in Figure 42.

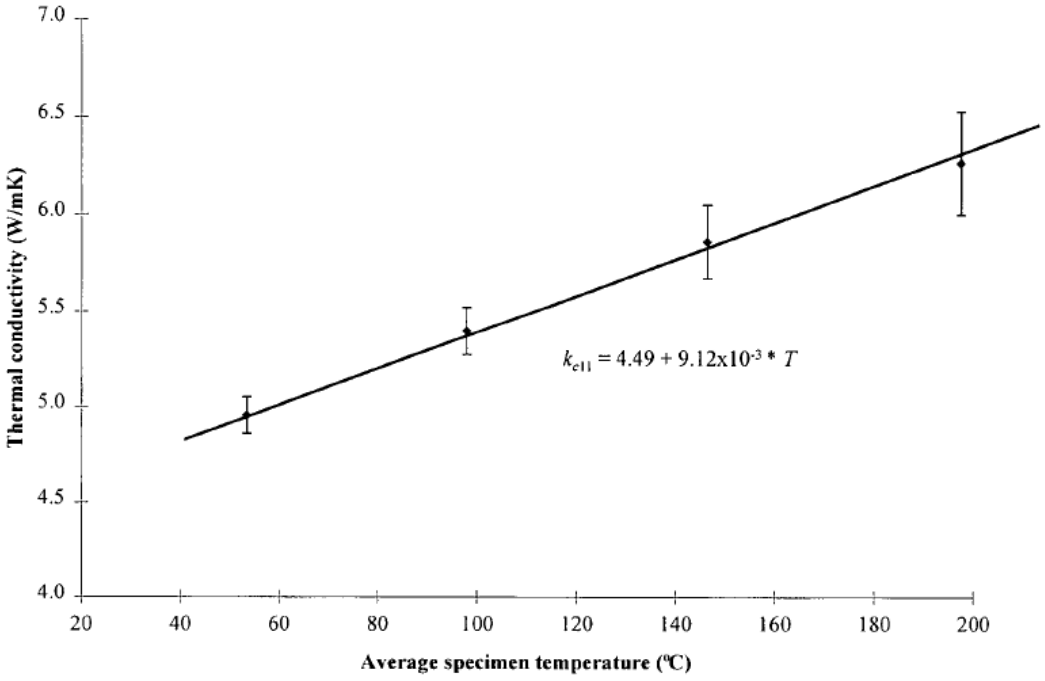

Figure 42: Longitudinal thermal conductivity (k_{c11}) obtained for AS4/8552 in cured state [60]

For the numerical analysis model, in order to simulate rubbery and glassy states of AS4/8552 composite system, transverse thermal conductivity properties (k_{c22}=k_{c33}) at both uncured and cured states, and longitudinal thermal conductivity (k_{c11}) property are calculated at a temperature of 100ºC using Figure 41 and Figure 42. Table 3 gives the average thermal conductivities of AS4/8552 used in ABAQUS analysis model.

Table 3 – Average thermal conductivities of AS4/8552 used in ABAQUS analysis model

Longitudinal Thermal Conductivity (k_{c11}) (W/mK)	**Transverse Thermal Conductivity** (k_{c22}=k_{c33}) (W/mK)	
Rubbery and Glassy States	Rubbery State	Glassy State
5.402	0.489	0.658

As mentioned earlier, Johnston [60] also determined the specific heat capacity (C_p) of AS4/8552 composite system for cured and uncured states by using a Perkin-Elmer Tas 7 DSC device. (Figure 43)

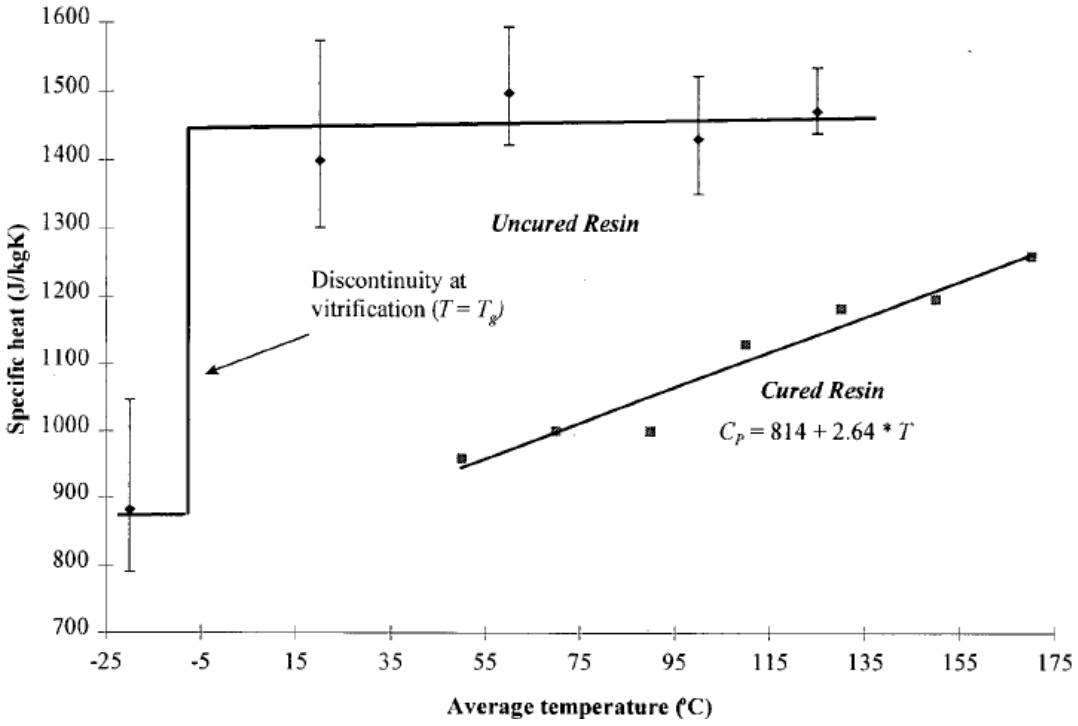

Figure 43: Specific heat capacity (C_p) obtained for AS4/8552 for cured and uncured resin [60]

Average specific heat capacity (C_p) values of the AS4/8552 composite system to be used in ABAUQS analysis model are calculated at 100ºC with the help of Figure 43. The results for both rubbery and glassy states are displayed in Table 4.

Table 4 – Average specific heat capacities of AS4/8552 used in ABAQUS analysis model

Specific Heat (C_p) (J/kgK)	
Rubbery State	Glassy State
1450	1100

On the other hand, isotropic material properties are used for the aluminum tools which are made of (Al 6061 series with T6 heat treatment. Table 5 gives the, Young's modulus (E), Poisson ratio (ϑ), CTE (α), specific heat capacity (C_p), thermal conductivity (k), and density (ρ) for the tool material. Change in tool material properties with respect to temperature is neglected.

Table 5 – Material properties of aluminum tools (6061 series, T6 heat treatment) used in ABAQUS analysis model [68]

Property	**Unit**	**Value**
E	MPa	68.9
ϑ	-	0.33
α	με/°C	25.2
C_p	J/kgK	896
k	W/mK	167
ρ	g/cm^3	2.7

4.2. ABAQUS ANALYSIS MODEL

4.2.1. FEM Models in the Literature

In the literature, there are many finite element analysis models simulating shape distortions of different composite systems [35, 44, 55, 61, 63, 64, 65].

Zhu et al. [61] constructed a transient coupled thermo-chemo-viscoelastic numerical model which aimed to find the optimal tool geometry. The model generated by Zhu et al. [61] is a 2-D plane strain finite element in which both warpage and spring-in problems are considered. First, the effect of composite part's curvature with changing CTEs of the tool and then the spring-in problem of the L-shaped composite part are studied. However, numerical model constructed for the spring-in problem does not take tool-part interaction into account properly since the composite part is connected to the tool surface during analysis which means no slip condition is assumed between tool and composite part.

Dong [44] generated a 3-D FEM model to observe spring-in of an L-shaped composite part made of T300/CYCOM 934 carbon epoxy unidirectional prepreg. As an important note, in the study of Dong [44], tool is not constructed for the numerical model, therefore tool-part interaction is neglected. The model also considers only the glassy state properties such that viscoelastic behavior of resin is not taken into account.

In the study of Wiersma et al. [62], first a 3-D numerical composite part model which is composed of 8-node brick elements is generated. Within this numerical analysis, only thermoelastic behavior of composite part causing the spring-in is examined and it is stated that the results of thermoelastic numerical model do not explain the total spring-in angles found in experiments. Therefore, Wiersma et al. [62] decided to improve the first numerical modelto include a cure cycle model to simulate the heat distribution in composite part and a viscoelastic model to include

the changes in thermoset resin properties. The extended numerical model generated by Wiersma et al. [62] is a 2-D model and it also considers tooling effects but no slip is allowed between tool and part. At the end of the study, it is concluded that improvement in cure cycle model is needed to have better spring-in angle predictions and this requires a more complex modeling strategy.

Dong et al. [63] developed a 2-D thermoelastic numerical finite element analysis (FEA) model by constructing typical structural composite parts such as stiffeners, corner shaped parts, and cylindrical shells etc... In this study, viscoelastic effects and tool effects are neglected, only composite part is modeled and thermoelastic effects are simulated. Regression-based shape distortion model is generated by using FEA results of each typical structural composite part for different dimensions. The aim here is to obtain a regression based model for any fiber or resin type and stacking sequence, and to eliminate the need for using an FEA model. Dong et al. [63] constructed structural tree method by using the generated regression models to calculate shape distortions of assemblies which are composed of typical structural composite parts.

Fernlund et al. [64] used 2-D process models which are generated in COMPRO to predict shape distortion on various sections of interest on a 3-D model. This technique is called as 2-D/3-D technique in the study. 2-D process models consider extrinsic and intrinsic process parameters existing during the cure process. For extrinsic process parameters, effects of lay-up, part and tool geometry, cure cycle, tool material, and tool surface are taken into account in the generated COMPRO model. On the other hand, for intrinsic process parameters, the factors such as anisotropy in the CTE and cure shrinkage of the resin are included. Moreover, autoclave conditions are modeled during numerical analysis [64] since convective heat transfer which is found as a function of pressure is applied to all boundaries of manufacturing assembly that are subjected to the autoclave gas. In addition to this, in the COMPRO model, a more realistic model is implemented such that degree of cure and temperature are used as state variables to calculate thermal and physical

properties at any time during the curing process. Here, degree of cure is obtained from a developed cure kinetics model and temperature is determined by the heat transfer analysis. However, predicting thermo-physical material properties instantly in the course of curing requires constructing complex constitutive models and extensive material characterization. Also, in order to find the convective heat transfer coefficient to simulate the autoclave environment, experiments need to be conducted. Another important point in study of Fernlund et al. [64] is that at the tool-part interface, slippage is not allowed between contacting surface and they are assumed to be bonded together. Consequently, it is suggested that the usage of full 3-D models give better results but they also state that 3-D modeling requires longer computation times.

Svanberg and Holmberg [65] simulated spring-in of angle bracket manufactured by the RTM technique. In ABAQUS, plane strain elements (CGPE6) are used to generate the analysis model. Epoxy system Araldite LY5052/Hardener HY5052 and E-glass weave, Hexcel 7781-127 are used as the composite material. For tool-part interaction, Svanberg and Holmberg [65] proposed three different boundary condition modeling methods such as freestanding, fully constrained, and frictionless contact conditions. In freestanding boundary condition, only the part is modeled and it is free to move in any direction during curing process, therefore tooling effects are completely disregarded. In fully constrained method, the angle bracket is constrained from all degrees of freedom such that a rigid tool is assumed. Demolding is simulated by removing the constraints defined on the composite part. Lastly, in the frictionless contact condition, a frictionless contact pair for the mating surfaces of composite part and tool is defined in ABAQUS. It is defined as frictionless since Svanberg and Holmberg [65] states that the tool surface is clothed with Myler film which has low coefficient of friction. According to Svanberg and Holmberg [65], the best results are obtained when the contact boundary condition is applied to the analysis model. Moreover, in the accompanying study of Svanberg and Holmberg [65], Svanberg and Holmberg [35] constructed a constitutive model including different glassy and rubbery material properties and chemical shrinkage.

The model is then applied to ABAQUS by user subroutines UMAT and UEXPAN for spring-in simulations of angle brackets performed in study of Svanberg and Holmberg [65].

In all of the aforementioned studies [35, 44, 55, 61, 63, 64, 65] which present spring-in simulation techniques, some of the models are simple that do not take the important spring-in mechanisms such as viscoelasticity of resin and the tool-part interaction. Other models are complex to construct, because in those models constitutive models, which take changing cure shrinkage and material properties as a function of temperature into account, are implemented in the analysis program with a user subroutine. Moreover, in some of the complex models, convection heat transfer coefficient within the autoclave chamber is experimentally found and implemented in the numerical analysis.

4.2.2. Modeling Strategy in ABAQUS

Modeling strategy in this thesis takes its basis from the study of Çınar et al. [55] in some aspects and adds new contributions to the model. Çınar et al. [55] established a three-step two dimensional (2-D) plane strain finite element model to investigate the spring-in behavior of corner shaped composite parts in ABAQUS. The numerical analysis is performed in general static case and it takes anisotropy in CTE, cure shrinkage, consolidation and tool-part interaction into account. The model of Çınar et al. [55] works on constant viscous, rubbery, and glassy state material properties of AS4/8552 composite system. For viscous state material properties, Çınar et al. [55] conducted a parametric study such that fractions of rubbery state properties are used since information on viscous state properties is not available. This way, the model is able to consider the effects of consolidation. However, viscous resin is not able to sustain considerable amount of residual stress. Therefore, the effect of consolidation on spring-in can be neglected [36, 58]. To take tool-part interaction into account, hard contact and classical isotropic Coulomb

friction are defined by Çınar et al. [55] between contacting surfaces of the composite part and the tool in ABAQUS. In Table 6, comparison between numerical model developed in this thesis and Çınar's numerical model is shown.

Table 6 – Comparison Between Numerical Model Developed in This Thesis and Çınar's Numerical Model

Numerical Model Developed in the Thesis	**Çınar's Numerical Model**
3-D full scale model is constructed.	2-D plane strain model is constructed.
Coupled temperature-displacement analysis type in ABAQUS is implemented.	General static analysis type in ABAQUS is implemented.
Apart from thermo-mechanical static solution, convection and conduction heat transfer solutions can be adopted if needed.	Only thermo-mechanical static solution can be obtained.
Viscous state material properties are not taken into account.	Viscous state material properties are taken into account.

The ABAQUS model created in this thesis is a three-step 3-D full model that runs coupled temperature-displacement analysis and uses C3D8RHT (8-node thermally coupled brick, trilinear displacement and temperature, reduced integration, hourglass control, hybrid, constant pressure) solid elements. Both the composite part and the tool are modeled according to the dimensions given in Figure 26 and Figure 27. In total, 50895 linear hexahedral elements are used. Figure 44 shows the finite element model of the U shaped composite part and the tool in assembled form built in Abaqus.

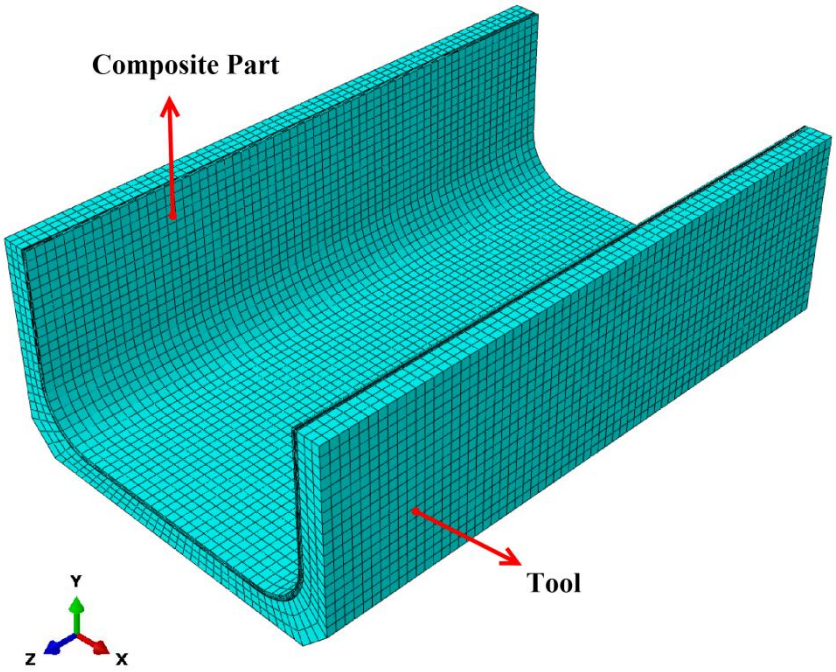

Figure 44: ABAQUS analysis model

While modeling the composite part, a solid part is created for the whole laminate and then partition cells are generated on the solid part to define each lamina. Solid and homogeneous type material section is assigned to each lamina with the related orientations. As mentioned earlier, there are 8 laminae in the laminate which has the lay-up configuration of $[45°/-45°/90°/0°]_s$. Tool, on the other hand, is modeled as a unique solid part and similarly, solid and homogeneous type material section is assigned in ABAQUS but this time isotropic material properties are used and no orientation is assigned to the tool material.

The ABAQUS model works on coupled temperature-displacement type analysis. Therefore, if needed, convection and conduction heat transfer can also be simulated in the numerical model. However, the numerical model constructed in this thesis does not solve any heat transfer problem as uniform temperature boundary conditions are assigned to the whole model which means the composite part and tool is subjected to the same temperature everywhere at any time instance. This is

because the surface temperature data obtained from experiment by monitoring the composite part and the tool surfaces at different locations revealed that maximum temperature gradient among all thermocouple measurements is within the range of 2℃. (Figure 33) Therefore, variation in the surface temperature fields for composite part and tool can be neglected and uniform temperature boundary conditions can be assigned. On the other hand, for thicker and larger composite parts where temperature field on the surface differs greatly, the present numerical model can be modified to take convection heat transfer mechanism into account. The convection coefficient of autoclave chamber can be determined experimentally and implemented in the model but this would require additional work. It should be noted that although the analysis model does not solve any heat transfer problem, ABAQUS requires a thermal conduction to be defined between contacting surfaces of the composite part and the tool.

The ABAQUS analysis model considers rubbery and glassy state properties of composite material and it consists of three steps as mentioned earlier. The first two steps are illustrated on the cure diagram of AS4/8552 composite system in Figure 45. In the third step, demolding process of the composite part from the tool is simulated.

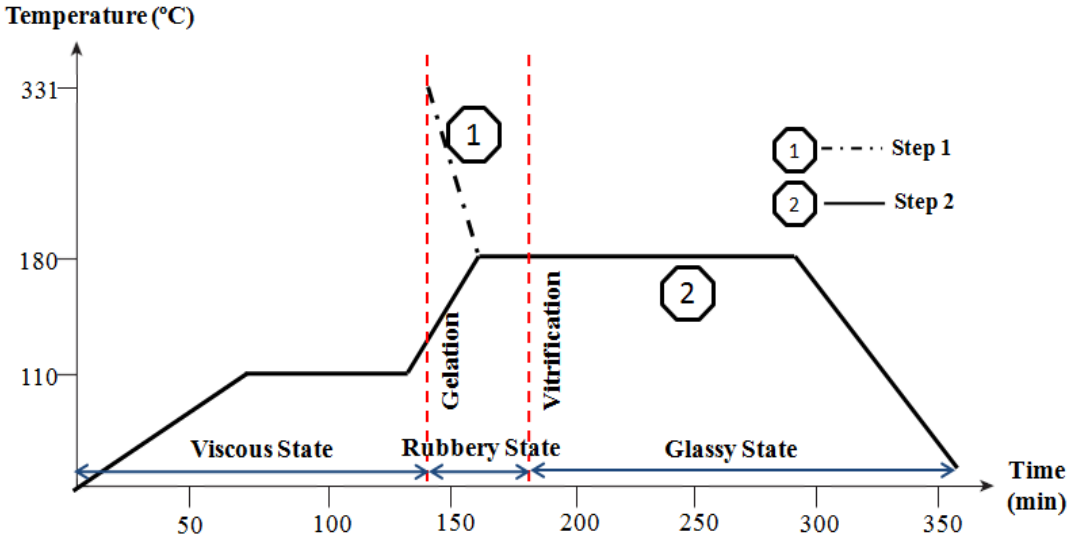

Figure 45: The first two analysis steps on the cure diagram of AS4/8552 composite system

During the first step shown in Figure 45, rubbery state material properties from Table 2, Table 3, and Table 4 are used and cure shrinkage mechanism is taken into account in the same manner Çınar et al. [55] handles the cure shrinkage. Cure shrinkage is considered as thermal contraction in through the thickness direction according to the simple thermal strain Equation (38):

$$\varepsilon_{33}^{cure} = \alpha_{33} \Delta T \tag{38}$$

where ε_{33}^{cure} is 0.48% and α_{33} is -31.7 με/℃ as can be seen in Table 2. The temperature gradient, ΔT, is then found to be 151ºC. Therefore at Step 1, in order to simulate cure shrinkage as thermal contraction, the initial temperature boundary condition is started from 331ºC and reduced to 180ºC which is the cure temperature on MRCC of AS4/8552 composite system. At the end of first step, a steady state solution is obtained in ABAQUS.

At Step 2, cooling down from cure temperature to room temperature is simulated. Therefore, the temperature boundary condition is brought to 25ºC in 2700 seconds. For a more realistic simulation, transient solution technique is preferred at this step.

During the first and second steps, displacement of four nodes at the corners of bottom surface of the tool is fixed in x, y, and z directions but no constraint is applied for the rotation boundary conditions. Figure 46 shows the displacement boundary condition applied to the corner nodes of the bottom surface of the tool.

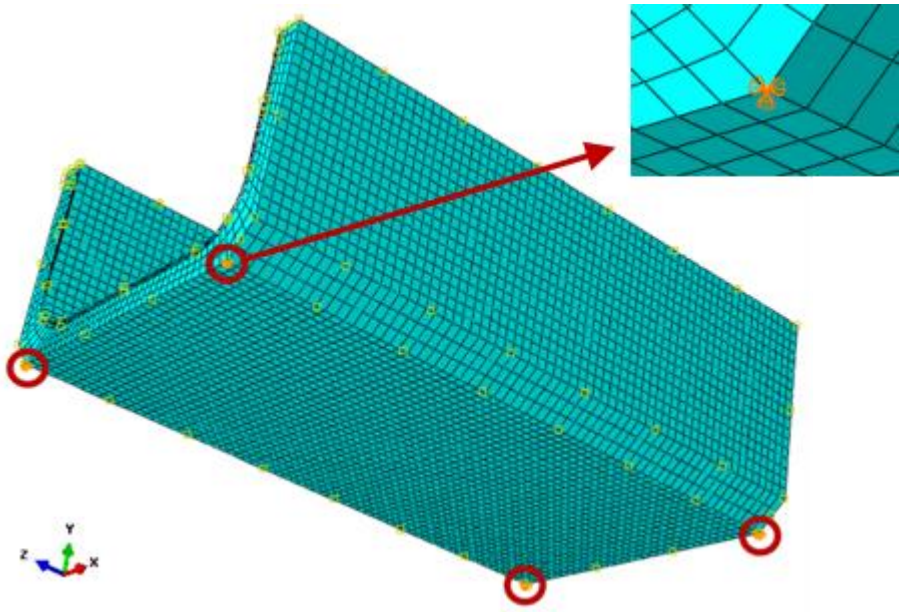

Figure 46: Displacement boundary condition applied to the corner nodes of the bottom surface of the tool

A pressure load of 0.78 MPa representing the combined autoclave chamber pressure and vacuum pressure is applied to the whole manufacturing assembly during the first and second steps as shown in Figure 47. At the third step, the pressure load is removed.

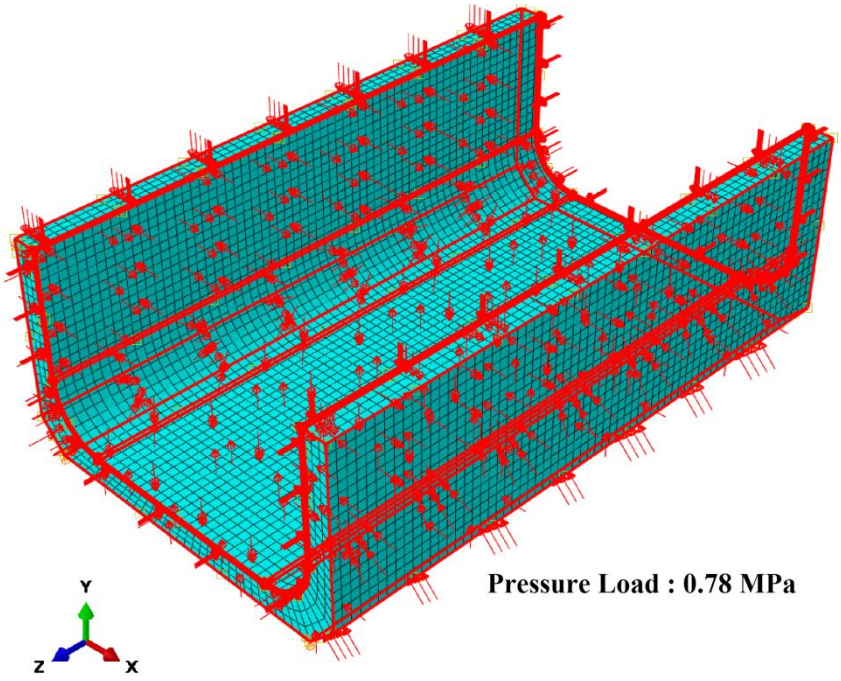

Figure 47: Pressure load applied to the whole manufacturing assembly

Tool-part interaction mechanism is modeled between the contact surfaces of composite part and tool during the first two steps of the analysis model. For this purpose, standard surface to surface contact interaction is defined in ABAQUS for the mating surfaces where tool surface is selected to be the master surface, and the surface of the composite part is selected to be the slave surface.

"Normal behavior", "tangential behavior" and "thermal conductance" properties are assigned to the surface to surface contact interaction. In the "normal behavior" mechanical contact property, "hard contact" is chosen since it transmits any contact pressure possible when in contact and ceases transmitting contact pressure when no contact is present between the mating surfaces. Hard contact also minimizes the penetration of the slave surface nodes into the master surface nodes along the locations of constraint [59]. In the "tangential behavior" mechanical contact property, isotropic Coulomb friction is defined between the contacting surfaces. The coefficient of friction, μ, is calculated according to the sliding stress, τ_{max}, on the

contacting surfaces which is accepted to be 0.2 MPa in Step 1 and Step 2 [55]. Equation (39) is used for determining μ:

$$\mu = \frac{\tau_{max}}{P} \tag{39}$$

where P represents the total pressure applied on the manufacturing assembly during cure and as mentioned earlier, it is 0.78 MPa. The coefficient of friction, μ, is then found to be 0.26. For the "thermal conductance" thermal contact property, a perfect thermal conductance which uses clearance-dependency is defined between the mating surfaces. In reality, engineering surfaces are not completely smooth and there always exists a surface roughness. These surface irregularities result in reduced heat transfer between contacting surfaces and conduction heat transfer is possible through the solid to solid contact points and through the interfacial gaps [69]. There are available studies in the literature in which thermal conductance models are presented [70, 71]. However, for the ease of calculation, in the present study, perfect thermal conductance between composite part and tool is assumed in the numerical model. To provide perfect thermal conduction meaning there is no thermal resistance between the contacting surfaces, thermal contact conductance (TCC) is selected to be a large number in the heat transfer analysis. Thermal contact conductance is determined in terms of the highest material conductivity (HMC) used in the model and the diagonal of the overall geometry bounding box (DOGBB) according to Equation (40) [66]:

$$\text{TCC} = (10000 \times \text{HMC}) / \text{DOGBB} \tag{40}$$

DOGBB is calculated by measuring the distance between the furthest two points on tool geometry. TCC is found to be 7.7×10^6 W/mK which is then approximated as

10^7 W/mK and applied to the model when the clearance between the mating surfaces of composite part and tool is assumed to be zero. On the other hand, TCC is assumed to be zero when the clearance between two mating surfaces reaches 10^{-5}mm. Thermal conduction interaction between two bodies is desired to be ceased even when an infinitesimal amount of clearance occurs. For this reason, the clearance is selected to be very little. Consequently, thermal conductance values and the related clearance values are shown in Table 7.

Table 7 – Thermal conductance and related clearance values defined in the analysis model

Conductance (W/mK)	**Clearance (mm)**
$7.7x10^6$	0
0	10^{-5}

In the last step, while holding temperature at the room temperature (25ºC), the tool is removed from the ABAQUS analysis model by using "model change" interaction in which all elements and nodes of tool are deactivated and only composite part remains. As the displacement/rotation boundary condition, displacement of the four corner nodes at the bottom surface of U-shaped composite part is fixed in x, y, and z directions and no rotational constraint is applied, as shown in Figure 48.

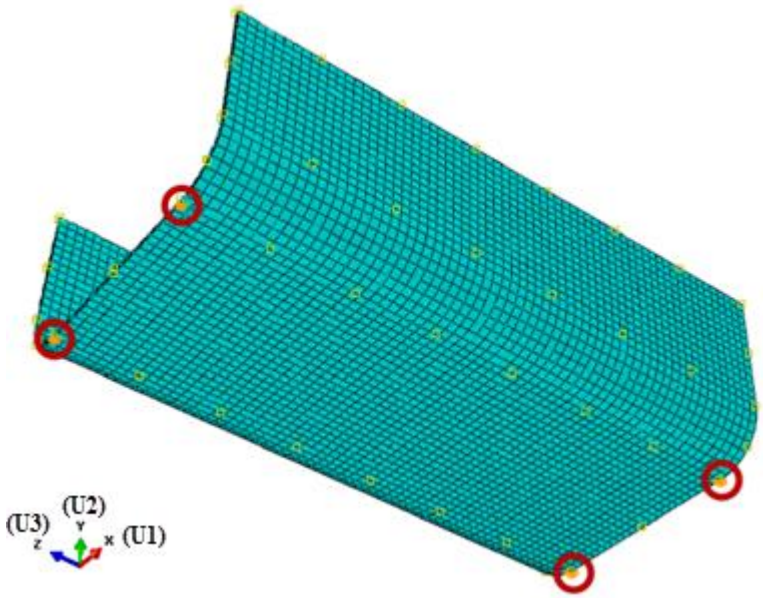

Figure 48: Displacement boundary condition applied to the corner nodes of the bottom surface of the composite part in step 3 of the analysis

During the analysis, ABAQUS 6.12-1 is linked to Intel Fortran Compiler 10.1 along with Microsoft Visual Studio 2010 in order to implement changing material properties for rubbery and glassy states. For that purpose a user subroutine called as USDFLD is written and this subroutine uses rubbery state material properties at Step 1 and then changes rubbery state material properties to glassy state material properties at Step 2 and Step 3 by employing field variables defined in ABAQUS "Edit Material" window. For example, as can be seen in Figure 49, rubbery state thermal conductivity material properties shown in the first row are implemented in the model at Step 1 when Field 1 variable is activated by entering 1. Similarly, for Step 2 and Step 3, glassy state material properties shown in the second row in Figure 49 are implemented when Field 2 and Field 3 variables are activated.

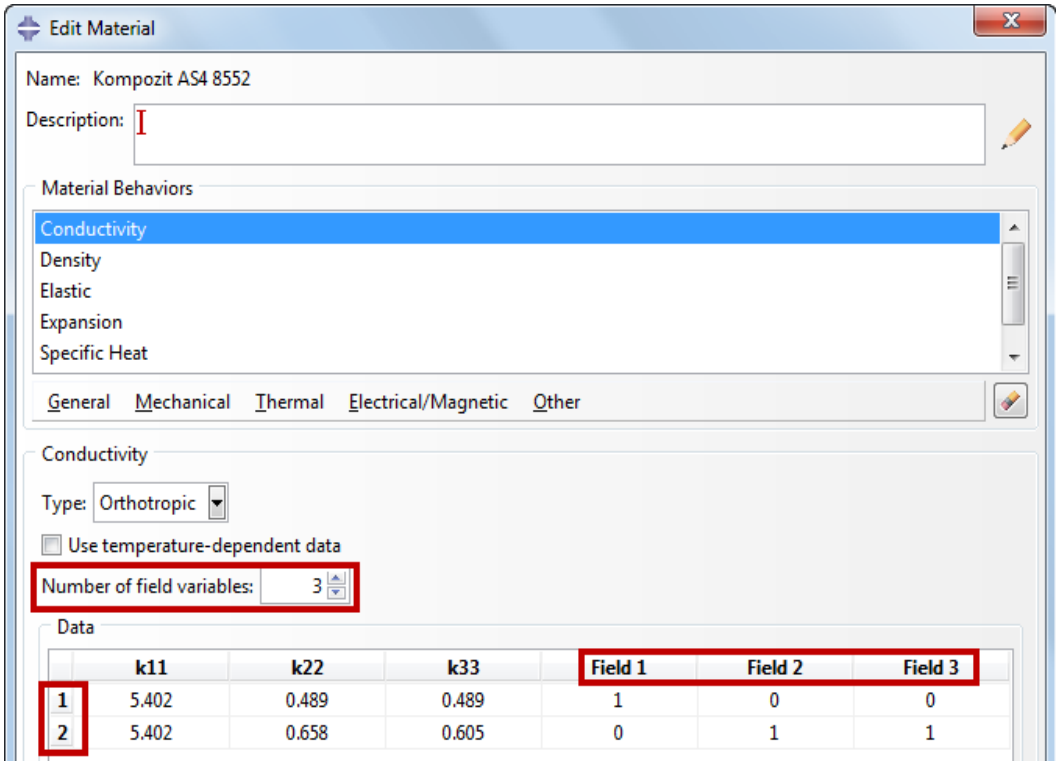

Figure 49: Defining field variables in ABAQUS Edit Material window

HP Z400 Workstation is used to simulate spring-in modeling and analysis in ABAQUS. Time elapsed during the solution is approximately one and a half hour. The results are provided in Chapter 5.

Up to this point, primary analysis model simulating the spring-in behavior of U-shaped composite parts is developed. The primary analysis model includes both composite part and tool. In this model, spring-in mechanisms: cure shrinkage of resin, tool-part interaction, and anisotropic material properties are taken into account by using glassy state and rubbery state composite properties. Apart from the primary analysis model, two more analysis models are developed in ABAQUS by modifying the primary analysis model. In one of these modified models, cure shrinkage effect on the spring-in problem is simulated by only using rubbery state material properties. In the other model, the effect of tool-part interaction is

investigated by removing tool from the analysis model. Both modified models are explained in the following sections.

4.2.3. The Effect of Cure Shrinkage on the Spring-in

In order to understand the effect of cure shrinkage, ABAQUS analysis model is modified in such a way that only rubbery state material properties are used. The purpose is to see the spring-in behavior of U-shaped composite part when only cure shrinkage and tool-part interaction mechanisms are taken into account. Therefore, the cooling down from the cure temperature to room temperature is not simulated in this model. The analysis consists of two steps. The previously described modeling strategy is employed during both steps. In the first step, which is shown in Figure 45 as Step 1, rubbery state material properties are used and cure shrinkage mechanism is modeled as thermal contraction. Therefore, the temperature of both composite part and tool is brought to 180ºC from 331ºC. In the second step, while holding the temperature constant at 180ºC as if the room temperature is reached, tool is removed from the analysis model and demolding process is simulated. The results are provided in Chapter 5.

4.2.4. The Effect of Tool-part Interaction on Spring-in

Tool-part interaction has an important effect on the spring-in mechanism. To see this effect, ABAQUS analysis model is modified such that tool is removed from the analysis model and surface to surface contact definition between the composite part and the tool is eliminated. The analysis model only considers composite part and it consists of two steps which are shown in Figure 45 as Step 1 and Step 2. The previously described modeling strategy is employed during both steps. In the first step, rubbery state material properties are used and cure shrinkage mechanism is modeled as thermal contraction. In the second step, cooling down from cure temperature to room temperature is simulated by using glassy state material

properties. The same boundary conditions and loads are applied to the composite part. The results are provided in Chapter 5.

CHAPTER 5

RESULTS AND DISCUSSIONS

In this thesis, spring-in problem of corner shaped composite parts which are made of AS4/8552 UD prepregs is investigated by three different methods. In the first method, spring-in problem is solved by employing an analytical model which is available in the literature. In the analytical model, a 2-D solution is obtained and the effect of two spring-in mechanisms, cure shrinkage and anisotropy in CTEs, is taken into account. In the second method, four composite parts are manufactured with autoclave forming process. During manufacturing process, the surface temperature of one of the composite parts and its tool is monitored at different locations to see the variation in temperature. Then, spring-in angles of the remaining composite parts are measured by using the optical scanning device. In the third method, a 3-D ABAQUS analysis model which considers the effective spring-in mechanisms cure shrinkage, anisotropic material properties, and tool-part interaction is developed. To have a realistic analysis model, changing material properties are implemented in the analysis model during the cure cycle for the composite parts. For that purpose, constant rubbery and glassy state material properties of the composite material available in the literature are used. Furthermore, effects of cure shrinkage and tool-part interaction mechanisms are studied separately by modifying the analysis model. In order to see the effect of cure shrinkage on the spring-in shape distortion, only cure shrinkage mechanism is simulated. To understand the effect of tool-part interaction, tool is removed from the analysis model and autoclave forming process is simulated in ABAQUS only for the composite part.

.

5.1. SPRING-IN ANGLE CALCULATION VIA ANALYTICAL MODEL

In the analytical model, a thermoelastic approach is utilized to determine the 3-D thermomechanial properties (effective stiffness matrix and CTEs) of symmetric and balanced laminates . In addition to these properties, effective cure strains of symmetric and balanced laminates are determined by an analytical approach. For cure shrinkage strain of one AS4/8552 ply, experimental data available in the literature is used. Then, the system of equations given by equations (4-36) are solved in MATLAB environment, and the total spring-in angle ($\Delta\theta_L$) of the U shaped $[45°/-45°/90°/0°]_s$ composite laminate composed of AS4/8552 layers due to anisotropy in CTEs and cure shrinkage is calculated analytically. Table 8 summarizes the spring-in angles calculated due to anisotropy in CTEs and cure shrinkage and the final spring-in angle.

Table 8 – Spring-in angles calculated by using the 2-D analytical model

Spring-in Angle due to Anisotropy in CTE's $\Delta\theta_{CTE}$ (°) *	**Spring-in Angle due to Cure Shrinkage $\Delta\theta_{CS}$ (°) ***	**Total Spring-in Angle $\Delta\theta_L$ (°) ***
1.72	-0.18	1.54

* Positive angle indicates that spring-in occurs towards the inside. Negative angle indicates that spring-in occurs towards the outside.

From Table 8, it can be seen that spring-in angle due to anisotropy in CTE's and spring-in angle due to cure shrinkage are opposite to each other since one of them is positive and the other one is negative. Spring-in angle due to cure shrinkage is found to be negative according to Equation (3) due to the fact that the through-thickness cure shrinkage strain of laminate ($\emptyset_r$) is larger than the in–plane cure shrinkage strain of laminate ($\emptyset_\theta$). This is because the fiber reinforcement through

the in-plane direction causes less cure shrinkage strain ($\varnothing_\theta$) than through the thickness cure shrinkage strain ($\varnothing_r$).

5.2. SPRING-IN ANGLE MEASUREMENT VIA EXPERIMENT

During the experiment which is the second method for spring-in investigation, first of all, surface temperature data of a specific composite part and tool is obtained during the cure process by installing thermocouples on predetermined locations as shown in Figure 31 and Figure 32. The aim is to see the temperature variation on the surfaces the composite part and the tool. If a great difference in thermocouple readings is observed, the temperature data would have to be entered as boundary condition in the ABAQUS analysis model. However, the maximum difference in thermocouple readings is found to be approximately 2°C during the complete cure cycle. (Figure 33) Therefore, the same homogeneous temperature field is assigned to all surfaces of both the composite part and the tool in the ABAQUS analysis model. Secondly, the contact surfaces of remaining three composite parts and tools are scanned after the autoclave forming process is ended. Corner angles of composite parts and tools, α_{ij} and β_{ij} respectively, are measured from six locations as shown in Figure 50 and Figure 51 by using CATIA. Table 9 and Table 10 give the measured corner angles of the composite parts and the tools.

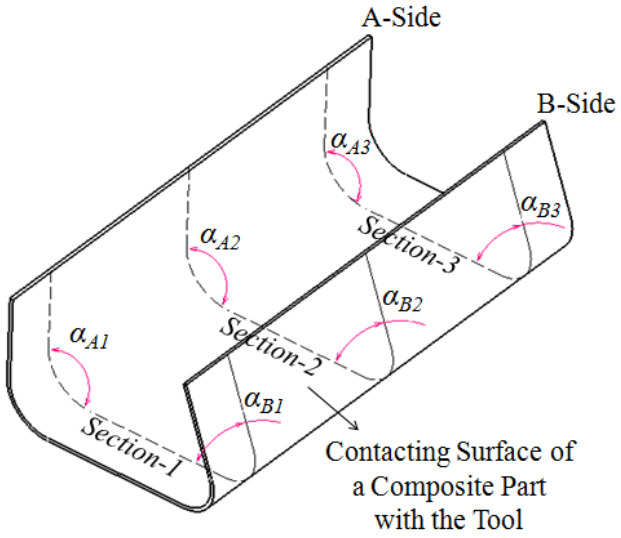

Figure 50: Angles α_{ij} *(i=A,B and j=1,2,3)* measured in CATIA for composite parts

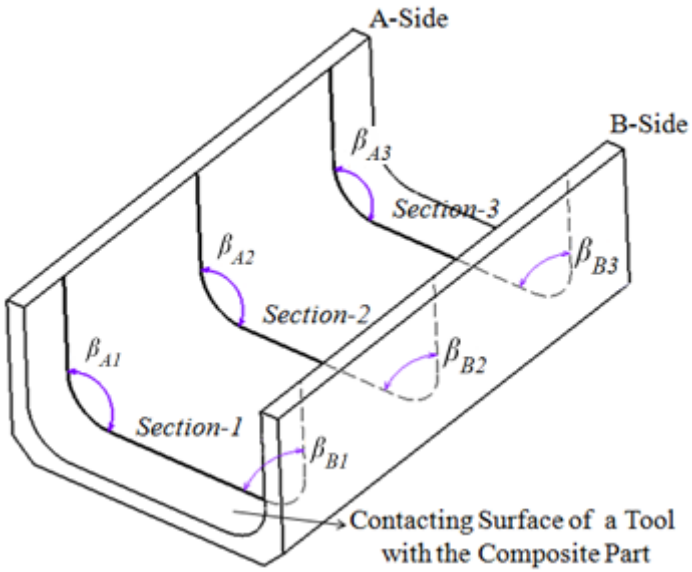

Figure 51: Angles β_{ij} *(i=A,B and j=1,2,3)* measured in CATIA for tools

Table 9 – Measured angles, α_{ij} *(i=A,B and j=1,2,3)* on each composite part

Composite Part	α_{A1}	α_{A2}	α_{A3}	α_{B1}	α_{B2}	α_{B3}
Part-1	89.11°	88.94°	89.06°	88.83°	88.91°	88.93°
Part-2	89.06°	89.06°	88.96°	88.88°	88.92°	88.91°
Part-3	88.73°	88.76°	88.59°	89.11°	88.66°	88.75°

Table 10 – Measured angles, β_{ij} *(i=A,B and j=1,2,3)* on each tool

Tool	β_{A1}	β_{A2}	β_{A3}	β_{B1}	β_{B2}	β_{B3}
Tool-1	89.92°	89.68°	89.56°	89.73°	89.77°	89.64°
Tool-2	89.63°	89.76°	89.87°	89.70°	89.48°	89.57°
Tool-3	89.63°	89.73°	89.93°	90.11°	89.79°	89.96°

Using Equation (37) and the angles provided in Table 9 and Table 10, spring-in angles of composite parts at three different sections are calculated. For the three U shaped composite parts, Table 11 gives the spring-in angles measured at three different sections.

Table 11 - Spring-in angles, $\Delta\theta_{ij}$ *(i=A,B and j=1,2,3)*

Composite Part	$\Delta\theta_{A1}$	$\Delta\theta_{A2}$	$\Delta\theta_{A3}$	$\Delta\theta_{B1}$	$\Delta\theta_{B2}$	$\Delta\theta_{B3}$
Part-1	0.81°	0.74°	0.50°	0.90°	0.86°	0.71°
Part-2	0.57°	0.70°	0.91°	0.82°	0.60°	0.65°
Part-3	0.91°	0.97°	1.34°	1.00°	1.14°	1.21°

* Positive angle indicates that spring-in occurs towards the inside. Negative angle indicates that spring-in occurs towards the outside.

The reason for measuring spring-in angles at multiple locations is to see the possible variation of the spring-in angle along the length of composite part.

Although the composite parts have the same U-shaped geometries with symmetric sides, spring-in angles are measured at both sides for all composite parts. Here, the purpose is to compensate the errors coming from manufacturing process and to have a unique average spring-in angle measurement which is expected to be more accurate. By looking at Table 11, it can be deduced that there is no obvious trend for spring-in angles along the length of the parts. This might be due to uncontrollable nature of composite manufacturing. It is also considered that longer U-shaped composite parts may have to be investigated to obtain a spring-in angle trend along the length of the composite part. The total average spring-in angle for the manufactured composite parts is found to be 0.85º.

5.3. SPRING-IN ANGLE CALCULATION VIA NUMERICAL ANALYSIS MODEL

In the third method, spring-in measurements are performed in ABAQUS for three different models. In the first model which is the primary analysis model, both composite part and tool are modeled and spring-in mechanisms cure shrinkage of the resin, tool-part interaction, and anisotropic material properties are simulated in a three-step analysis model with constant glassy state and rubbery state composite properties. The coefficient of friction, μ, between tool and part is taken as 0.28 in this model. Details related to the primary analysis model are provided in section 4.2.2. For the primary analysis model, displacement solutions obtained from ABAQUS at the end of each step are shown in Figure 52, Figure 53, and Figure 54.

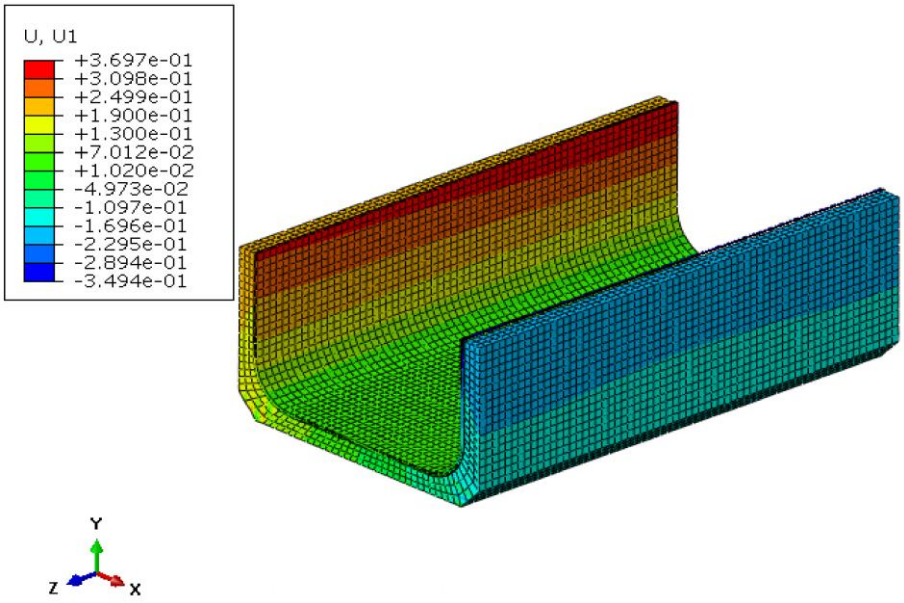

Figure 52: Primary analysis model - displacement in U1 direction (global-x direction) at the end of Step 1 (Deformation Scale Factor: 1, unit: mm, and μ=0.28)

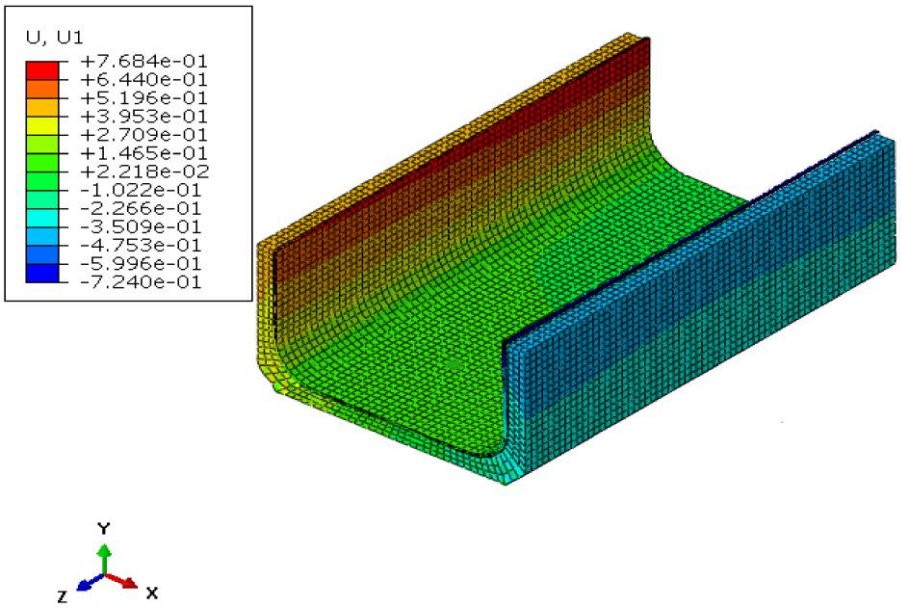

Figure 53: Primary analysis model - displacement in U1 direction (global-x direction) at the end of Step 2 (Deformation Scale Factor: 1, unit: mm, and μ=0.28)

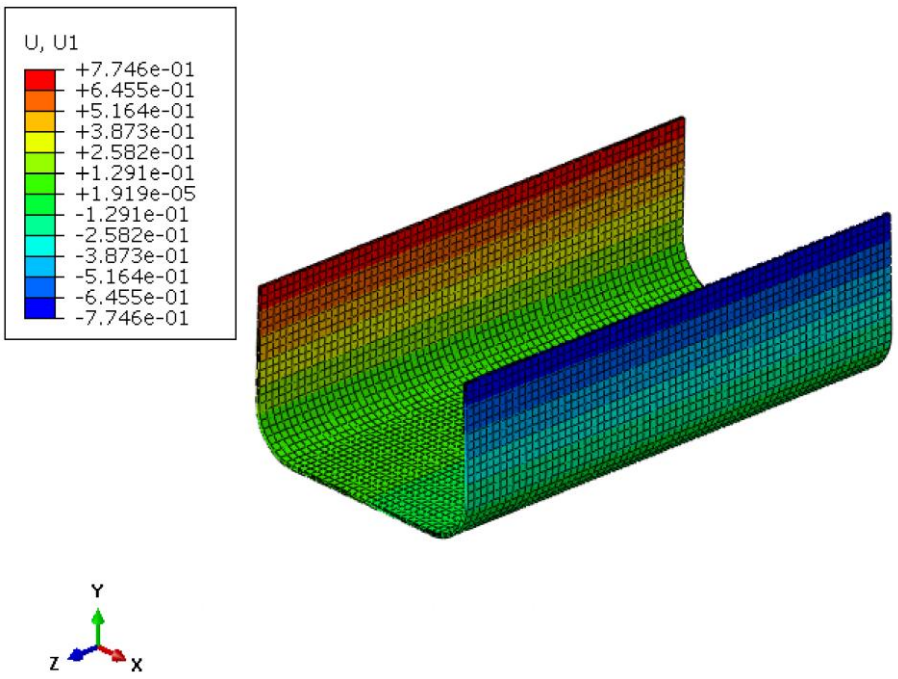

Figure 54: Primary analysis model - displacement in U1 direction (global-x direction) at the end of Step 3 (Deformation Scale Factor: 1, unit: mm, and μ=0.28)

In the first model, the effect of coefficient of friction, μ, between tool and part is also investigated by choosing a higher and a lower coefficient of friction values from the original coefficient of friction value, 0.28, found in the literature. For that purpose, coefficients of friction values, 0.36 and 0.20 are given as input to primary analysis model. The following displacement results shown in Figure 55, Figure 56, and Figure 57 are obtained when μ is chosen as 0.36:

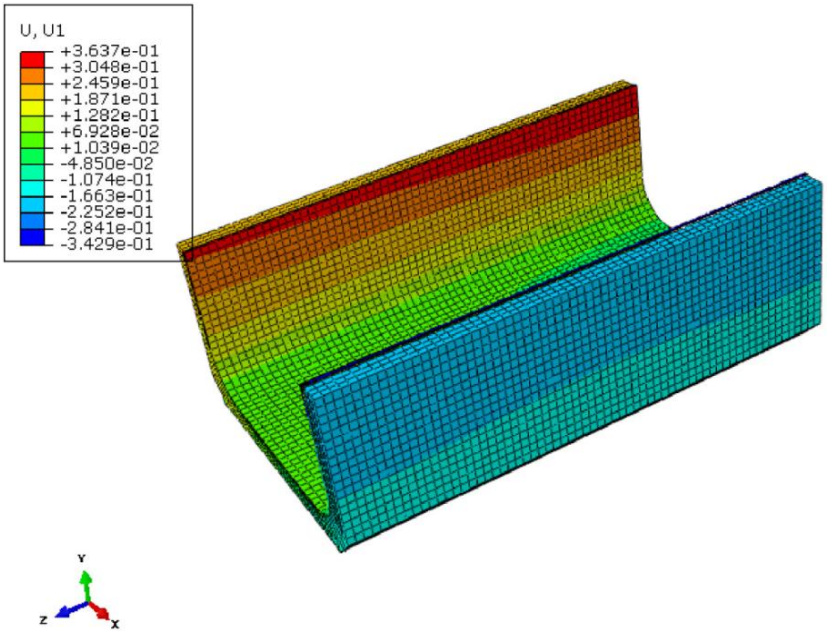

Figure 55: Primary analysis model - displacement in U1 direction (global-x direction) at the end of Step 1 (Deformation Scale Factor: 1, unit: mm, and μ=0.36)

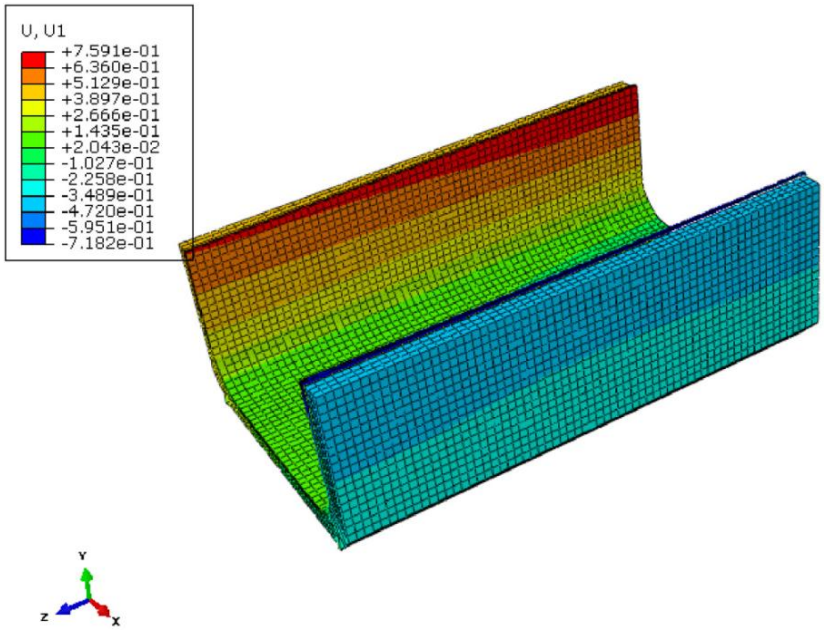

Figure 56: Primary analysis model - displacement in U1 direction (global-x direction) at the end of Step 2 (Deformation Scale Factor: 1, unit: mm, and μ=0.36)

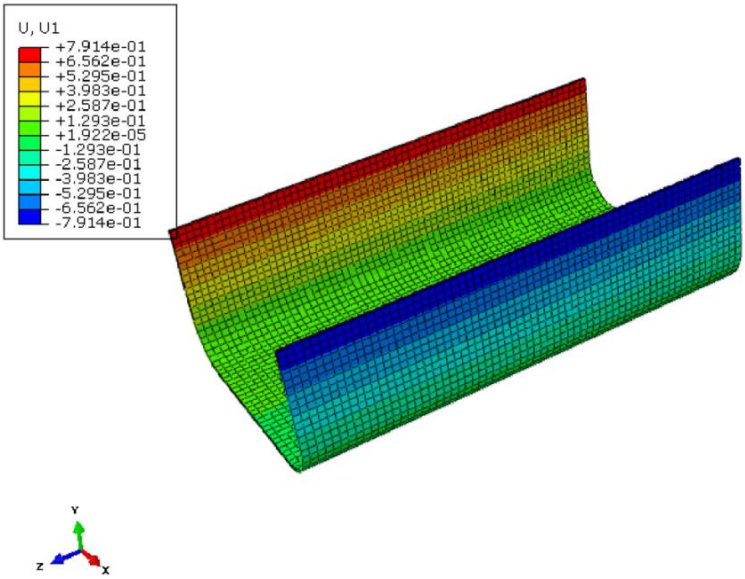

Figure 57: Primary analysis model - displacement in U1 direction (global-x direction) at the end of Step 3 (Deformation Scale Factor: 1, unit: mm, and μ=0.36)

The following displacement results shown in Figure 58, Figure 59, and Figure 60 are obtained when μ is chosen as 0.20:

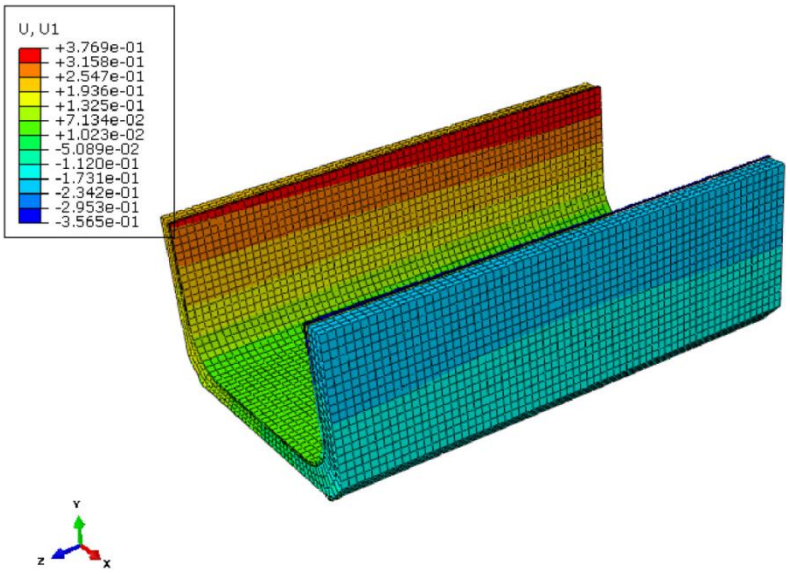

Figure 58: Primary analysis model - displacement in U1 direction (global-x direction) at the end of Step1 (Deformation Scale Factor: 1, unit: mm, and μ=0.20)

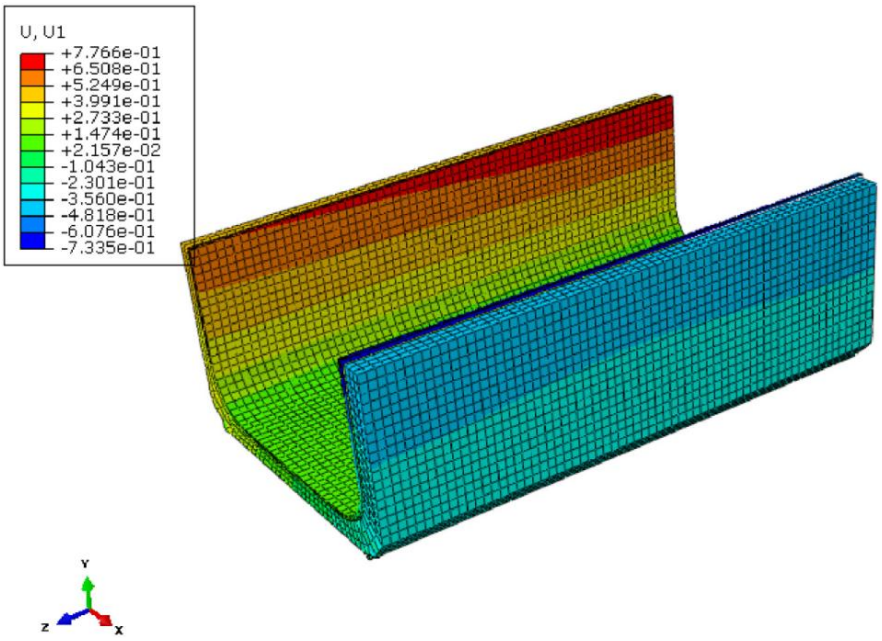

Figure 59: Primary analysis model - displacement in U1 direction (global-x direction) at the end of Step2 (Deformation Scale Factor: 1, unit: mm, and μ=0.20)

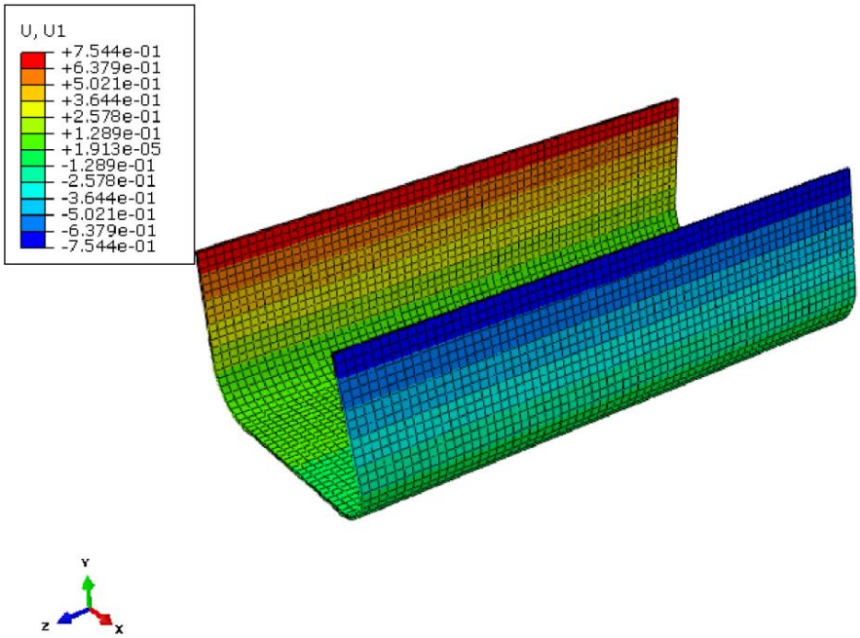

Figure 60: Primary analysis model - displacement in U1 direction (global-x direction) at the end of Step3 (Deformation Scale Factor: 1, unit: mm, and μ=0.20)

In the first model, the spring-in solutions were obtained for different coefficient of friction values, μ as 0.20, 0.28, and 0.36. By looking at Figure 54, Figure 57, and Figure 60, it is observed that higher coefficient of friction results in higher spring-in angles. This is because when the friction between composite part and tool increases, the amount of residual stresses locked in the composite part also increase. The spring-in angles obtained from these models are summarized in Table 12.

Table 12 – Spring-in angles calculated by using different coefficient of friction (μ) values in primary analysis model

ABAQUS Model	**Spring-in Angle (°)***
Primary Analysis Model (μ=0.28)	0.92
Primary Analysis Model (μ=0.36)	0.93
Primary Analysis Model (μ=0.20)	0.91

* Positive angle indicates that spring-in occurs towards the inside.

In the second model, the effect of cure shrinkage on the spring-in mechanism is studied and for that purpose only cure shrinkage is simulated along with the defined tool-part interaction and rubbery state material properties are used for composite part. Details related to the analysis model simulating cure shrinkage effect are provided in section 4.2.3. For the two-step analysis model simulating cure shrinkage effect, displacement solutions obtained from ABAQUS at the end of each step are shown in the Figure 61 and Figure 62.

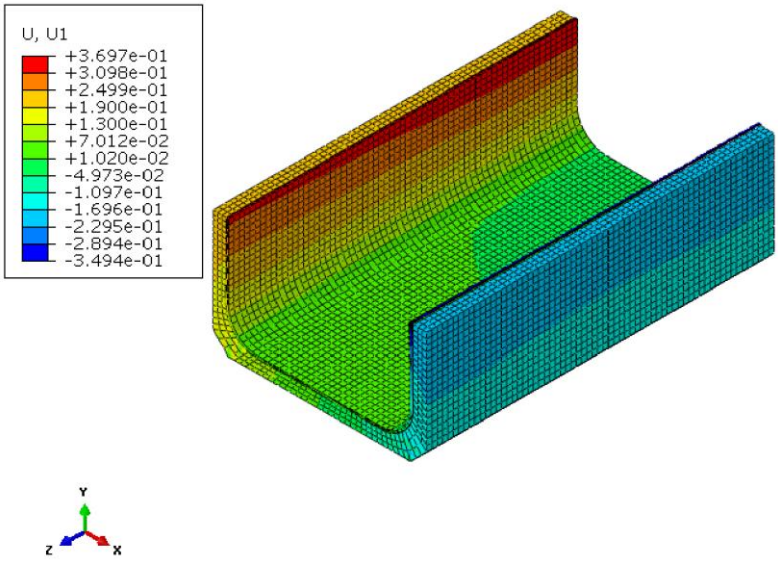

Figure 61: Analysis Model Simulating Cure Shrinkage Effect - displacement in U1 direction (global-x direction) at the end of Step 1 (Deformation Scale Factor: 1 and unit: mm)

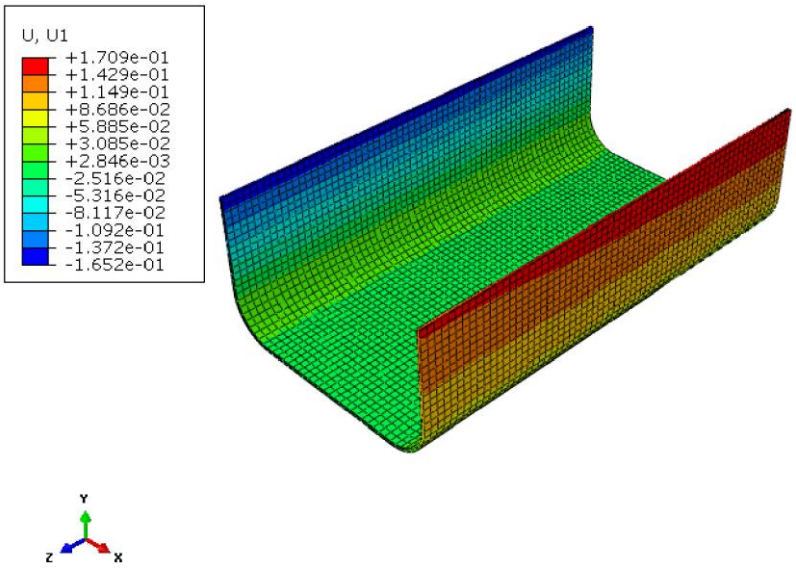

Figure 62: Analysis Model Simulating Cure Shrinkage Effect - displacement in U1 direction (global-x direction) at the end of Step 2 (Deformation Scale Factor: 1 and unit: mm)

Finally, in the third model, the effect of tool-part interaction is investigated. Tool is removed from the model and only the spring-in behavior of composite part is examined without the tool. Details related to the analysis model without tool are provided in section 4.2.4. For the two-step analysis model without the tool, displacement solutions obtained from ABAQUS at the end of each step are shown in Figure 63 and Figure 64.

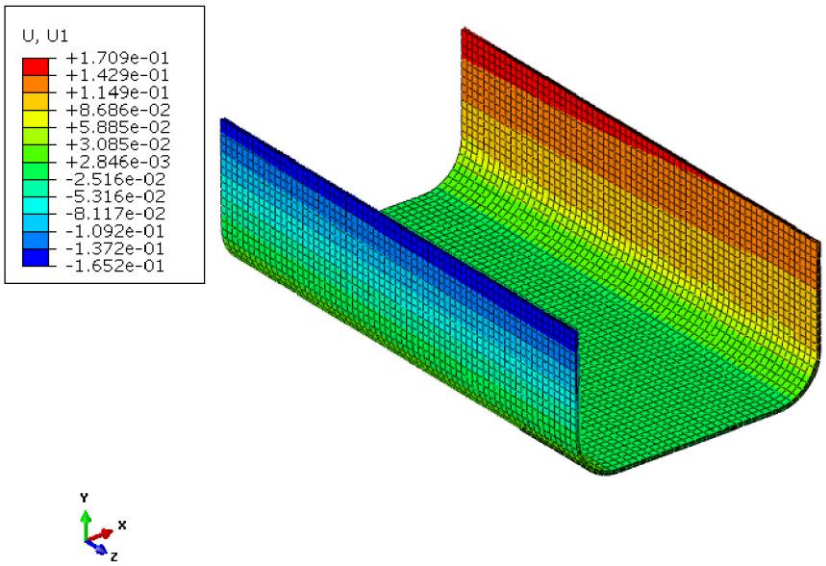

Figure 63: Analysis Model without Tool - displacement in U1 direction (global-x direction) at the end of Step 1 (Deformation Scale Factor : 1 and unit : mm)

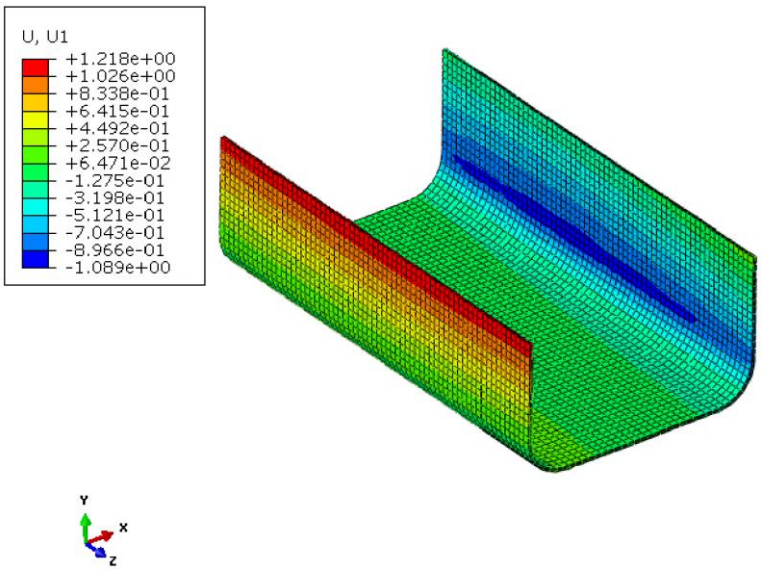

Figure 64: Analysis Model without Tool - displacement in U1 direction (global-x direction) at the end of Step 2 (Deformation Scale Factor : 1 and unit : mm)

In Figure 64, it is seen that the displacements in U1 or global-x direction are not symmetric with respect to both sides of U-shaped geometry. This might be due to a shift in the line of symmetry of lay-up and/or lack of tool-part interaction. Even though the laminate used in the thesis is symmetric and balanced, the symmetry line shifts around the corners since the length of layers change from the inner layer to the outer layer. Therefore, the effects of ±45° layers with respect to symmetry line are different from each other. However, it is also seen that when the same analysis is performed in ABAQUS with lay-up configuration of $[0°]_8$, symmetric displacement results are obtained at the end. (Figure 65) This is because no bending-stretch couplings occur in $[0°]_8$ lay-up configuration since all layers have the same orientation.

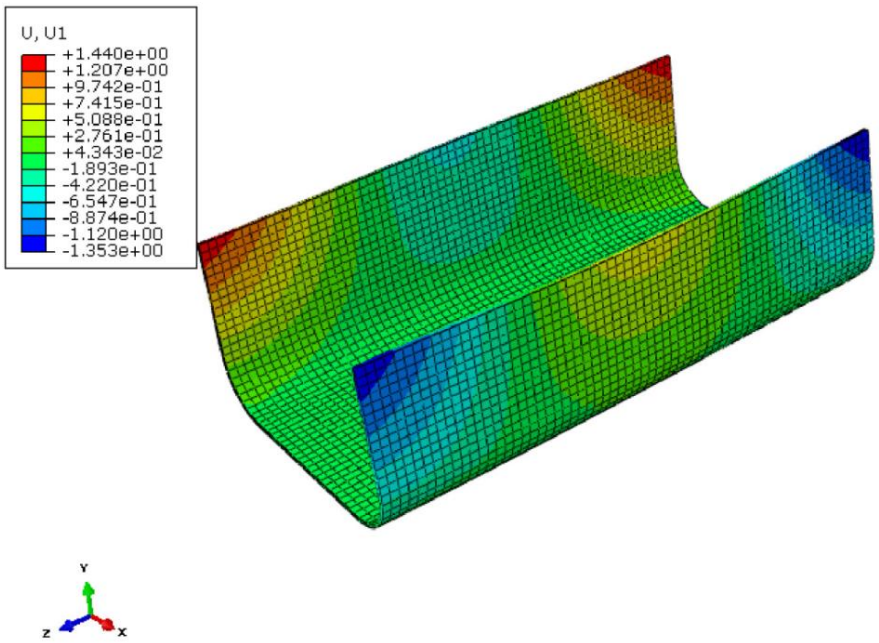

Figure 65: Analysis Model without Tool and with Lay-up Configuration of $[0]_8$ - displacement in U1 direction (global-x direction) (Deformation Scale Factor : 1 and unit : mm)

Calculated average spring-in angles for the all three models are presented in Table 13. In ABAQUS models, spring-in angles are measured from three locations along three sections on one side of the U-shaped composite parts. The same sections defined during experimental spring-in measurements are also used for spring-in angle measurements in numerical analysis models. Consequently, the spring-in angles are averaged along these three sections.

Table 13 – Spring-in angles calculated by each ABAQUS analysis model

ABAQUS Model	Spring-in Angle (°)*
Primary Analysis Model (μ=0.28)	0.92
Analysis Model Simulating Cure Shrinkage Effect	-0.21
Analysis Model without Tool	1.11

* Positive angle indicates that spring-in occurs towards the inside. Negative angle indicates that spring-in occurs towards the outside.

From Table 13, it is seen that analysis model without the tool predicts a higher spring-in angle than the primary analysis model. The main reason for this is that friction between tool and part is neglected and geometric constraints on composite part due to tool are removed.

It is also seen in Table 13 that spring-in angle found by the analysis model simulating cure shrinkage effect is negative. As already explained in the previous chapter, cure shrinkage is simulated as thermal contraction by only using rubbery state properties. CTEs at rubbery state are negative while CTEs at glassy state are positive as shown in Table 2. Therefore, the effect of cure shrinkage causes spring-in distortion towards the outside. Moreover, as can be seen in Table 8 and Table 13, spring-in angle found by the analysis model simulating cure shrinkage effect is in agreement with the spring-in angle due to cure shrinkage found by analytical model.

5.4.COMPARISON OF SPRING-IN ANGLES FOUND BY ANALYTICAL MODEL, EXPERIMENT AND NUMERICAL ANALYSIS MODEL

The spring-in angles for the U-shaped composite part found by analytical model, experiment and numerical analysis model are summarized in Table 14.

Table 14 –Comparison of Spring-in Angles Found by Three Different Methods

Model	Spring-in Angle (º)*
Analytical Model	1.54
Experiment	0.85
Numerical Analysis Model	0.92

* Positive angle indicates that spring-in occurs towards the inside.

By looking at Table 14, it can be deduced that numerical analysis model which simulates autoclave forming process of U-shaped composite parts finds spring-in angle as 0.92º which is in good agreement with the average experimental spring-in angle that is 0.85º. Analytical model, on the other hand, finds higher spring-in angle when compared to other methods. This is because the 2-D analytical model works with Cauchy strains and it does not consider the third dimension which is the length of part. Also, the analytical model does not take the tool-part interaction and the autoclave pressure into account.

CHAPTER 6

CONCLUSIONS

In this thesis, spring-in problem encountered in U-shaped composite parts which are made of Hexcel's AS4/8552 unidirectional (UD) prepregs with lay-up configuration $[45°/-45°/90°/0°]_s$ is investigated by analytical, experimental and numerical methods. First of all, a simple two dimensional (2-D) geometrical model available in the literature is implemented and spring-in is calculated according to this model. Secondly, using autoclave forming technique, U-shaped composite parts are manufactured and spring-in measurements are performed on these parts by using optical scanning device. Finally, a three dimensional (3-D) numerical model in ABAQUS is constructed by taking tool-part interaction, cure shrinkage and state transformations of resin into account. Then spring-in simulation is performed by using constant rubbery and glassy state material properties for U-shaped composite parts.

Spring-in angle 1.54º calculated with analytical method is observed to be higher than spring-in angles determined by the numerical and the experimental methods. Therefore, it is concluded that although 2-D analytical model is a fast method to predict spring-in behavior of a corner shaped composite part, it overestimates the spring-in angle.

It can be deduced from the overestimated results of analytical model that tool-part interaction is an important spring-in mechanism which must be taken into account for proper spring-in estimation. The importance of tool-part interaction mechanism is also seen in the numerical analyses. The numerical analysis performed without the tool gave spring-in angle of 1.11º which is higher than the spring angle of 0.92º found by primary analysis model which includes tool model and, therefore; tool-part interaction.

The effect of cure shrinkage causes a spring-in behavior towards the outside for a U-shaped composite part. This is validated by both analytical and numerical results. Negative spring-in angles of -0.18º and -0.21º are obtained from the analytical and numerical models, respectively. Negative spring-in angles mean that the spring-in occurs towards the outside. It can be stated that analytical model and numerical model make a good agreement while calculating spring-in angle due to cure shrinkage mechanism.

As mentioned earlier, spring-in angle 0.92º found by primary analysis model which is the basic numerical model developed in ABAQUS is very close to the average spring-in angle 0.85º obtained via experiment. Therefore, ABAQUS analysis model is found to be satisfactory since it yields acceptable spring-in angle prediction with respect to the real case spring-in angle measured during experiment. It is concluded that the ABAQUS analysis model can be used to predict the spring-in angle of a composite part so that more accurate tools can be manufactured beforehand. This reduces manufacturing costs and time.

For future studies, in order to have a more realistic numerical analysis model, heat transfer inside the autoclave chamber can be modeled. For that purpose, convection coefficient should be experimentally determined and implemented in the analysis model. Also, to see the variation of spring-in along the length of U-shaped composite parts, experiments and numerical analyses with longer composite parts should be conducted. In addition to these, spring-in behavior of a different type of reinforcement such as woven fabric reinforcement can be studied in the numerical analysis and experiments. Plane stress and strain models of the composite parts can be developed to make comparisons against the 2D analytical prediction presented in this thesis.

REFERENCES

[1] Harris, B., (1999). Engineering Composite Materials. London: The Institute of Materials.

[2] Mohan, M., (2008). The Advantages of Composite Materials in Marine Renewable Energy Structures. Paper presented at RINA Marine Renewable Energy Conference. pp.1-3

[3] Biron, M., (2014). Thermosets and Composites. 2nd ed. San Diego, USA: Elsevier.

[4] Ratna, D., (2009). Handbook of Thermoset Resins. 1st ed. UK: Smithers.

[5] Lamers, E. A. D., (2004). Shape distortions in fabric reinforced composite products due to processing induced fibre reorientation. 1st ed. The Netherlands: FEBO druk, Enschede.

[6] Ibeh, C.C., (2011). Thermoplastic Materials: Properties, Manufacturing Methods, and Applications. 1st ed. : CRC Press.

[7] Todd Johnson (2008). Thermoplastic vs Thermoset Resins. [ONLINE] Available at: http://composite.about.com/od/aboutcompositesplastics/a/Thermoplastic-Vs-Thermoset-Resins.htm. [Last Accessed 13 July 2014].

[8] Henning, F., Krause, W., (2005). Long-Fiber Reinforced Thermoplastics Tailored for Structural Performance. ACCE, 5th Automotive and Composites Conference. USA.

[9] Daniel, M.I., Ishai, O., (1994). Engineering Mechanics of Composite Materials. 1st ed. New York: Oxford University Press.

[10] Tong, L., Mouritz, A. P., and Bannister, M. K., (2002). 3D Fiber Reinforced Polymer Composites. 1st ed. Sydney: Elsevier.

[11] Bilisik, K., (2013). Three-dimensional braiding for composites: A review. Textile Research Journal. 83 (13), pp.1414-1436

[12] Campbell, F.C., (2003). Manufacturing Processes for Advanced Composites. Missouri: Elsevier.

[13] Vasiliev, V. V., Morozov, E. V., (2001). Mechanics and Analysis of Composite Materials. 1st ed. Oxford: Elsevier.

[14] Harper, A. C., Petrie, M. E., (2003). Plastics Materials and Processes: A Concise Encyclopedia. John Wiley & Sons, Inc..

[15] Laurenzi, S. and Marchetti, M. (2012). Advanced Composite Materials by Resin Transfer Molding for Aerospace Applications, Composites and Their Properties, Prof. Ning Hu (Ed.), ISBN: 978-953-51-0711-8, InTech, DOI: 10.5772/48172. Available from: http://www.intechopen.com/books/composites-and-their-properties/advanced-composite-materials-by-resin-transfer-molding-for-aerospace-applications

[16] Hoa, V. S., (2009). Principles of the Manufacturing of Composite Materials. 1st ed. USA: DEStech Publications.

[17] Hexcel (2005). Prepreg Technology. France: Publication No. FGU 017b.

[18] West System, (2010). Vacuum Bagging Techniques. 7th ed. Bay City: Gougeon Brothers.

[19] Bersee, H.E.N., Lindstedt, S., Niño, G., Beukers, A., (2007). DIAPHRAGM FORMING OF THERMOSET COMPOSITES. 16TH INTERNATIONAL CONFERENCE ON COMPOSITE MATERIALS. pp.1-2

[20] Lavender CE (2010). Guide to Vacuum Bagging. [ONLINE] Available at: http://www.lavender-ce.com/wp-content/uploads/guide-to-vacuum-bagging.pdf. [Last Accessed 15.07.2014].

[21] Hexcel, (2013). HexPly 8552 Product Data. 1st ed. France: Hexcel Composites Publication.

[22] FAA-H-8083-31, (2014). Aviation Maintenance Technician Handbook - Airframe. 1st ed. USA

[23] Fernlund, G., Poursartip, A., Twigg, G., and Albert, C., (2002). RESIDUAL STRESS, 2 IN AUTOCLAVED COMPOSITE PARTS. Vancouver: The University of British Columbia.

[24] Antonucci V., Giordano M., Cusano A., Nasser J., Nicolais L., (2006). Real time monitoring of cure and gelification of a thermoset matrix. Composites Science and Technology. 66, pp.3273–3280

[25] ACP Composites (2013). Prepregs. [ONLINE] Available at: https://www.acpsales.com/upload/what-are-prepregs.pdf. [Last Accessed 16 July 2014].

[26] Leutz, D., (2011). Draping Simulation: Modelling different Materials and Processes. München: SGL GROUP.

[27] PAM-QUIKFORM for CATIA V5 (2007). [ONLINE] Available at: http://www.plmmarketplace.com/software/pam-quikform-for-catia-v5.html. [Last Accessed 17 July 2014].

[28] Woytowich, Brian J., (2008). Detection of delamination defects in carbon fiber laminate composites using ultrasound and the Hilbert-Huang transform. Massachusetts: Tufts University

[29] P. Camanhoa, P., G. Da´vila, C., Pinhoc, S., Iannucci, L., Robinson, P., (2006). Prediction of in situ strengths and matrix cracking in composites under transverse tension and in-plane shear. Composites. 37 (Part A), pp. 165–176

[30] Wisnom, M.R., Gigliotti, M., Ersoy, N., Campbell, M., Potter, K.D. , (2006). Mechanisms generating residual stresses and distortion during manufacture of polymer–matrix composite structures. Composites. 37 (Part A), pp.522-529

[31] Twigg, G., Poursartip, A., Fernlund, G., (2004). Tool–part interaction in composites processing. Part I: experimental investigation and analytical model. Composites. 35 (Part A), pp.121-133

[32] Albert, C., Fernlund, G., (2002). Spring-in and warpage of angled composite laminates. Composites Science and Technology. 62 (), pp.1895-1912

[33] Wijskamp, S., (2005). Shape Distortions in Composite Forming. 1st ed. The Netherlands: PrintPartners Ipskamp B.V.

[34] Salomi, A., Garstka T., Potter K., Greco, A., Maffezzoli, A., (2002). Spring-in angle as molding distortion for thermoplastic matrix composite. Composites Science and Technology. 68, pp.3047-3054

[35] Svanberg, J.M., Holmberg, J. A., (2004). Prediction of shape distortions Part I. FE-implementation of a path dependent constitutive model. Composites. 35 (Part A), pp.711-721

[36] Svanberg, J.M., (2002). Predictions of manufacturing induced shape distortions-high performance thermoset composites. Sweden: Department of Applied Physics and Mechanical Engineering, Lulea University of Technology.

[37] Ersoy, N., Tugutlu, M., (2010). Cure Kinetics Modeling and Cure Shrinkage Behavior of a Thermosetting Composite. POLYMER ENGINEERING AND SCIENCE. 50, pp.84-92

[38] Shokrieh, M.M., Safarabadi, M., (2011). Three-dimensional analysis of micro-residual stresses in fibrous composites based on the energy method: a study including interphase effects. Journal of Composite Materials. 46 (6), pp.727-735

[39] Nawab, Y., Tardif, X., Boyard, N., Sobotka, V., Casari, P., Jacquemin, F., (2012). Determination and modelling of the cure shrinkage of epoxy vinylester resin and associated composites by considering thermal gradients. Composites Science and Technology. 73, pp.81-87

[40] Hoa, S.V., Ouellette, P., Ngo, T.D., (2009). Determination of Shrinkage and Modulus Development of Thermosetting Resins. Journal of Composite Materials. 43 (783).

[41] Yoon, K. J., Kim, J-S., (2001). Effect of Thermal Deformation and Chemical Shrinkage on the Process Induced Distortion of Carbon/Epoxy Curved Laminates. Journal of Composite Materials. 35 (253).

[42] Russell, J.D., Madhukar, M.S., Genidy, Lee, A.Y., (2000). A New Method to Reduce Cure-Induced Stresses in Thermoset Polymer Composites, Part III: Correlating Stress History to Viscosity, Degree of Cure, and Cure Shrinkage. Journal of Composite Materials. 34 (1926).

[43] Zeng, X., Raghavan, J., (2010). Role of tool-part interaction in process-induced warpage of autoclave-manufactured composite structures. Composites. 41 (Part A), pp.1174-1183

[44] Dong, C., (2009). Modeling the Dimensional Variations of Composites Using Effective Coefficients of Thermal Expansion. Journal of Composite Materials. 43 (2639).

[45] Wisnom, M. R., Potter, K. D., and Ersoy, N., (2007). Shear-lag Analysis of the Effect of Thickness on Spring-in of Curved Composites. Journal of Composite Materials. 41 (1311)

[46] Radford, D.W., Rennic, T.S., (2000). Separating sources of manufacturing distortion in laminated composites. Journal of Reinforeced Plastics Composites. 19 (8), pp.621-641

[47] Chen, H-J. and Tsai, S.W., (1996). Three-Dimensional Effective Moduli of Symmetric Laminates. Journal of Composite Materials. 30 (906).

[48] Goetschel, D.B., and Radford, D.W., (1997). Analytical development of through–thickness properties of composite laminates. Journal of Advanced Materials, 28(4), pp.37–46.

[49] Akkerman, R., (2002). On the properties of quasi–isotropic laminates. Composites Part B: Engineering, 33, pp.133–140.

[50] Roylance, D., (2001). Transformation of Stresses and Strains, Department of Materials Science and Engineering, MIT, USA.

[51] Ersoy, N., Garstka, T., Potter, K., Wisnom, M.R., Porter, D., Clegg, M., Stringer, G., (2010). Development of the properties of a carbon fibre reinforced thermosetting composite through cure. Composites. 41 (Part A), pp.401-409

[52] HexTow, AS4, (2013). Product Data. France: Hexcel.

[53] HexPly, 8552 Epoxy Matrix, (2013). Product Data. France: Hexcel.

[54] FREKOTE, 700-NC, (2009). Technical Data Sheet. Germany: Henkel

[55] Çinar, K., Öztürk, U. E., Ersoy, N., Wisnom, M.R., (2013) Modeling manufacturing deformations in corner sections made of composite materials. Journal of Composite Materials, 0(0) 1–15.

[56] ZAIMOVIC-UZUNOVIC, N., LEMES, S., (2010) Influences Of Surface Parameters On Laser 3d Scanning, 10th International Symposium on Measurement and Quality Control.

[57] Khoun, L., Centea, T., Hubert, P., (2009). Characterization Methodology of Thermoset Resins for the Processing of Composite Materials -- Case Study: CYCOM 890RTM Epoxy Resin. Journal of Composite Materials. 44 (1397)

[58] Ersoy, N., Garstka, T., Potter, K., Wisnom, M.R., Porter, D., Stringer, G., (2009) Modelling of the spring-in phenomenon in curved parts made of a thermosetting composite. Composites. 41 (Part A), pp.410-418

[59] SIMULIA, ABAQUS 6.12-1. ABAQUS Analysis User's Manual.

[60] Johnston, A.A., (1997). An Integrated Model of the Development of Process-Induced Deformation in Autoclave Processing of Composite Structures. Canada: Department of Metals and Materials Engineering, The University of British Columbia.

[61] Zhu, Q., Geubelle, P.H., (2002). Dimensional Accuracy of Thermoset Composites: Shape Optimization, Journal of Composite Materials. 36 (647)

[62] Wiersma, H.W., Peeters, L.J.B., Akkerman, R., (1998). Prediction of springforward in continuous-fibre/polymer L-shaped parts. The Netherlands: Department of Mechanical Engineering, University of Twente.

[63] Dong, C., Zhang, C., Liang, Z., Wang, B., (2003) Dimension variation prediction for composites with finite element analysis and regression modeling, Composites. 35 (Part A), pp.735-746

[64] Fernlund, G., Osooly, A., Poursartip, A., Vaziri, R., Courdji, R., Nelson, K., George, P., Hendrickson, L., Griffith, J., (2003). Finite element based prediction of

process-induced deformation of autoclaved composite structures using 2D process analysis and 3D structural analysis, Composite Structures. 62, pp.223-234

[65] Svanberg, J.M., Holmberg, J.A., (2004). Prediction of shape distortions. Part II. Experimental validation and analysis of boundary conditions, Composites. 35 (Part A), pp.723-734

[66] Ruiz, M. J. G., (2009). Thermal Analysis in ANSYS. Columbia: Mechanical Engineering Department, Universidad EAFIT.

[67] Dynamic Mechanical Analysis (DMA), (2013). USA: PerkinElmer Inc.

[68] ASM Aerospace Specification Metals Inc. (2001). [ONLINE] Available at: http://asm.matweb.com/search/GetReference.asp?bassnum=MA6061t6. [Last Accessed 25 June 2014].

[69] Misra, P., Nagaraju, J., (2010). Thermal gap conductance at low contact pressures (<1 MPa): Effect of gold plating and plating thickness, International Journal of Heat and Mass Transfer. 53, 5373-5379

[70] Milanez, F., Yovanovic, M. M., Mantelli, M.B.H., (2003). Thermal Contact Conductance At Low Contact Pressures, 36th AIAA Thermophysics Conference, Orlando, FL

[71] Cooper, M. G., Mikict, B. B., Yovanovich M. M., (1969), Thermal Contact Conductance. International Journal of Heat and Mass Transfer, 12, pp.279-303